LONDON'S GLOBAL UNIVERSITY

UNIVERSITY COLLEGE LONDON
Department of Civil, Environmental & Geomatic Engineering

DISSERTATION:

Seismic Analysis & Fragility Assessment of Reinforced Concrete Structures through Numerical Modelling

Cory George
15115628

A dissertation submitted in partial
fulfilment for the degree in Master of Science in
MSc Earthquake Engineering and Disaster Management

Supervisor:
Dr. Arash Nassirpour

September 2018

DISSERTATION SUBMISSION / PLAGERISM FORM

ABSTRACT

This research investigates the differences observed in structural responses produced by the Opensees and Seismostruct numerical modelling software. The study aims on developing models to represent low rise reinforced concrete structures which will be studied under both static and dynamic loading. The structures are modelled using well known numerical modelling approaches; lumped plasticity and distributed plasticity. Each program has specific methods to apply these approaches however the aim is to generate accurate models in both to ensure proper results. The lumped plasticity approach would be applied in Opensees and the distributed plasticity in Seismostruct.

The nonlinear analyses conducted in this study were nonlinear static pushover analysis and the nonlinear time history analysis. To conduct the nonlinear time history analysis, 20 well known earthquake records typically used by earthquake engineers are utilized. To gain further insight on the impact the results from each software, may have on a wider scale, a probabilistic assessment was conducted showing how the responses from the programs can affect risk.

The results from the pushover analysis resulted seimostruct producing conservative results, where the frames yielded at lower base shears compared to that of Opensees. However when conducting the nonlinear time history analysis, Opensees produced lower peak responses compared to Seimostruct. This therefore shows that precautions are required when selecting numerical modelling techniques to conduct analysis. It illustrates that some level of understanding of the structure to be analysed as well as the limitations of each approach is required to get a better undertsnding.This research would provide some insight on what should be considered when using these modelling approaches.

ACKNOWLEDGEMENTS

First of all, I am grateful to The Almighty God for establishing me to complete this dissertation.

I owe my deepest gratitude to my supervisor Dr Arash Nassirpour PhD. I am extremely grateful and indebted to him for his expertise, continuous encouragement and valuable guidance extended to me.

I am deeply grateful Associate Professor Carmine Galasso, Degree Programme Director of MSc Earthquake Engineering and Disaster Management for making it possible study in his department at the University College London. I am also thankful for his continuous encouragement throughout the study year and for making this experience possible.

I want to take this opportunity to record my sincerest thanks to all the faculty members ,research assistants and classmates of the 2017- 2018 year group in the Department of Earthquake Engineering and Disaster Management for their help and encouragement, for if it wasn’t for the combined effort I would not be able to be completing this dissertation.

I also want to thank my parents for their unceasing encouragement and support, for without them I would not be present today.

Finally, I place on record, my sincerest appreciation to those who directly or indirectly, have lent their helping hand on this journey. Your assistance will not be forgotten as it aided in my completion of this dissertation.

TABLE OF CONTENTS

Contents

LIST OF TABLES

LIST OF FIGURES

Chapter 1.0

INTRODUCTION

1.1 Background

The emergence of performance based earthquake engineering seeks to enable more accurate and transparent assessment of life safety risks and damage by simulating the nonlinear response of a structural system to seismic excitation. (Filippou and Fenves 2004, Zendaoui, Kadid and Yahiaoui, 2016). The first generation of performance-based assessment provisions, such as FEMA 273 and 356 (ASCE 1997; ASCE 2000b) and ATC 40 (ATC 1996), provided an excellent first step toward codifying approaches that embrace nonlinear analysis to simulate system performance and articulate performance metrics for the onset of damage up to structural collapse. These nonlinear analysis techniques are generally seeking practical design applications to assess the performance of buildings under static and dynamic loads.

However, new performance based guidelines, according to FEMA -273 (1997), states that buildings are required to be analysed using nonlinear static pushover analysis or non-linear dynamic analyses to regulate the global and local demands. Therefore, the use of nonlinear analysis demands the availability of robust and computationally efficient models for performing analyses in a reasonable amount of time (Coleman and Spacone 2001).

Therefore, accurate and computationally efficient numerical models that represent the cyclic loading of plastic hinges in beam–column elements, including the effect of degradation, are thus required to simulate the seismic response and evaluate the performance of structural systems (Scott and Fenves 2006).In this research the use of two well-known modelling techniques will be used in Opensees and Seismostruct programs and the responses would both be compared.

1.2 Aims and Scope

The aim of this research is to understand the impact and extent of utilising different numerical software (Opensees, Seismostruct) on the obtained seismic performance and consequently the damage assessment, by focusing on low-rise reinforced concrete structures. To achieve this research goal, three mid-rise RC residential buildings, each 2 storey high and having same plan dimensions with different structural member configurations, were selected and analysed in both software and their resulting seismic responses are compared using a modified capacity spectrum method (FRACAS).The chosen RC buildings configurations are classified as generic building type C1L (Low-Rise Concrete Moment Frame) according to HAZUS documentation provided by FEMA. Three generic buildings were analysed using both Nonlinear Static Pushover Analysis and Nonlinear Time History Analysis (NLTHA) where the buildings performances for three limit states including slight damage, moderate damage and collapse were determined from the Nonlinear Static Pushover analysis. Then the fragility assessment is performed where the fragility curves are developed for the three limit states and fragility curves of the three buildings in both software are compared to determine the sensitivity of the software.

1.3 Objectives:

1) A comprehensive review of available literature on comparing the seismic evaluation through the considered software (Opensees and Seismostruct).
2) Identify the advantages and disadvantages of each software by focusing on their approach to modelling components and estimating the nonlinearity in both material and geometry.
3) Identifying and modelling a number of existing residential buildings with highest possible detailing and components through each software.
4) Analysing the numerical models through Static Pushover and Non Linear Time History Analysis, to evaluate the seismic performance of the building and its potential deficiencies.
5) Identify the most applicable damage states and thresholds based on the results obtained through each model.
6) Deriving and comparing the analytical Fragility Functions.

1.4 Thesis Organisation

This research contains seven sections that explain the seismic responses of the three low rise RC generic buildings modelled as 2dimensional frame and 1, three dimensional building. The design of the generic structures were obtained from a structural member database produced by Berry et al ( ) and analysed using the Nonlinear Static Pushover Analysis (NLSPOA) and Nonlinear Time

History Analysis (NLTHA) using both software. Three limit states were then determined from Push over curves and fragility curves were developed for the three buildings in the x direction for the 2 dimensional frame.

Chapter 1 – Background

This chapter gives a general background of the research including the purpose and understanding of how numerical analysis is conducted in specific software and how it approaches modelling components as well as considerations that need to be addressed for engineers who intend on conducting numerical analysis using these programs. Also in this chapter the main objectives of the research and thesis is outlined.

Chapter 2 – Theoretical Background

This section provides a comprehensive review available literature on comparing the seismic evaluation through the Opensees and Seismostruct software. First, a discussion about techniques used to model structural elements in order to simulate the response of reinforced concrete buildings subjected to seismic activity. Secondly, previous studies and history on the development of the concentrated and distributed plasticity nonlinear modelling techniques. Third, the advantages and disadvantages of the both nonlinear modelling techniques are discussed. Finally, the approach each software uses to model the components and estimating nonlinearity in both material and geometry using the concentrated and distributed plasticity.

Chapter 3 – Methodology

This section describes the approach used to conduct the study in the form of a flow chart.

Chapter 4 - Design

This chapter discusses the description and RC design of the three generic RC frames. It first describes the structural configuration of the sample generic frames under investigation illustrating their elevation view. Then a description of the structural database being used and purpose in this research project. Finally, all the building member cross sections illustrated as well as the associated structural properties are listed.

Chapter 5 – Numerical Structural Model

This chapter explains the nonlinear modelling of the three, 2 dimensional RC frames and 3 dimensional building for numerical simulation in Opensees and Seismostruct with the intention of ensuring both models are identical. The geometric and material nonlinearities and materials types (i.e. Reinforcement and concrete) used in this research are highlighted and discussed. The results are the natural periods and the first three translational modes.

Chapter 6 - Pushover Analysis

This chapter focuses on the nonlinear static pushover of the building models discussed in the chapter four and five. Firstly, the modal analysis results are shown including the modal periods and shapes to validate numerical models in Opensees and Seismostruct models. The target displacement is determined. The chapter concludes with a discussion

Chapter 7 – Nonlinear-Time History Analysis

This chapter contains the assessment of the nonlinear dynamic time history analysis in great detail by comparing the seismic responses of the three sample generic two dimensional frames. The results are presented and compared with PA's results. The fundamental periods would then be used to develop representations of the Intensity Measure (IM) vs Engineering Demand Parameters (EDP) plots. The chapter concludes with a discussion of the results.

Chapter 8 –Fragility Analysis

This chapter discusses the development of the modified capacity spectrum method and the procedure used to generate the fragility curves. A comparison of the fragility curves for two frames models are shown aiming to show the sensitivity of the results or responses from each software.

Chapter 9 - Further Analysis

The chapter contains the investigation of the structural response regarding a 3 dimensional structure using fibre based model in Opensees and comparing with the force based concentrated plasticity and displacement based distributed plasticity in Seismostruct. A pushover analysis is conducted and the results are compared and discussed.

Chapter 10 - Conclusion

Main conclusion and remarks are presented

Chapter 2.0

LITERATURE REVIEW

2.1 ELEMENT MODELING

In order to simulate the response of under designed reinforced concrete buildings subjected to seismic activity, it is essential to take into account the flexure behaviour of beams and columns, shear behaviour of columns and failure in connections. These behaviours are simulated using numerical models to replicate the non-ductile behaviour of structural elements in which the results can be further used to perform collapse risk assessments. Currently, there are five idealized model types **(See figure 2.1)** that can be used to represent the inelastic flexural response of beam – column elements which are used to estimate the lateral displacements due to flexure, bar slip and shear. These fall into two main categories. These are 1) lumped plasticity at the ends of the element or 2) distributed plasticity along its length **(NIST GCR 10-917-5, 2010).**

- Firstly, as illustrated in figure 1 below, the most simplified approach , lumped plasticity, implies that all inelastic deformations is concentrated at the ends of the element.
- The second approach that has become very popular is the distributed plasticity approach. This modelling method is can be idealised as either having an inelastic response within a specified length (finite length hinge model) **(Figure 2-3.c),** or a fibre section formulation **(Figure 2-3.d).**The fibre section considers the inelastic behaviour to be distributed along the length of the member using plate like sections consisting of the structural member properties along the member length in each fibre cross section. The last model type is the considered the most complex numerical modelling technique, which discretizes the member cross section into finite elements along the member length. **(Figure 2-3.e)**

Presently, the fibre model type **(Figure 2-3.d)** is the most commonly used approach due to its computational efficiency. This approach utilizes uniaxial stress–strain relationships for both concrete and steel reinforcement resulting in the ability to model, various concrete regions and steel reinforcement independently.

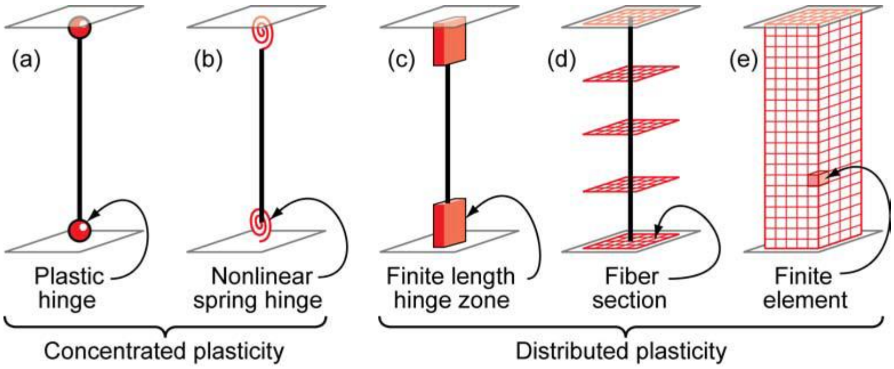

Figure 2-1 Idealization of structural component (from NIST GCR 10-917-7, 2010)

These existing models may not accurately predict the shear capacity for columns that undergo flexural yielding before shear failure due to the fact that they don't account for degradation of shear strength with inelastic flexural deformations. However, they are appropriate for flexure-controlled columns or pure shear failures. In addition to the above, no guidance is provided for simulating the response once shear failure is detected. According to (ATC-95 (2013), models that are computationally efficient, calibrated to a wide range of column failure modes, have the ability to transit between shear and flexure failures, capable of simulating the degrading lateral-force response including in cycle and cyclic degradation, compatible with joint and bar slip response and ability to adjust to different boundary conditions should be used to simulate nonlinear response of existing columns leading to shear and subsequent axial failure.

In retrospect of the above mentioned issues, three models were developed by Elwood (2004), LeBorgne and Ghannoum (2009), and Haselton et al. (2008) which were overcame these concerns and contain the main features suggested by ATC -95 (2013) listed above. A review of Haselton et al.(2008), is presented in chapter 5 as it is used in this study.

2.2 Previous studies and development of Concentrated and Distributed plasticity models.

2.2.1Concentrated Plasticity

The lumped plasticity model as mentioned in section 2.1, is conceptualised by modelling elements with its nonlinear capabilities concentrated at member ends. The general model can be envisioned by separating a line element into linear elastic and elastic perfectly plastic components. The elastic member accounts for the strain hardening characteristics of the reinforcing steel, while the elastic perfectly plastic member accounts for yielding (plastic deformations) of the reinforcement concentrated in the plastic hinges at the element ends. The plastic hinges are represented as zero length rotational springs elements. The plastic behaviour of the rotational springs when subjected to seismic loads, is provided by means of hysteresis models which have a better chance of capturing the nonlinear degrading response of members. This is due to calibration of the springs to test data of various reinforced concrete sections on moment –rotation and hysteresis curves.

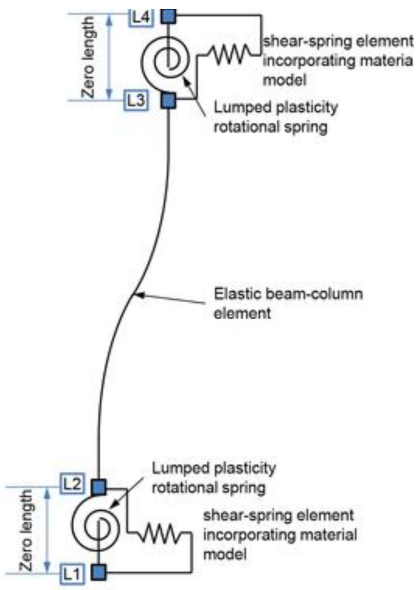

Figure 2-2 Showing elastic beam column line element and zero length lumped plasticity rotational springs

The earliest component model element was introduced by Clough and Johnston (1967) and was only restricted to the bilinear-type hysteresis moment rotation**.** This model was known as the two component model whereby both elastic and inelastic components acted in parallel with each other. Following this, further research was conducted by Giberson (1967) resulting upgrading the model removing the restriction. This updated model was referred to as the one component model as it consisted of two rotational springs attached in series at the ends of an elastic element. This model is more popular than the two component model because of its simplicity and the fact that the member end deformations depends exclusively on the moment acting at the end. This therefore, allows for modelling various complex hysteretic responses. There were later models which were developed allowing the variation of the location of the plastic hinges which was found to perform well in low rise structures according to (Roh, Reinhorn and Lee, 2018).The results showed that this model provided a good evaluation of the base shear and global responses compared to its ability to capture inter-storey deformations and local responses.

Presently, there exist several hysteretic models with calibrated parameters that can be used to represent moment-rotation relationships for non-linear springs. Such models include cyclic stiffness degradation in flexure and shear, (Takeda et al .1970), pinching under reversal, Brancaleoni et al. (1983) and fixed end rotations at the beam – column joint interface due to bar pull out (Filippou and Issa 1988). Therefore the choice of hysteretic models depends on the user.

2.2.2 Distributed Plasticity

According to Spacone and El-Tawil, 2004, distributed plasticity approaches are more accurate than lumped plasticity approaches, because in reality, it is impossible to achieve all inelastic behaviour at the ends of a member. The behaviour of the cross section is either in agreement with plasticity theory of stress and strain responses or derived by discretization of the cross section into fibres, as illustrated in spread plasticity fibre models. An assumption of these models is that the strains are linearly distributed over the cross section. The fiber based models are catergorized into two types; displacement- based (stiffness-based) and forced-based (flexibility-based). Displacement- based requires a predefined displacement shape-function to interpolate the displacements along the element length with respect to the nodal displacements and force-based (flexibility-based) requires using interpolation functions to estimate the forces along the element length with respect to the nodal forces. These will be discussed in more detail in its application in Seismostruct in chapter 6.

The distributed plasticity approach behaviour is examined by numerical integrations through the member cross sections and along the member length. Uniaxial material models are defined to capture the nonlinear hysteric axial stress –strain characteristics in the cross section. The plane sections remain plane assumption is reinforced, where uniaxial material fibers are numerically integrated over the cross section to obtain axial forces and moment stresses as well as incremental moment curvature and axial force strain relations. The cross sections are then integrated numerically at discreet sections along the member length, using displacement or force interpolation functions (Kunnath et al.1990, Spacone et al. 1996).

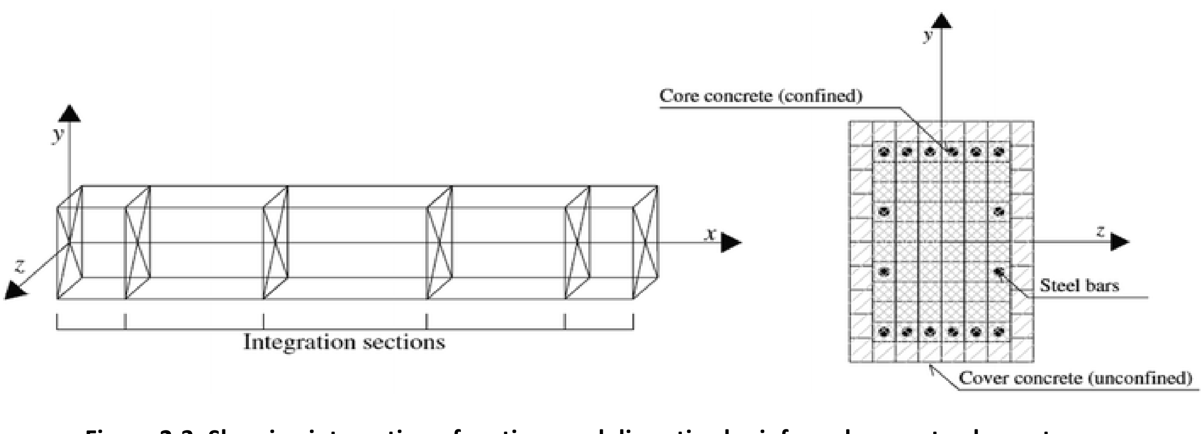

Figure 2-3: Showing integration of sections and discretized reinforced concrete element

Distributed fiber formulations do not generally report plastic hinge rotations, however, it provides the resultant strains in concrete cross sections. This is due to the strain demands having a highly sensitive response to moment gradient, integration method, element length and strain hardening parameters. Therefore, the strain demands and threshold damage state limits should be referenced with concentrated hinge models, which considers plastic hinge rotations. (Nassirpour, 2018).

Although there has been continuous research and development to the concentrated and distributed plasticity modelling there are some considerations that need to be highlighted when conducting numerical analyses. Therefore, following section provides a summarised insight into the advantages and disadvantages of the abovementioned numerical modelling techniques.

2.3 ADVANTAGES AND DISADVATAGES OF LUMPED AND DISTRIBUTED PLASTICITY.

2.3.1 Lumped Plasticity

Advantages

- Simplicity reduces computation effort, computational costs and storage requirements and improves the numerical stability of computations.
- Can specify complex behaviour.
- Lumped plasticity models include hysteretic rules for the hinge behaviour, which can account for many physical phenomena for example cyclic degradation in stiffness and strength, pinching under reversal.
- Applicable to various types of components such as beams, shear walls connections
- Preferred for performance based simulations
- Captures interface effects such as bar pull out and shear sliding.

Disadvantages

(Almeida, J .P. Tarquinii, D.and Beyer,K, 2014)

- They are over simplified e.g. important aspects of the cyclic behaviour of reinforced concrete members such as the post-yield response and axial-flexural interaction which can produce inaccurate results.

- The use of empirical control parameters in limits the generality as the values of these parameters are usually selected by trial and error to produce model response that fit with experimental results of a limited number of reinforced concrete components.

- Selection of parameters for representing the experimental hysteretic behaviour because a). The model parameters depend not only on the section characteristics but also, on the load and deformation history, thus limiting the generality of the approach.

- Inability to describe adequately the deformation softening behaviour of reinforced concrete members. This is observed as the reduction in lateral resistance of an axially loaded cantilever column under monotonically increasing lateral tip displacement.

- It has to be mentioned that such models usually lead to better response estimates for steel rather than for concrete structures.

- Localization occurs if a trilinear approximation of the moment –curvature relation with softening branch is defined for the plastic hinge.

- Cannot capture axial force- moment interactions.

- Model parameters are calibrated on a dataset consisting of mainly columns with flexure dominated failures model parameters are pre-defined, and therefore, it is not capable of

2.4.2 Distributed Plasticity models advantages and disadvantages

(Almeida, J .P, Tarquinii, D. and Beyer, K, 2014)

Advantages

1. Can capture the spread of plasticity.
2. Hysteretic behaviour is implicitly defined at the uniaxial material stress-strain level.
3. Capture flexural deformation and its spread along an assumed number of integration sections along element.
4. P -delta effects: they can be accounted for in the finite element formulation.
5. Sectional response (local level) can capture axial load –moment interaction
6. Are independent of cross sections.
7. Does not require a predetermined length where the inelasticity can occur.
8. Less reliant on calibration of elements.

Disadvantages

- The definition of the integration scheme and number of integration sections requires expertise.
- Computational Cost: For structures composed of many elements and a large number of fibres per section, computing time can increase considerably for nonlinear dynamic time histories.
- Anchorage slip (strain penetration): requires explicit (separate) modelling, e.g. with a zero length element.
- Cannot capture complex response (softening, pinching) modes easily.(Nassipour,2018)
- Assumes a strain-hardening response.

2.5 SOFTWARES

2.5.1 Opensees

The Open System for Earthquake Engineering Simulation (Opensees) is a software framework for simulating the seismic response of structures. Opensees has been developed as the computational platform for research in performance-based earthquake engineering at the Pacific Earthquake Engineering Research Centre. (PEER) by Frank McKenna and Gregory L. Fenves. It has different material models, elements and solution algorithms used for conducting structural and dynamic analyses. The software is based on finite element methods and interprets scripts of tool command language (Tcl). Furthermore, it is an open-source and gives access to all earthquake engineering researchers and students. The main advantage is that the user must create the model manually and define all the steps throughout the procedures. This however enable interested researchers the ability to gain an analytical skills in manual numerical modelling. It has recently been upgraded to include a graphical user interface (GUI) however this may take away from understand the functions and commands of the software. An disadvantage is that some material models may not perform as they should, i.e. confined elements. They figure below provides a visual of the processing interface of the software.

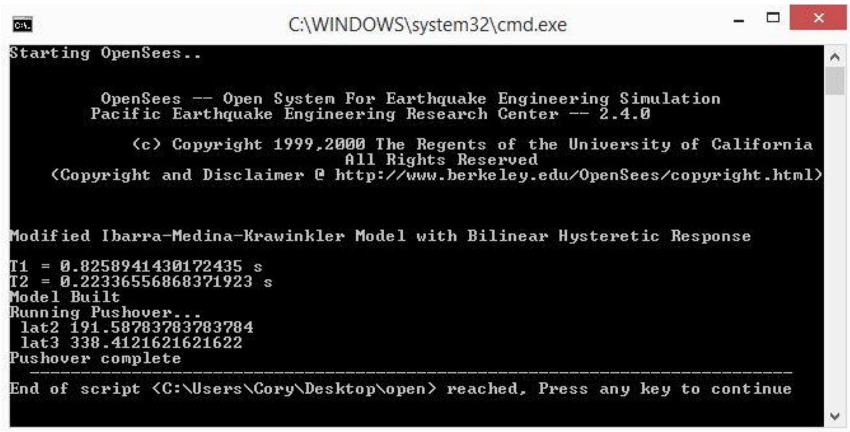

Figure 2-4: Showing Opensees processing interface for pushover analysis.

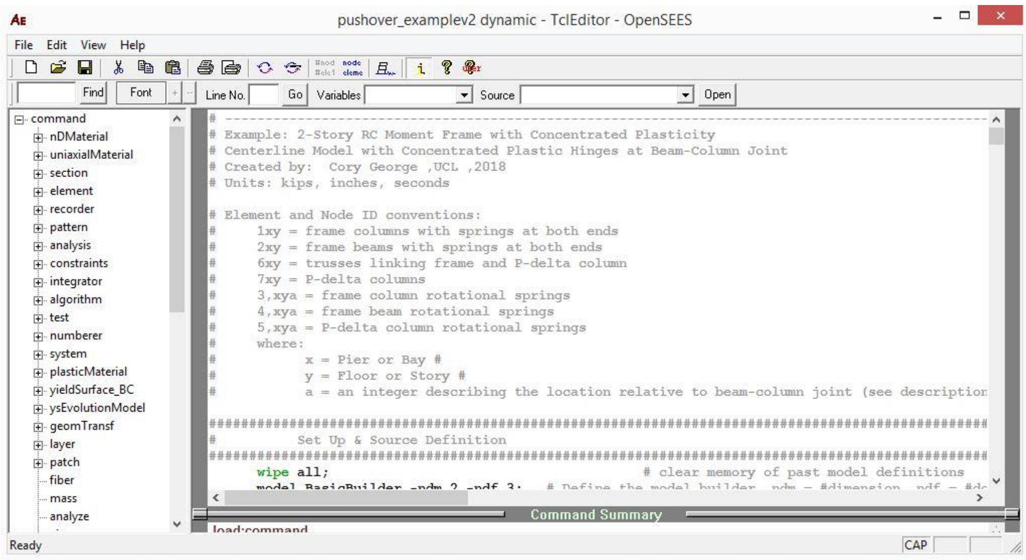

Figure 2-5: Shows an example of a tcl-script for a dynamic time-history analysis.

Simulation strategies for nonlinear beam-column in Opensees

There are three different beam-column element options available in Opensees (McKenna, 2011) to simulate nonlinear material response. The first method consist into model the column using lumped plasticity in which the nonlinear behaviour is concentrated at the ends of an elastic element. The other two modelling solutions allow the simulation of nonlinear response using a distributed plasticity formulation based on finite-element methods. For the purposes of this research, only the lumped plasticity option would be discussed.

Lumped plasticity Element

As discussed in section 2.2, the lumped plasticity can be introduced consists of an elastic beam-column element with two zero-length elements at both the element extremities. The zero-length elements are associated to a rotational hinge model with hysteretic rules able to capture the flexural behaviour of the elements. The behaviour of rotational hinge is associated to a uniaxial material that express the plastic hinge behaviour in terms of moment-rotation relationship, however, caution is advised in implementing the stiffness property of the element connecting the elastic beam –column element to the hinges. The moment- rotation relation can be represented as monotonic backbone curves. These curves are often calibrated to a particular monotonic response. These are bilinear, trilinear, elastic – nonlinear hardening and lastly a monotonic curve including capping or residual strength.

Modified Ibarra-Medina-Krawinkler Deterioration Model

The Ibarra- Medina -Krawinkler model (IMK) analytical model developed by Ibarra et al (2005), is implemented in Opensees (Mckenna, 1997) and is used to represent the concentrated plasticity zero length element. The monotonic curve used to represent the response of the IMK model is the bilinear curve shown in Figure 6 below. The model specifies the demand limits of the structural member also simulating the strength deterioration (negative slope) once the maximum moment capacity (M_c) is reached. If the model is asymmetrical, a similar response is seen upon but for a negative moment capacity.

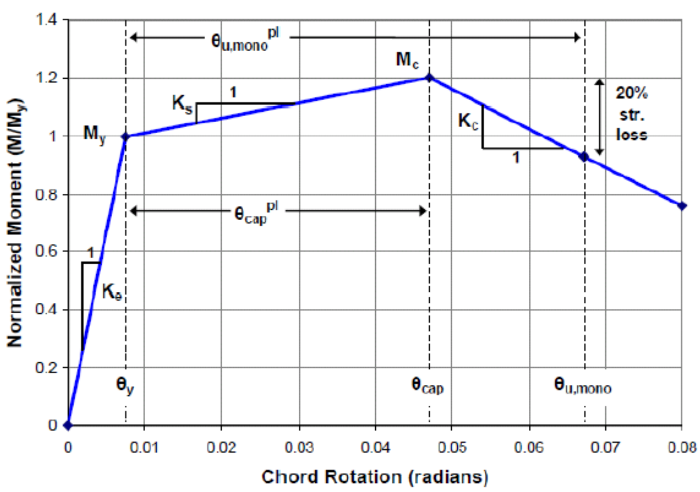

Figure 2-6: Showing monotonic bilinear backbone curve (elastic perfectly plastic with linear hardening)

The characteristics that defines the monotonic curve in the modified IMK model as shown in figure 6, are initial elastic stiffness K_e, the effective yield moment strength M_y, the post yield strength ratio M_c / M_y or $\theta_{cap\ pl}$, and the residual moment strength $M_r = {}_kM_y$. The backbone curve can be described by three deformation parameters. These are the;

- Pre capping plastic rotation, $\theta_{p,}$ which is associated with the components behaviour prior to local instabilities (buckling of reinforcing bars). This represents the initiation of the loss of strength.
- Post capping plastic rotation θ_{pc}; which is associated with component behaviour after the occurrence of local instabilities. The smaller the value, the sooner the component reaches zero bending strength capacity therefore building collapse is imminent.
- The ultimate rotation θ_u, which is associated with failure modes consisting of sudden strength loss of a structural component (e.g., ductile tearing). (Ibarra, 2013).

If the hysteretic/cyclic behaviour of a structural component is asymmetric, the aforementioned parameters is also defined for positive and negative loading directions as illustrated in figure 7.

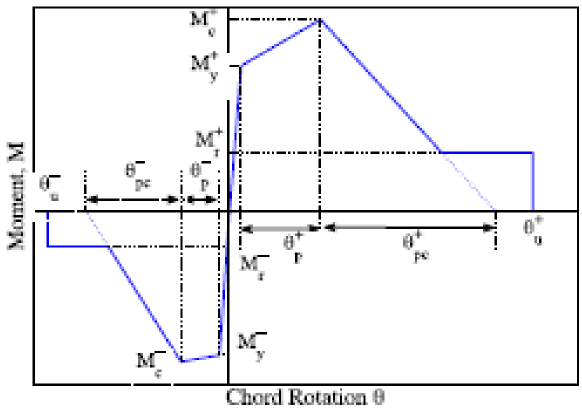

Figure 2-7: Showing the modified (IMK) model behaviour to positive and negative loading

Description of hysteretic models without degradation

The hysteretic models available to conduct nonlinear analysis are: a bilinear, peak-oriented, and pinched hysteretic response, which represents is a modification to the traditional hysteretic models needed to incorporate the deteriorating backbone curve.

Modified Ibarra-Medina-Krawinkler (IMK) deterioration model with bilinear hysteretic response

This numerical model is able to consider asymmetric cyclic deterioration in strength and stiffness in order to simulate the behaviour of composite steel beams. It is also able to consider the residual strength of steel components when subjected to monotonic/cyclic loading. This model is based on the standard bilinear hysteretic rules with kinematic strain hardening. These basic rules are preserved once post-capping and residual strength branches are included. However, it is necessary to consider the demand limitations as shown in Figure 8 when the backbone curve includes a section with negative gradient.

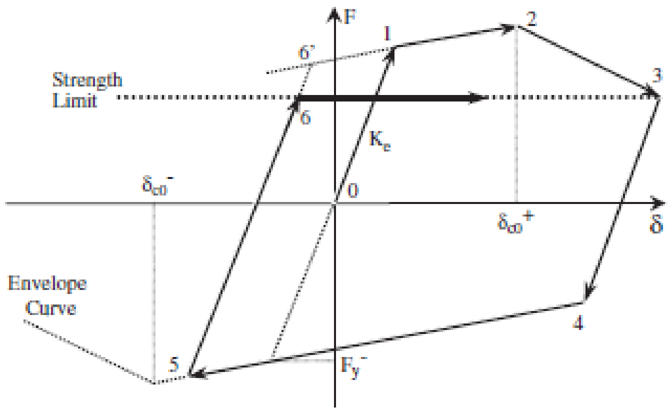

Figure 2-8 .Bilinear hysteretic response model with strength limit

Modified Ibarra-Medina-Krawinkler (IMK) deterioration model with peak-oriented hysteretic response:

This numerical model is able to consider asymmetric cyclic deterioration in strength and stiffness in order to simulate the behaviour of reinforced concrete beams that primarily fail in a flexural mode. This model has been calibrated with more than 200 RC beams (Lignos and Krawinkler 2012). This model keeps the basic hysteretic rules, however this curve is upgraded to incorporate strength capping and residual strength. The inclusion of a negative post capping stiffness however does not have an impact on the simple rule of the model. (Lignos and Krawinkler 2012)

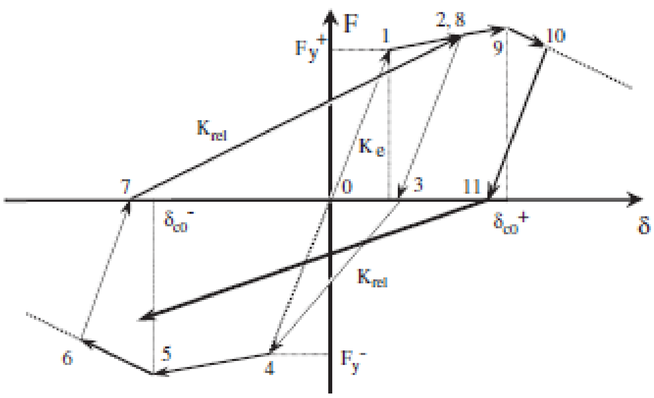

Figure 2- 9 Peak oriented hysteretic response model

Modified Ibarra-Medina-Krawinkler (IMK) deterioration model with Pinching model with hysteretic response.

This numerical model is able to consider asymmetric cyclic deterioration in strength and stiffness in order to simulate the behaviour of reinforced concrete beams that fail primarily fail in a shear mode. This model is also able to simulate the hysteretic behaviour of shear connections, beam-to-column gusset plate connections and wooden components. The pinching model is similar to the peak-oriented model, except that reloading consists of two parts. (Lignos and Krawinkler 2012)

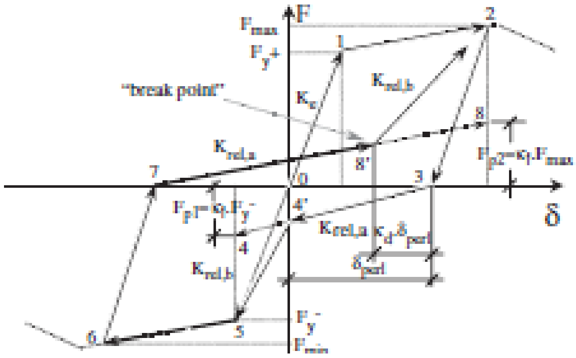

Figure 2-10 a Pinching hysteretic model basic rules

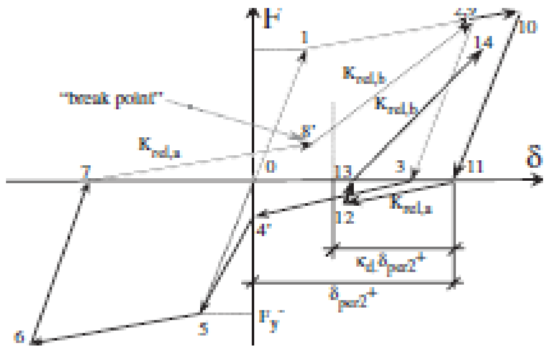

Figure 2-10 b Modification of hysteretic model

2.5.2 Seismostruct

This finite element program is has the ability to estimate large displacement responses of 2 and three dimensional models when conducting dynamic and static analyses. The programs also has the ability to consider for both material inelasticity and geometric nonlinearities. Seismostruct has built in database that stores structural materials models along such as steel, concrete, alloys and fiber- reinforced plastic. Additionally, it consists of three dimensional elements that utilize the material model configurations.

In order to generate a building with accuracy, Seismostruct uses offers the option if spread plasticity distributed along the members length and cross section. The loading capabilities offered in this program consists of static forces, displacements and earthquake ground motions for dynamic analysis. Furthermore, the program it allows for different types of analysis to be conducted. These are modal (eigenvalue) analysis, static analysis, static pushover analysis, static adaptive pushover analysis, incremental dynamic analysis, dynamic analysis and response spectrum analysis. (Seismosoft, 2016)

There are four nonlinear modelling strategies that can be implemented in this software, that utilize the two formulations above mentioned.

- Inelastic force-based frame element where plasticity is distributed along the entire length of the structural member inelastic.

- Inelastic force-based frame element where inelasticity is spread within a fixed length of the element. (Scott and Fenves (2006)).
- Inelastic displacement –based frame element, where the displacements and the plasticity is distributed along the length of element.
- Inelastic displacement–based frame element where the concentrated plasticity–displacement based element is within the plasticity concentrated at two element ends.

The modelling strategy applied to each column and beam was the distributed plasticity strategies. While the evaluated numerical models are based on different assumptions, input parameters for these elements are primarily physical properties such as section geometry and uniaxial behaviour of materials. The main advantages of this software is it incorporates a visual interface, which reduces the configuration time of models. Other aspects are that Seismotruct can be used directly with other programs such as excel. Finally, it has an advanced post-processing facility, including the ability to format output graphs and deformed shapes, which increases working efficiency. The main disadvantages are that the computational-times can be lengthy especially for nonlinear time history analysis also material and element configurations may not always be reliable.

Chapter 3.0 Methodology

This chapter outlines the procedure implemented in this study to investigate the response of the frames to nonlinear linear analysis in both Opensees and Seismostruct. The method is outlined schematically using a flow chart. (See below)

1) Description of the 3 generic 2d frame structural configuration and 3d structural frame building.

- Structural Configuration
- Member cross section description
- Member structural detailing
- Material properties

2) Structural Modelling with Opensees and Seismostruct

- Opensees – Elastic Beam-column elements with rotational springs at the each end representing lumped plasticity (zero length inelastic element).Obtain input parameters specifically calibrated for the member cross sections for each frame.
- Seismostruct – Structural members are modelled using materials consisting of nonlinear properties. The inelastic behaviour is distributed along the length and cross section.

3) Structural Analysis using Opensees and Seismostruct

- Eigenvalue Analysis – To validate models in both programs.
- Nonlinear Static Pushover Analysis – Develop and compare pushover curves.
- Nonlinear Dynamic Time History Analysis – Using 20 unscaled ground motion sets (PEER), to obtain the nonlinear response of each frame.

4) Modified Capacity Spectrum Analysis (FRACAS).

- Determine damage limit states to be used in FRACAS.
- Compare the damage limit states with global damage limit states presented in FEMA. (HAZUS)

5) Data Analysis and Assessment of Results

Figure 3-1: Showing flow chart illustrating the analysis procedure.

Chapter 4

Description and Design of Reinforced Concrete Buildings

4.1 Introduction

In this chapter, the structural characteristics and of the three low rise reinforced concrete (RC) generic frames are discussed. The three typologies used in this case study have the same height, bay width and number of bays whose lateral force resisting system consists of low code reinforced concrete moment-resisting system. However, to compare seismic responses, the members in the each frame are varied, resulting in classifying the three frames as weak, mid, strong frame.

The structural database used in this study is the Pacific Earthquake Engineering Research Centre's Structural Performance Database (PEER) (2005). This database was developed by Berry, Parrish, and Eberhard (Berry et al. 2004) at the University of Washington. It consists of cyclic and monotonic tests results from 306 rectangular columns and 177 circular columns, where the data was transformed into equivalent cantilevers for ease of comparison (Berry et al.2004).The database provides reports on the column geometry, and reinforcement information, the failure mode, and force displacement history. (Haselton et al 2007).

This database was utilized as the parameters required for the Ibarra-Medina–Krawinkler rotational spring to be implemented in Opensees, was developed by Haselton, Liel, Lange and Deierlein (Haselton et al. 2007) using this database. The study was aimed at developing a database, to present a beam-column element models calibrated for predicting flexural response leading to global collapse of RC frame buildings. The lumped plasticity element model developed by Ibarra et al (2005) is used to model the behaviour of reinforced concrete beam column elements where the backbone curve and its respective cyclic rules provide for versatile modelling of cyclic response also capturing the negative stiffness of post peak response, enabling the modelling of the strain softening. This behaviour is critical for simulating the collapse of RC frame structures. The Ibarra element model plastic rotation capacity and cyclic deterioration parameters were calibrated to 255 reinforced concrete column test. They were able to produce predictive equations that can be used to determine a specific columns element model parameter for input into analysis. The parameters used for each structure would be presented in chapter 6.

4.2 Buildings Description

The three low rise RC buildings had the story heights i.e. first story having height of 15 feet and the second storey having height being 12 feet. The bay width in the x direction is 16.4 feet center –to center span length. (See Figure below), however each lateral resisting system variation is described below.

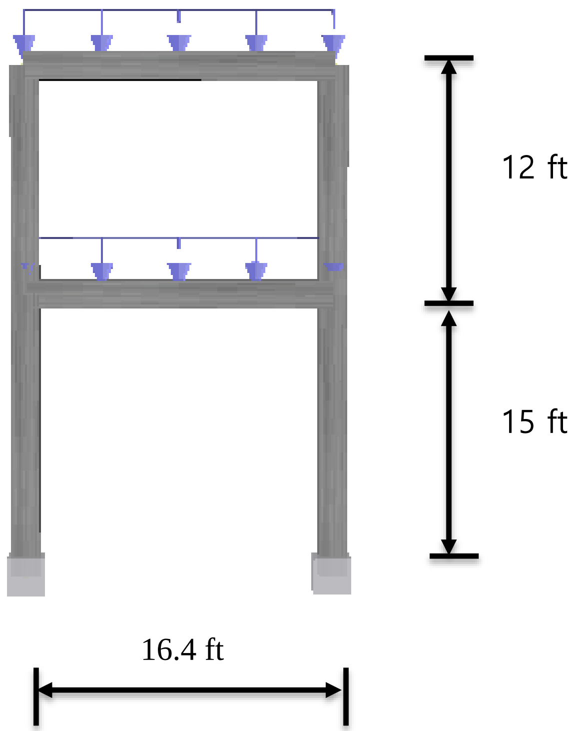

Figure 4-1: Showing 2d frame structural dimensions

Frame 1 consists of beams and columns having cross sections of 7.78 inches by 7.78 inches, **Frame 2** beam and column elements with 13.77 inches by 13.77 inches and **Frame 3**, with the largest sections with 17.96 inches by 17.96 inches. These configurations are compared as they are simple representations of RC structures that can be idealised as reinforced concrete houses.

Table 4 -1: Showing design cross sections and structural properties

Frame	Cross section	Reinforcement	Cross section layout
1	7.78 x 7.78 in Cover = 0.47 in	Longitudinal bars : 4 #5 bars Transverse Bars : # 2 bars @0.5 in c/c	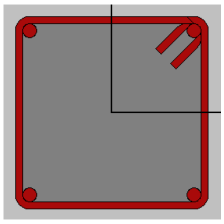
2	13.77 x 13 .77 in Cover = 0.88 in	Longitudinal bars : 4 # 9 bars Transverse Bars : #3 bars @ 3 in c/c	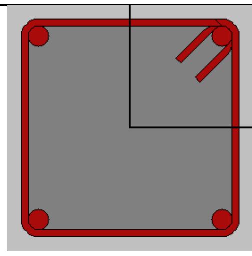
3	17.96 x 17.96 in Cover = 1.497 in	Longitudinal bars Corner: 4 # 9 Interm: 2 # 8 Transverse bars : #3 @7.9in c/c	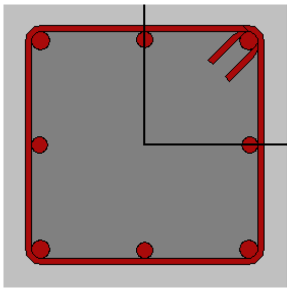

Table 4-2: Showing structural material properties

Frame	Characteristic Comp. Strength of Concrete, Fck (Ksi)	Modulus of Elasticity, Es ,(Ksi)	Yield stress of long. Reinf. (Ksi) Fyl
1	3.132	3190.37	53.808
2	5.047	4924..84	62.366
3	5.69	5230.79	63.671

4.3 Masses and Loading

Gravity loads

The gravity loads based on the tributary areas is applied as a distributed load along the beams of the original frame members while the gravity loads from the original frame columns are applied as point loads on the nodes on the first floor and second floor leaning columns. The leaning columns were modelled only in Opensees to represent p-delta effects. The concept of the inclusion of the leaning column is to simulate P-Δ effects where the leaning column receive load from gravity loads only. It is connected to the frame using axially-rigid truss elements. The gravity loads were applied as constant time series load pattern because they always act on the frame. Any lateral resistance provided by leaning columns in ignored as its base is pinned at the base and between floors.

Table 4 – 3: Showing the dead loads and point loads for each frame

Frames	Distributed load (kips/in)		*Point loads (kips) (Pdelta column)	
	First floor beam	Second floor beam	First floor NO	Second floor
1	0.05	0.04	6.10	5.15
2	0.08	0.06	11.93	8.97
3	0.11	0.08	17.94	12.90

Lateral Loads

The lateral loads were calculated based on the effective weights of each floor. This weight includes the dead load from beams, columns and a 4 inch slab. The loads are then distributed in proportion to the individual floor weight and elevation. The loads are applied to nodes along the height of the frame. It is also worth mentioning that the seismic masses is applied and distributed equally as point loads at the beam –column joints of each floor. A summary of the lateral loads for the 3 frames are illustrated in the table below. A summary of the lateral loads for each frame are shown in the table below.

Table 4-4: Showing lateral loads for each frame

Floor	Lateral loads (Kips)		
	FRAME 1	FRAME 2	FRAME 3
2	5.557233034	8.17918895	10.87
1	3.430276924	5.635543456	7.91
TOTAL	8.99	13.81	18.79

Chapter 5.0

Numerical structural Model

5.1 Introduction

In earthquake engineering, the finite element model is usually the approach utilized for design and analysis of structures. The purpose of this approach is mainly to determine and adopt an accurate and reliable numerical structural model to perform linear and non-linear analysis. In this research, the frames are modelled using the two well-known software packages: Opensees and Seismostruct. In order to verify the accuracy of the finite element models, the natural frequencies of the numerical models are determined and compared.

5.2 Basic Model Description

The frame is represented as two-dimensional model. The model consists of beam –column elements, where masses from tributary as well as gravity loads are applied on beams. From the figure below, the original frame is idealised consisting of pier 1 and pier 2 .The leaning column which is modelled as pier 3 is introduced to account for P- delta effects. This is modelled only in Opensees as Seismostruct considers these effects differently. This would be discussed further in the next section. The leaning column is connected to the original frame by rigid links.

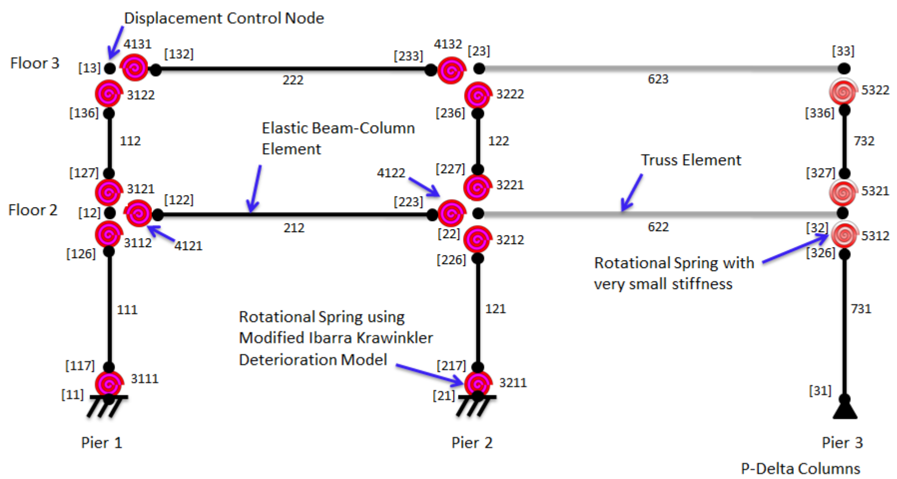

Figure 5-1: Schematic representation of concentrated plasticity Opensees model with element number labels, node number labels and springs representing zero length elements (Opensees.berkeley.edu, 2018)

5.2 Material

Defining the elastic column elements

The materials used in both programs are defined based on the material properties from the Haselton et al. (2007) database. In Opensees, the beam- column elements are modeled as elastic elements while the nonlinear behavior is concentrated at the ends of which will be represented as zero-length rotational springs which is further discussed in the sections below. The elastic properties required for the Opensees model are the sectional area, moment of inertia and Young's modulus of elasticity. The formula used to calculate the modulus of elasticity in Opensees; Ec = 57000 $57000\sqrt{f'c}\ psi$ (Review of Building Code Requirements for Structural Concrete (ACI 318-95) and Commentary (ACI 318R-95) by ACI Committee 318, 1996).The reinforcing steel is not modeled in these elements as the nonlinear action is represented by the rotational springs. The table below provides a summary of the Opensees input parameters.

Table 5-1: Showing input parameters for Opensees software

Frame	C.S.A (in^2)	Moment of inertia (in^4)	Young's Modulus E (ksi)
1	60.52	305	3190
2	189.61	2994	4049
3	322.5616	8667	4303

However, in Seismostruct, the material model used for concrete is the Mander et al.(1988) based on its nonlinear stress-strain relationship. See figure ( ) below. This concrete model is utilised because it considers the high strain rate with the concrete strength and stiffness increasing with loads being applied rapidly. It can also be used for various reinforcement configurations and in unconfined concrete. The confinement effects provided by the lateral transverse reinforcement are incorporated where the confining pressure is assumed throughout the entire stress strain range. The main input parameters required for this nonlinear concrete model are compressive and tensile strength, strain at peak stress. The previously introduced structural database, provides the characteristic compressive stress, f_{ck}, therefore, this value was converted in Seismostruct to obtain the mean compressive strength.

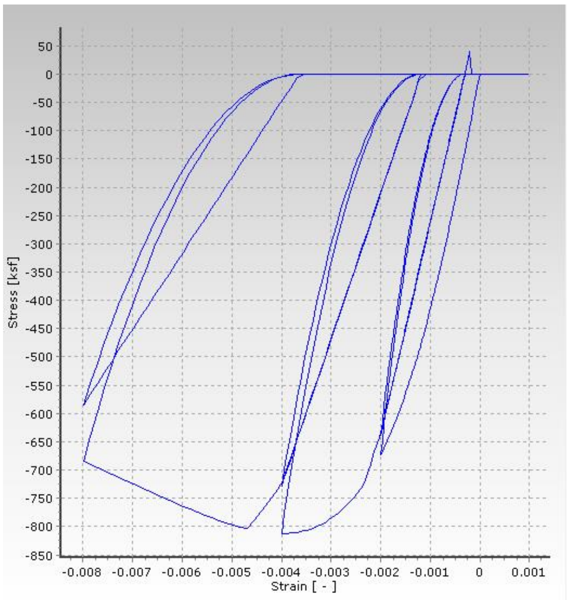

Figure 5-1: Showing Mander (1988) Concrete material model frame 1 , (Seismostruct (2016))

The nonlinear model chosen in Seismostruct was the bilinear steel model. See figure below). This uniaxial bilinear stress –strain model has the capability to continue in the elastic range throughout the duration of loading. This characteristic is referred to the kinematic strain hardening. This function is assumed to have a linear response when the reinforcement is yielding.

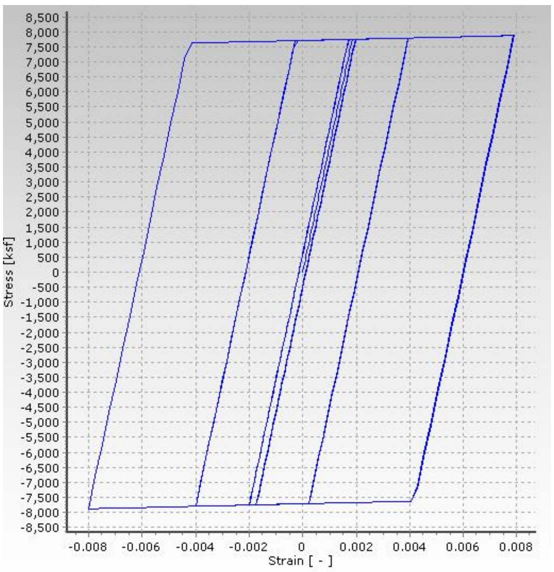

Figure 5-2 : Showing bilinear steel model frame 1(Seismosoft (2016))

This steel model is simple and input parameters are easily attainable. However, according to Seismostruct (2016) due to its very simple nature it is not suited for modelling reinforced concrete members subject to complex loading histories where significant load reversals might occur. This type was still selected as it represents the bilinear action represented by the bilinear rotational springs being used in Opensees. The reinforcing steel properties for each reinforced concrete section was also provided in the database and was directly used as input in the Seismostruct.

5.3 Elements

5.31 Opensees

In Opensees, when using the lumped plasticity approach, the elements are modelled as elastic beam column elements and since it is a two dimensional frame the nodes are allowed 3 degrees of freedom considering bending and axial deformations. As previously mentioned, the cross sectional properties, reinforcement and type of element are all manually defined. The inelastic system depends on the nonlinear concept to absorb the forces acting on the structure. In order to perform the analysis the nonlinear element used is the concentrated plasticity rotational spring developed by Krawinkler (2005).This is implemented as uniaxial material known as the Modified Ibarra-Medina-Krawinkler deterioration model with bilinear hysteretic response (bilinear material).

5.32 Lumped Plasticity Element: Modified (IMK) Krawinkler Deterioration Model

This element is modelled as zero-length spring elements connected at each end of the elastic elements. These elements are referred to as rotational springs which represent the structure's nonlinear behaviour. This concept is a simplification of an elements actual behaviour, however, according to Eads (2013), if implemented adequately, errors associated in the global dynamic response of the structure would not be introduced. It must be noted that the plastic hinges are only defined at the original frame column bases and not the leaning column. The parameters used for the nonlinear rotational springs are provided in Table 5-2 below, and are based on the properties provided by Hasselton et.al (2007).

Table 5-2: Modelling parameters used for nonlinear rotational springs used in case study

No.	Ibarra-Medina-Krawrinkler Parameters	Frame 1	Frame 2	Frame 3
1	Yield Moment ,My (kips-in)	227	1695	3100
2	Ratio of capping moment to yield moment Mc /My	1.04	1.04	1.3
3	Basic strength deterioration , Ls	1000	1000	1000
4	Unloading stiffness deterioration , Lk	1000	1000	1000
5	Accelerated reloading stiffness deterioration ,LA	1000	1000	1000
6	Post capping strength deterioration ,LD	1000	1000	1000
7	Exponent for basic strength deterioration , cS	1	1	1
8	Exponent for unloading stiffness deterioration cK	1	1	1
9	Exponent for accelerated reloading stiffness deterioration ,cA	1	1	1
10	Exponent for post capping strength deterioration , cD	1	1	1
11	Plastic rotation capacity for positive loading ,θp_P	0.13	0.08	0.025
12	Post capping rotation capacity for positive loading ,θ_pcP	0.08	0.24	0.15
13	Residual strength ratio for negative loading	0.4	0.4	0.4
14	Rate of cyclic deterioration for positive loading	1	1	1

The Pacific Earthquake Engineering Research Center provided a summary of the various cross sections along with the model parameters. The figure below provides a visual representation of the use of the parameters on the back bone curve.

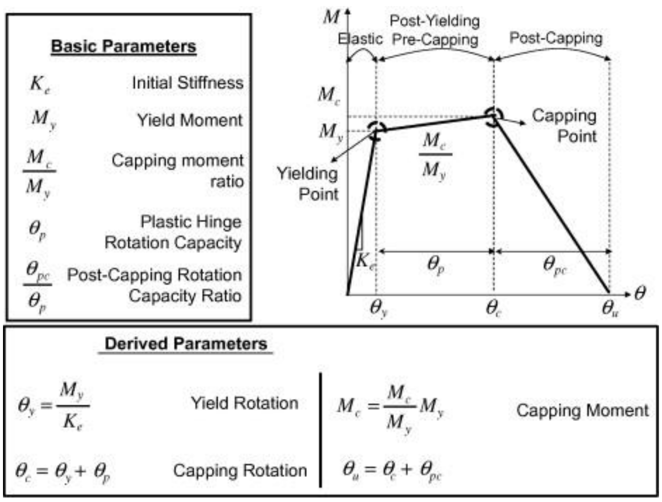

Figure 5-3 : Showing component backbone curve and its parameters (Hasselton et al. 2007)

The PEER database, provided a summary of these parameters however they can be calculated using the equations below.

- **Equation .1** - Plastic Hinge Rotation Capacity (Haselton et al. 2007)

- $\boldsymbol{\theta\ cap\ ,pl = 0.12\ (1 + 0.55a_{sl})(0.16)^{v}(0.02 + 40\ \rho sh)^{0.43}\ (0.54)^{0.01f'c}(0.66)^{0.1sn}(2.27)^{10.\rho}}$

Where; a_{sl} = bond slip indicator, 1 — ρ_{sh} = area ratio of transverse reinforcement

v = axial load ratio — s_n = rebar buckling coefficient

s = stirrup spacing — d_b = longitudinal rebar diameter

f_y = yield strength of rebar — c units = variable,1

- **Equation .2** - Post -Capping Rotation Capacity (Haselton et al. 2007)

- $\boldsymbol{\theta\ cap_{,pc} = (0.76)(0.031)^{v}\ (0.02 + 40\rho sh)^{1.02}\ \leq 0.10}$

Where; $v = {}^{P}/_{Ag\ fc}$ ρ_{sh} = transverse steel ratio

- **Equation 3** - Post Yielding Hardening Stiffness

- $\boldsymbol{{}^{Mc}/_{My} = (1.25)\ (0.89)^{\ v}\ (0.91)^{0.01\ \text{cunits}\ f'c}}$

Where; $v = {}^{P}/_{Ag\ fc}$ f'_c = compressive strength of concrete

These experiments did not consider changes in moment capacity due to axial-moment interaction effects as the analytical software does not have this capability.From table ( ) ,it is seen that all of the "L" deterioration parameter variables to 1000.0, all of the "c" exponent variables to 1.0, and both "C" rate of cyclic deterioration variables to 1.0. This is done to simplify the model and to compare with Seismostruct, also cyclic deterioration was ignored for the pushover analysis. The residual strength was not quantified in the (Haselton et al 2007) database however the value used in the table was provided from past research which uses an average residual strength used in a similar research for reinforced concrete buildings. (Zareian et al. 2012).

5.33 Stiffness Modifications to Elastic Frame Elements and Rotational Springs

According to (Eads ,2013), since a frame member is modeled as an elastic element connected in series with rotational springs at either end, the stiffness of these components must be modified so that the equivalent stiffness of this assembly is equivalent to the stiffness of the actual frame member. This would prevent numerical problems and allow all damping to be assigned to the elastic element.

The same conception was done for the nonlinear portion of the assembly, where nonlinear assembly is matched to the actual frame member. This is done via modifying the strain hardening coefficient (the ratio of post-yield stiffness to elastic stiffness) of the spring, $\alpha_{spring,}$ this is shown below:

- Actual Frame member strain hardening coefficient $\alpha_{s,mem}$
- Strain hardening coefficient of the spring is denoted $\alpha_{s,spring}$

- **Equation 4 -**

- $\alpha_{s,spring} = \frac{\alpha_{s,mem}}{1+n(1-\alpha_{s,mem})}$

5.34 P delta columns and rigid links

Leaning Columns and Frame Links

The leaning columns are modeled as elastic beam-column elements. These columns have second moments of inertia and cross sectional areas larger than the actual frame columns representing collective effect of all gravity columns in the frame. These columns are pinned at each connection and provide no bending restraint in a frame. They don’t contribute to lateral resistance, however carries gravity loads. When using leaning columns, it must be known that the p-delta effects can have large effects on post peak degradation even if they appear negligible for an elastic structure. (Nassirpour, 2018)

The columns are connected in this system are connected using rotational spring elements with very small stiffness values, so that the columns do not attract significant moments. Truss elements are used to link the frame and leaning columns system, allowing the P-Delta effect to be transferred. Similar to the leaning columns, the trusses have areas larger than the frame beams, which represents the collective effect of all the gravity beams. They are however assumed to be axially rigid. (Eads, 2013)

5.35 Hysteretic behaviour

The hysteric model used in this study follows the rules of the bilinear hysteretic model. The backbone and its associated hysteretic rules provide for versatile modelling of cyclic behaviour. (See figure 5-4). Other hysteretic models (peak and pinch) are not considered. According to (Medina and Krawinkler, 2003, and Ibarra and Krawinkler, 2005) the sensitivity of structural response parameters (i.e. EDP and collapse capacity) to variation of hysteric models is relatively small except for pinching hysteretic model with severe stiffness degradation. Once As long as there is good detailing, pinching can be ignored, therefore in this research we only consider the bilinear hysteretic model for structural component.

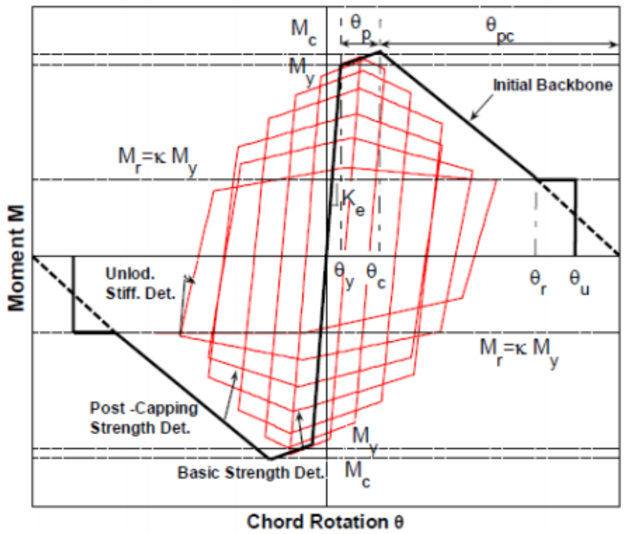

Figure 5-4 : Showing the Modified IMK deterioration model with bilinear hysteretic response

An important aspect of this model is the ability to represent negative stiffness branch of post-peak response, which enables modelling of strain-softening behaviour associated with physical phenomena such as concrete crushing, rebar buckling and fracture, and bond failure. The component model incorporates four cycles' deterioration modes once the yielding point is passed in cyclic loading. This element model requires the specification of seven parameters to control both the monotonic and cyclic behaviour of the model: My, θ y, Ks, θ cap, and Kc, λ, and c.2 .The connection between these model parameters and the physical behaviour of beam-column elements is explored in table below.

Table 5-3: Description of model parameters and associated physical behaviour and properties (Haselton et.al (2007)

Model Parameter	Description	Physical Behaviour contributing to parameter	Physical properties /possible predictors	References
My	Yield moment	1) Longitudinal rebar yielding. 2)Concrete cracking 3) Concrete crushing	1) Stress Block 2) Section geometry 3) Axial load (ratio), 4)Material strengths and stiffness's	Basic beam theory Fiber moment - curvature; Fradis,2003;Panagiotakos,2001
θy	Chord rotation , yield	same as above	1) Section geometry 2)Level of shear cracking 3)Shear demand 4) Axial load (ratio), material 5) Stiffness's/strengths.	Fardis, 2003;Panagiotakos 2001;Fiber moment-curvature
θcap	Chord rotation (mono) at onset of strength loss (capping)	1) Longitudinal rebar buckling /fracture 2) concrete core failure 3) Minimal lateral confinement	1) Confinement 2) Axial load (ratio) 3) Geometry 4) reinforcement ratio	Fardis, 2003;Panagiotakos 2001; Berry 2003
Mc/My (or Ke)	Hardening stiffness	1) Steel strain hardening, 2)Nonlinearity of concrete, 3)Bond-slip flexibility	1) Steel hardening modulus 2) Section geometry, 3) Interm. long. steel	Fiber moment-curvature and plastic hinge length approach;Zarelian 2006
θpc (or Kc)	Post capping stiffness	1)Post rebar buckling 2) Behaviour after loss of core concrete confinement.	1)Rebar slenderness between stirrups 2) Small stirrup spacing.	Ibarra, 2005/2003;Zareian2006
λ	Normalised hysteretic energy dissipation capacity (cyclic)	1) Concrete crushing 2) Stirrup fracture 3)Rebar buckling, longitudinal steel fracture.	Confinement, stirrup spacing ,axial load (ratio)	Ibarra, 2005/2003;Zareian2006
c	Exponent Term to model rate of deterioration	same as above	same as above	Ibarra, 2005/2003

5.4 Seismostruct

In Seismostruct the element type used was the inelastic forced based frame element. To conduct nonlinear analyses, the material nonlinearity can be accounted for by two methods. The lumped plastic hinge and distributed (fibre model) inelasticity elements. The lumped plasticity approach is dependent on the length of the plastic hinge and can be considered as inaccurate compared to the fibre model. (Semere, 2016).Due to the influx of computational tools the distributed inelasticity elements is the approach used by many researchers. The distributed inelasticity approach has the ability to represent spread plasticity within the element cross section and along the element length.

A main benefit in using this element is that there is no length or pre calibration response parameters required,(Semere,2016).The fibres associated with the uniaxial stress strain stress strain relationship which characterises the cross sectional behaviour and sectional stress-strain state of the element is determined by the integration of each fibre. The figure below illustrates the discretization of a typical reinforced concrete cross -section.

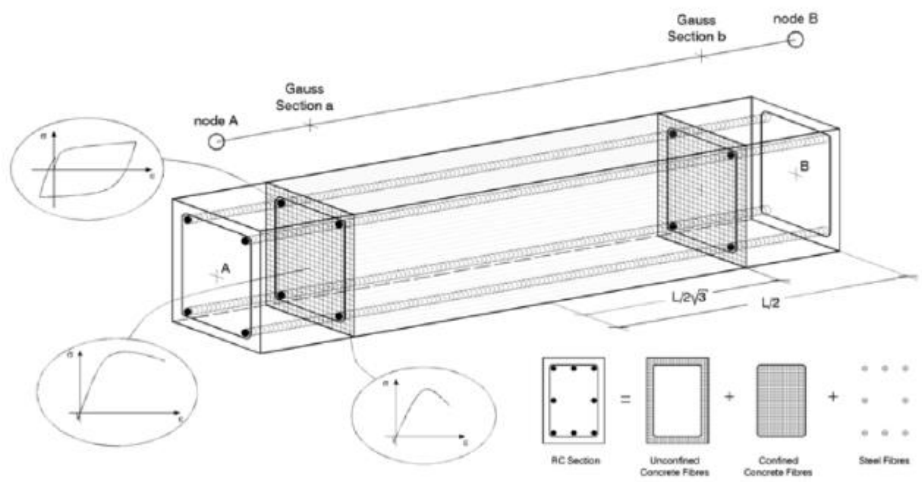

Figure 5-5: Showing discretisation of a reinforced concrete cross section (Seismosoft, 2016)

The fibre based elements can be modelled using two methods. The displacement –based formulation, which assigns displacement shape function to a finite element and then solving the main equations based on the stiffness of the element. This formulation is also based on a linear variation of curvature along the element. On the other hand, the forced based formulation implements a force field which is constructed on the element's flexibility. According Calabrese et al. (2010), the force based method has shown generate accurate results compared to the displacement based method. This is due to the displacement based method is unable to capture the real deformation shape in the presence of material inelasticity. In the forced based method, the solution is approximated by integration points along the element length. The number of integration points that can provide reliable results at a global level is 4.

(Seismosoft 2016).In addition to the integration points, it is recommended that the Gauss-Lobatto integration scheme is utilized for force based elements. The figure below illustrates the Gauss- Lobatto integration sections.

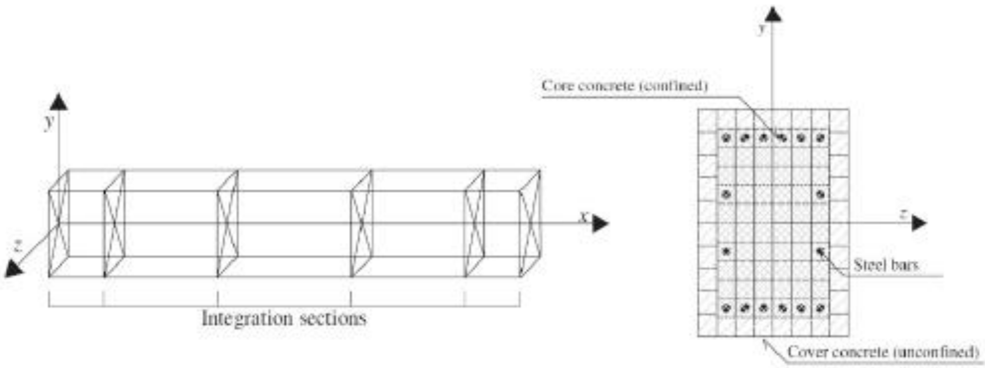

Figure 5-6 : Showing Gauss – Lobatto integration sections.(Seismostruct 2016)

In this research paper, the forced based beam column elements is utilized in Seismostruct model. The number of section fibres used is 100 beam column element. This is to reduce computational time. See figure 5-6 above. The number of integration points with the Gauss –Lobatto rule, used for the beam and column elements was 5 for all frames. The selection of integration point was done to reduce the issue associated with localization. This however does may not consider the convergence issues. Finally, the P- delta effects at a global level are accounted for in Seismostruct via an internal software function.

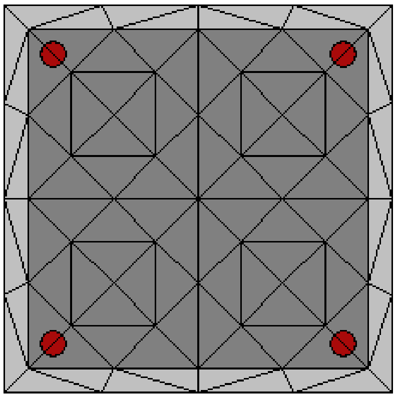

Figure 5-7: Showing discretization pattern of the section (Seismosoft, 2016)

5.41 Numerical Solution Algorithms

The iterative solution algorithm used in both programs was the Newton-Raphson method. This algorithm was used in both pushover and nonlinear time history analysis. (See script in appendix).The algorithm is implemented with prescribed displacement increments, which provide the most rapid converging process to determine the structural response.

5.42 Damping (nonlinear analysis)

In the non-linear time history analysis, The Rayleigh damping function is applied to represent viscous damping the frame. It expresses the damping matrix as a linear combination of the mass matrix and stiffness matrix as shown in the equation 5 below. (Chopra, 1995)

Equation 5

- $C = a_0\mathbf{M} + a_1\mathbf{K}$

Where; a_0 is the mass proportional damping coefficient

a_1 is the stiffness proportional damping coefficient.

M is the mass matrix

K is stiffness matrix

A damping ratio of 5 % was assigned to the first and second modes of the 2 dimensional frames which is usually applied for reinforced concrete structures. In order for the model to respond properly, stiffness proportional damping is applied only to the frame elements. Damping is neither applied to the rigid truss elements linking the frame to the leaning column nor the leaning columns.

5.5 Natural periods and Mode shapes

Natural periods and mode shapes for all inelastic frames were generated in both programs. The gravity loads were converted into masses in order to conduct the Eigen analysis assessment. Figure 5-8 and Table 5-4 illustrates the results of the natural periods. Figure 5-9 illustrates the first four mode shapes obtained with Seismostruct, which complies with the Opensees models with minimal differences.

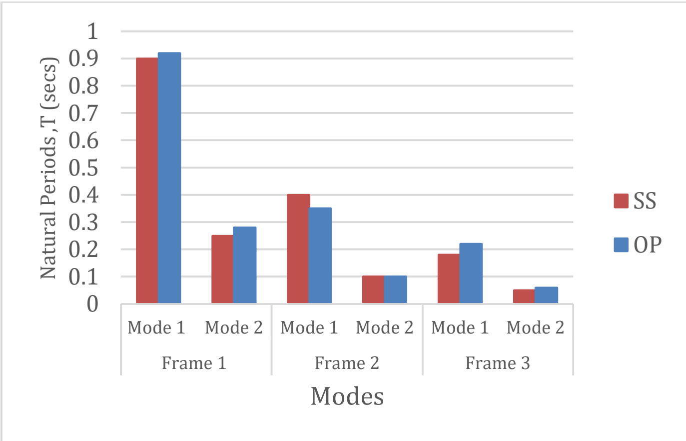

Figure 5-8: Showing natural periods of the numerical models

Table 5-4 showing natural periods of the different numerical models

Software	Frame 1		Frame 2		Frame 3	
	T 1 (secs)	T 2 (secs)	T 1 (secs)	T 2 (secs)	T 1 (secs)	T 2 (secs)
SS	0.9	0.25	0.4	0.13	0.18	0.05
OP	0.92	0.28	0.35	0.1	0.22	0.06
Difference %	2	3	5	3	4	1

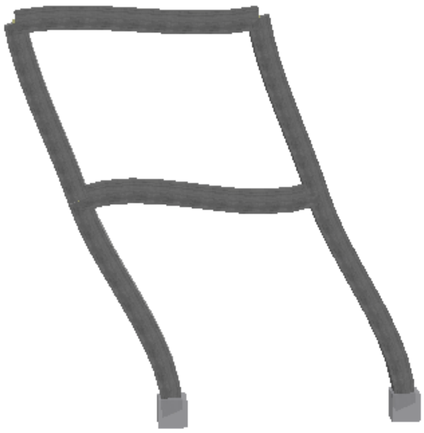 Figure 5-9 A showing the 1*st* mode shape frame 3 in Seismostruct	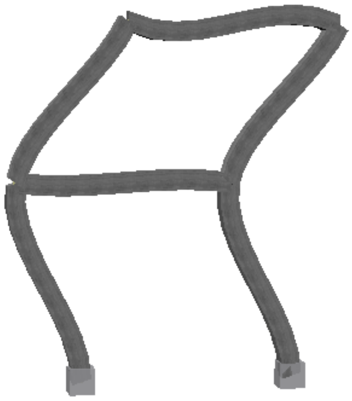 Figure 5-9 B showing the 2*nd* mode shape frame 3 in Seismosrtuct
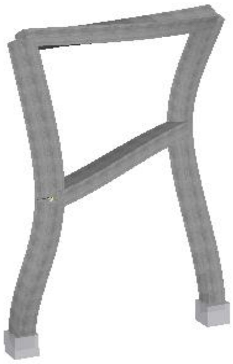 Figure 5-9 C showing the 3rd mode shape frame 3 in Seismosrtuct	 Figure 5-9 D showing the 4th mode shape frame 3 in Seismosrtuct

5.6 Discussion

The results shows that the models generated in both programs are match with minor differences observed in models implemented in Seismostruct and Opensees with regard to the first natural period. A max of 5 % however is seen for frame 2 in the first or fundamental natural period. Furthermore, in Seismostruct, the contribution of the reinforcement to the stiffness is not included. For all frames, in both programs, there were significant discrepancies observed in the higher modes.

Chapter 6.0

Push over analysis

The Non- linear Static Analysis was executed using both Opensees and Seismostruct software packages. The performance requirements of each frame was done in comparison to Hazus MR4 technical manual, which provides the damages states in the structure. According to the Hazus data base, these includes four damage states;

- Slight Structural Damage – Flexural or shear type hair line cracks in some beams and columns near joint or within joints.
- Moderate Structural Damage- Most beams and columns exhibit hairline cracks. Ductile frames elements have reached yield capacity which is indicated by larger flexural cracks and some concrete spalling. Non ductile frames may exhibit larger shear cracks and spalling
- Extensive Structural Damage – Some of the frame element shave reached their ultimate capacity indicated in ductile frames by large flexural cracks, spalled concrete and buckled main reinforcement; no ductile frame elements may have suffered shear failures or bond failures at reinforcement splices or broken ties or buckled main reinforcement in columns which may result in partial collapse.
- Complete structural damage – Structure is collapsed or in imminent danger of collapse due to brittle failure no ductile frame elements or loss of frame stability. Approximately 13 %(low-rise), 10 %(mid-rise) or 5 %(high-rise) of the total area of C1 buildings with Complete damage is expected to be collapsed.

The inter-storey drift limits of each frame would be determined at specific stages of the pushover curve and compared to the Hazus damage states.

The pushover curves for the different frames were developed by computing the nonlinear static analyses of the numerical models. The analysis was done in one direction utilising a height –wise distribution of the lateral loads proportional to each the weight of each floor and elevation. It was conducted with constant gravity loads while simultaneously increasing the lateral loads until failure of the frames or 20 % loss of capacity is reached.

The results are presented below.

It is worth mentioning that opensees, provided shear reactions at all frame bases, however only the base shear reactions from the original frame bases were used to calculate the total base shear as the leaning column had a pinned connection.

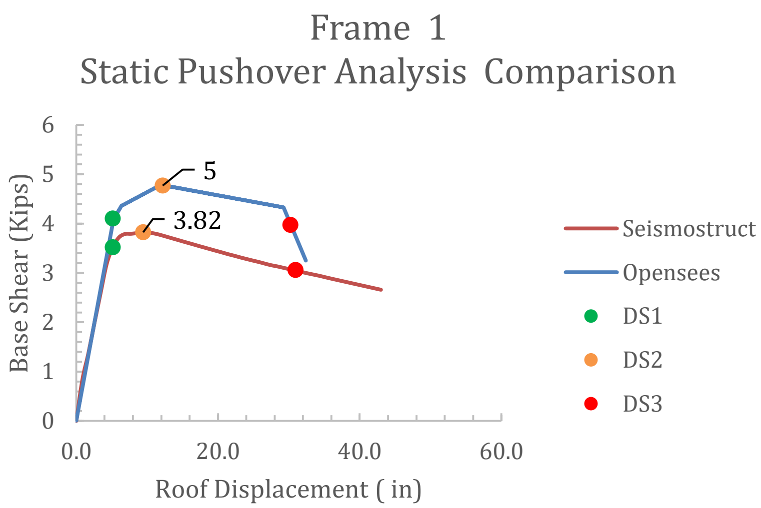

Figure 6-1: Showing the pushover curves for frame 1

The comparison illustrates that Frame 1 in both programs produce pushover curves that differ significantly. The maximum shear capacities from the Opensees and Seismostruct programs resulted in 5 kips and 3.82 kips respectively. It can also be seen that the displacements at the maximum shear capacities follow the same trend with the Seismostruct having lower displacement compared to Opensees. The curves however showed similarity in the initial elastic stiffness region. The pushover curve produced by Seismostruct, exhibited nonlinear action at an earlier stage in comparison to Opensees signifying that it has a lower yielding strength. From the plot we can say that Seismostruct produces conservative results compared to Opensees. A similar pattern was observed for frames 2 and 3.The maximum shear capacities for frame 2 resulted in 37 kips and 30.8 kips and frame 3 , 84 kips and 71 kips for Opensees and Seismostruct respectively. See figures below.

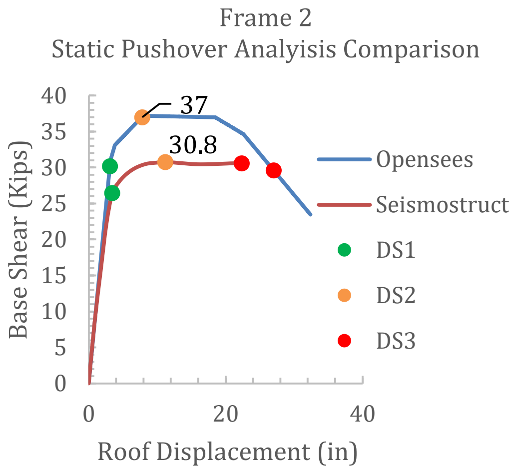

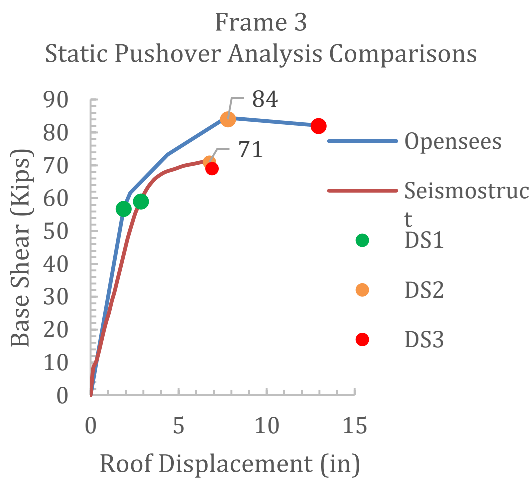

Figure 6-2A: Showing pushover curves frame 2 **6-2B: Showing pushover curves frame 3**

Also displayed on the push over curves are the manually selected damage states. The damage states for each of the curves were determined at critical areas of the push over curve. The yielding point, the maximum strength and the ultimate strength. The damage states were compared to the damage states provided by Hazus damage states for low rise concrete moment frames (C1 L). These damages states were developed for many different building typologies.

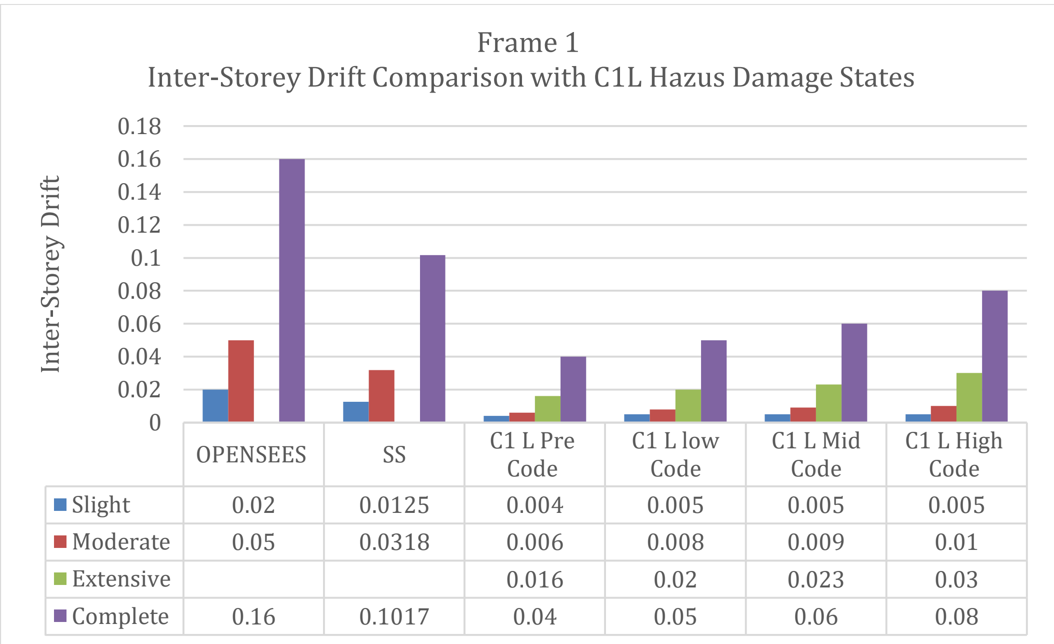

	OPENSEES	SS	C1 L Pre Code	C1 L low Code	C1 L Mid Code	C1 L High Code
Slight	0.02	0.0125	0.004	0.005	0.005	0.005
Moderate	0.05	0.0318	0.006	0.008	0.009	0.01
Extensive			0.016	0.02	0.023	0.03
Complete	0.16	0.1017	0.04	0.05	0.06	0.08

Figure 6-3: Showing frame 1 damage state comparisons with HAZUS MR4 damage states

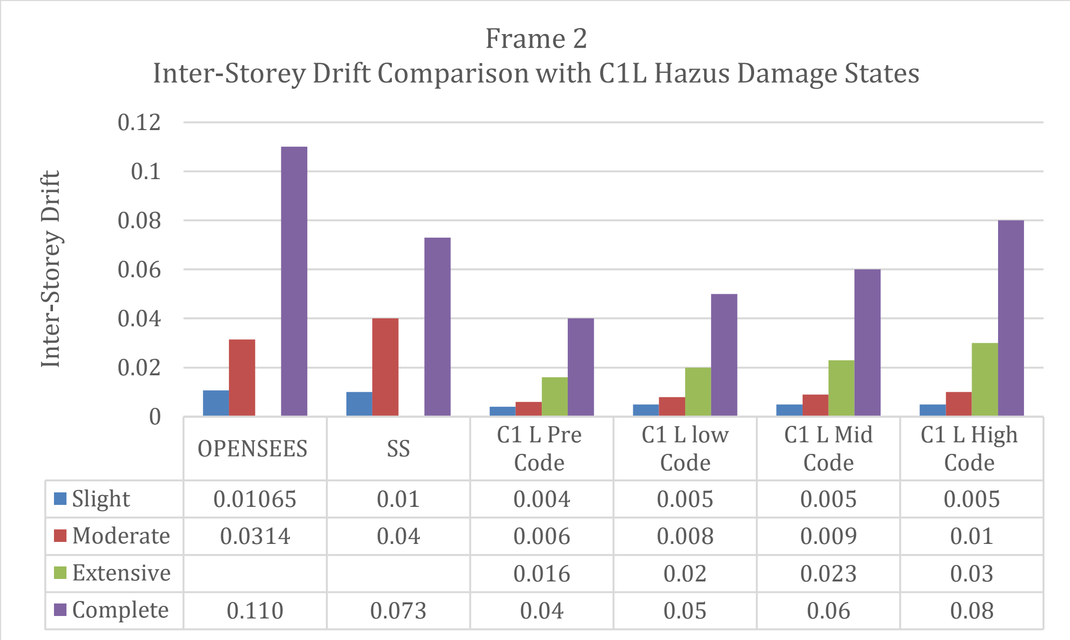

	OPENSEES	SS	C1 L Pre Code	C1 L low Code	C1 L Mid Code	C1 L High Code
Slight	0.01065	0.01	0.004	0.005	0.005	0.005
Moderate	0.0314	0.04	0.006	0.008	0.009	0.01
Extensive			0.016	0.02	0.023	0.03
Complete	0.110	0.073	0.04	0.05	0.06	0.08

Figure 6-4: Showing frame 2 damage state comparisons with HAZUS MR4 damage states

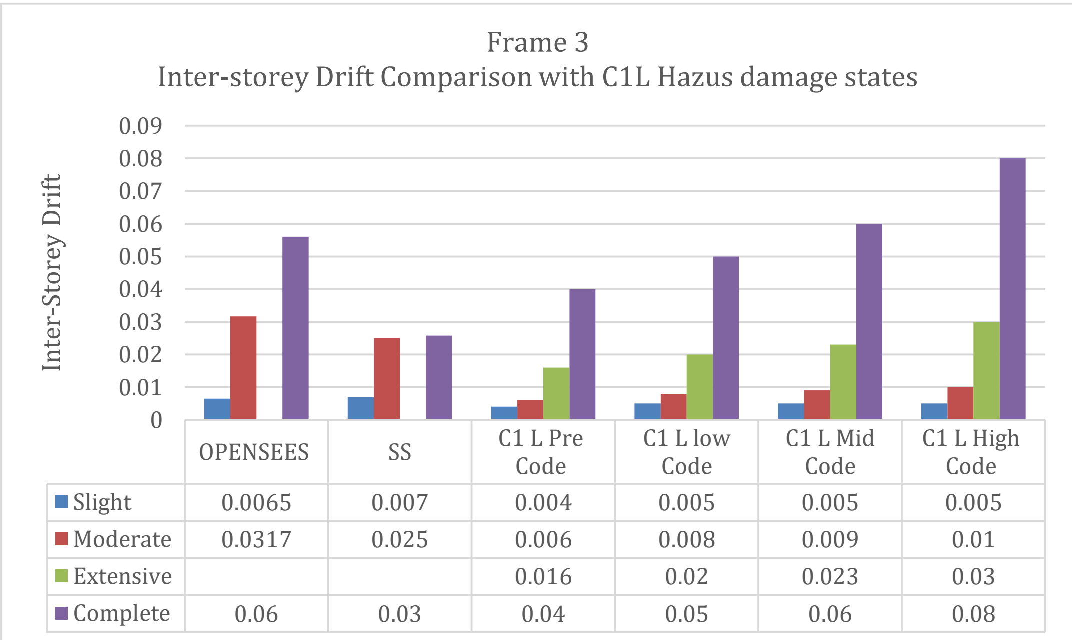

	OPENSEES	SS	C1 L Pre Code	C1 L low Code	C1 L Mid Code	C1 L High Code
Slight	0.0065	0.007	0.004	0.005	0.005	0.005
Moderate	0.0317	0.025	0.006	0.008	0.009	0.01
Extensive			0.016	0.02	0.023	0.03
Complete	0.06	0.03	0.04	0.05	0.06	0.08

Figure 6-5: Showing frame 3 damage state comparisons with HAZUS MR4 damage states

The figures below shows comparison of the strength of each frame, where frame 1 can be classed as weak with max displacement and least shear capacity, frame 2 medium strength and frame 3 high strength capacity and least displacement. It shows how the stiffness increases as the strengths increase as the initial elastic stiffness range gets steeper indicates as the cross sections and associated reinforcement results in an increase of the initial stiffness. This graph also shows that the stiffer the structure the less displacement it is able to undergo before failure as frame 1 has least stiffness and frame 3 most stiffness. This could be the reason why frame 2 and three failed in Seismostruct. The frames in Opensees show similar results however frame 1 and 2 was able to reach max displacements of 32.22 inches, however frame 3 did not reach the displacement again due to the stiffness. The frame does not have enough ductility to reach a displacement shown by frame 1 and 2.

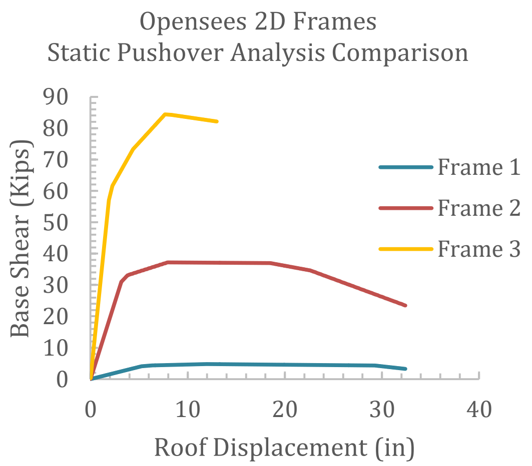

Figure 6-6 Showing Opensees PO curves comparisons

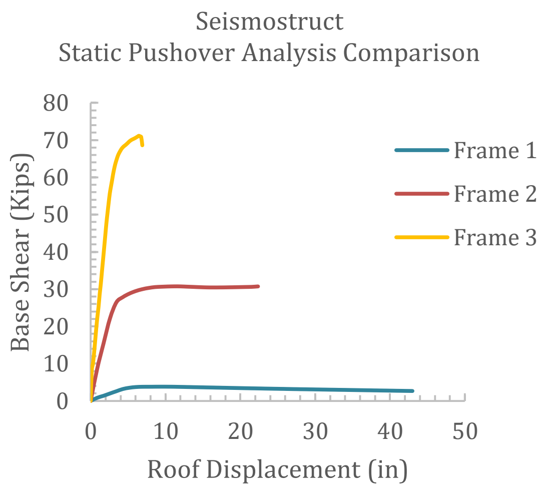

Figure 6-7 Showing SS PO curve comparisons

6.1 Inter-storey Drifts from Pushover Analysis

The Figures below provides a description of the inter-storey drift from the pushover analysis. These curves show that Opensees produced generally larger inter-storey drifts at storey 1 with maximum values of 0.16, 0.11 and 0.06.Tho resulting in larger drift values, both software's resulted in having close results. The results for both software for the storey 2 however were less than the results observed in the first storey. This is a clear indication of soft storey action occurring during the analysis as well as P-delta effects would be the cause of failure for the structure. Storey 2 drift ratios also had close results between both software with a max variation occurring in frame 1 with a difference of 6 %.

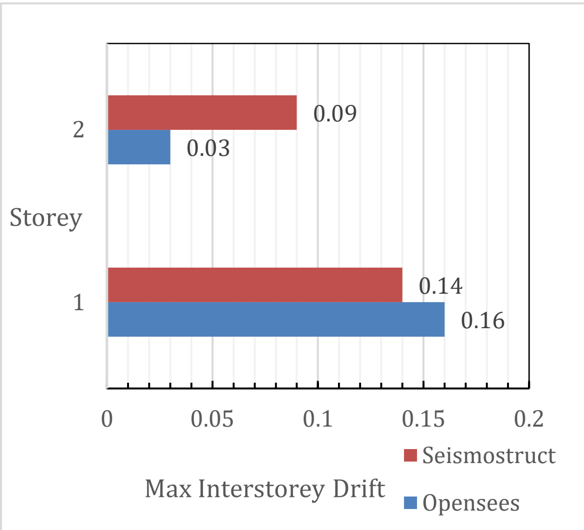

Frame 1

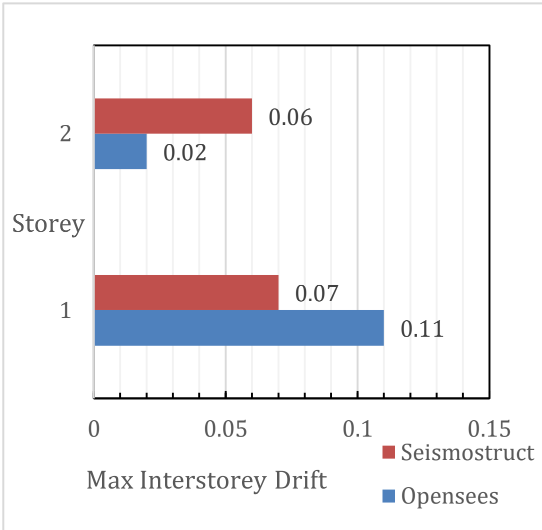

Frame 2

Figure 6-8: Showing MISD comparisons FRAME 1

Figure 6-9: Showing MISD comparisons FRAME 2

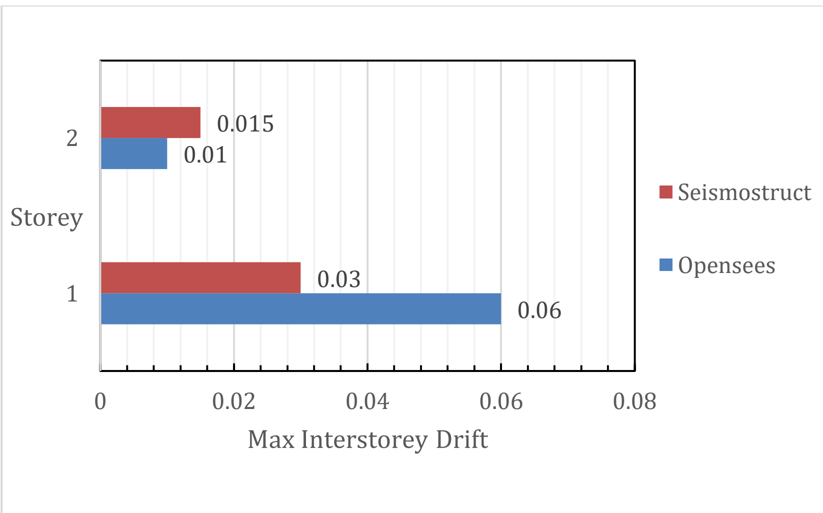

FRAME 3

Figure 6-9: Showing MISD comparisons for Frame 3

6.2 Discussion

FRAME 1

This result can be due to the fact that Opensees uses the Ibarra –Medina –Krawrinkler concentrated plasticity rotational spring model which captures the response of plastic hinges formed at the end of an element. This model which uses set parameters, which doesn't change during analysis. These calibrated parameters are intended to mimic the nonlinear response of a number of single beam-column element with specific structural characteristics under nonlinear forces. In reality, no one structure is the same, each consisting of various structural characteristics, resulting in their nonlinear responses being different. These responses change during the application of loading, therefore the use of concentrated springs may be not fully grasp the true response of the structure.

On the other hand, Seismostruct utilize the force based distributed plasticity along the element , with fibre section models for beams and columns with nonlinear concrete and steel material properties defined in figures above using 5 integration points. As stated previously, Seismostruct models consider the plasticity distributed along the element which check the responses of the each fibre along the length and cross sections of the elements during the analysis which change during the analysis. Therefore, Seismostruct is able to obtain the stress and strains of elements which efficiently resulted in the pushover curves resulting lower yield strength compared to Opensees.

After conducting the pushover analysis in Seismostruct, the action effects was check to determine the maximum moment experienced by the defined structural members, where the resulting moments were slightly lower than the yielding moment of the columns from the database. Another reason for this can be due to the concentrated plasticity springs were developed from only 255 reinforced concrete specimen, therefore the database may not be fully representative of the effects experienced by the elements in Opensees leaving room for errors. Whereas Seismostruct does not require calibration of empirical response parameters against the response of an actual or ideal frame element to loading, as the responses are calculated in Seismostruct.

From the plots we can see that apart from the fact that the demands for the both curves were different, Opensees pushover curve was again able to show the stages a nonlinear member experiences under loading which is known as the monotonic backbone curve. After the initial, elastic stiffness stage, based on the effective elastic stiffness, the yield strength is reached, and from that point the frame enters the nonlinear range which is known as the plastic deformation capacity section or the post yielding or pre – capping portion, reaching a maximum demand of 5 kips and displacement of 12 inches. This portion of the curve is defined on the capping moment ratio (Mc/My), 1.04 which uses the yield moment, My and the capping moment, Mc produced at the maximum base shear. The yield moment as stated earlier was 227 kips had a base shear of 4.1 kips. The higher capping moment ratio, the steeper the slope resulting in higher capping moment. Once the capping strength was achieved it can be seen that strength deterioration has occurred indicating the beginning of the softening stage. These stages are not clearly shown in the pushover curve produced by Seismostruct which is one of the advantages of using the rotational springs. Since Seismostruct uses the force based distributed plasticity along the element, this type of formulation assumes a strain hardening response and fails to capture strain softening hence in Opensees, there are distinct points along the curve and in Seismsostruct a negative slope is seen after the maximum strength is achieved. See tables below showing the yield and maximum strengths of each pushover curve for each frame.

Frame 2

Similar to frame 1, the Opensees pushover curve is able to provide distinct points compared to Seismostruct for reasons previously indicated. However the Seismostruct pushover curve showed that the post yield strength was maintained until there was a iteration error causing Seismostruct to not be able to apply load, when compared to frame 1, where the strength was reduced post yield. This error may be due to the structure failing or Seismostruct may not being able to show the strain softening resulting in the pushover curve shown above. According to Seismosoft (2016), forced based frame elements require a number of iterations to be conducted to ensure equilibrium internally is reached. If equilibrium is not achieved there would result in errors. After manipulating the program properties advised by Seismostruct team, the same error was seen therefore, the structure is deemed to have failed. Opensees on the other hand, due to its mathematical nature, if the structure fails, it is able to continue the analysis until the end point specified in the script is reached. The Opensees curve also showed some similarity in reaching the max demand strength of 37 kips and maintained this in the post capping stage until strain softening is experienced at a displacement of 17 inches.

Frame 3

This frame did not follow the pattern as the first 2 frames regarding the initial elastic stiffness. The Seismostruct pushover curve seemed to have decreased midway of the elastic region. It simply states that there was a sharp reduction in the frames elasticity or stiffness upon loading. This may be due to the longitudinal or transverse steel reinforcement being used in the design suggest by Berry et al.(2006).To reiterate the structural design and beam –column material and sectional properties modelled in Seismostruct produced the parameters used for the concentrated rotational plasticity springs required as input for the Opensees script. Despite the discrepancies associated with initial elastic stiffness, the push over curve for Seismostruct showed early failure until iteration error was obtained. As suggested by the Seismostruct team, the software settings were changed however once the load phase steps was changed from 100 to 50 steps the pushover curve produced the figure below.

Chapter 7.0

Nonlinear time history Analysis Results

7.1 Introduction

Seismic analysis entails determining the response of a structure during an earthquake. The nonlinear time history analysis provides a more reliable assessment of earthquake performance compared to the nonlinear static analysis. It is mainly applied when retrofitting existing structures. This analysis is also used when higher modes and structural behaviour after the first mechanism is of interest. Additionally, it provides estimates of both the peak and residual deformations. In nonlinear time history analysis, the nonlinear properties such as material properties are incorporated in the numerical model and considered as part of the time domain analysis.

For the dynamic analysis, the damping of the frames were considered globally and locally. The critical damping was applied to the initial stiffness of the frames. As suggested in previous research, for reinforced concrete structures, 5 percent damping ratio is applied to the first and second modal frequencies of each frame.

7.2 Seismic Input motions

To conduct this analysis, 20 well known earthquakes which are typically used by researchers were used to determine the responses.This database was developed by the US Federal Emergency Management Agency as a selection of ground motion records used to conduct the collapse assessment of structures using nonlinear dynamic analysis methods. This database is used highly utilized in the earthquakes engineering field when conducting structural or dynamic analysis.

The database includes a ground motion recording from sites located at a distances greater than or equal to 10 km from fault rupture, (far field record set (22 NS and 22 WE individual components for 22 seismic events), and a set of ground motions recorded from sites located less than 10 km from the fault rupture, referred to as near field record set (28 NS and 28 WE individual components for 28 events).

These far field records also have magnitudes larger than 6.5 but with a maximum of 7.6.They were recorded from sites located in either soft rock or stiff soil conditions according to Eurocode 8 and generated from thrust or strike slip source zones. The strongest ground motions have PGA greater than 0.2 g and have PGV greater than 15 cm/s. (Pioldi and Rizzi, 2017)

The table below provides a summary highlighting the main properties of the set of earthquakes.

Table 7-1: Showing main properties of the 22 far field set of P 695 earthquakes (Pioldi and Rizzi, 2017)

EQ ID	EARTHQUAKE						Station Name - Owner
	M	PGA (g)	year	Name	Dur. (s)	fs (Hz)	
12011	6.7	0.52	1994	Northridge, USA	29.99	100	Beverly Hills, Mulhol-USC
12012	6.7	0.48	1994	Northridge, USA	19.99	100	Canyon Country -USC
12041	7.1	0.82	1999	Duzce, TURKEY	55.9	100	Bolu-ERD
12052	7.1	0.34	1999	Hector Mine , USA	45.31	100	Hector.SCSN
12061	6.5	0.35	1979	Imperial Valley, USA	99.92	100	Delta - UMAMUCSD
12062	6.5	0.38	1979	Imperial Valley, USA	39.035	200	El CENTRO Array #11
12071	6.9	0.51	1995	Kobe , Japan	40.96	100	Nishi-Akashi - CUE
12072	6.9	0.24	1995	Kobe Japan	40.96	100	Shin-Osaka - CUE
12081	7.5	0.36	1999	Kocaeli, Turkey	27.085	200	Duzce - ERD
12082	7.5	0.22	1999	Kocaeli, Turkey	30	200	Arcelik - KOERI
12091	7.3	0.24	1992	Landers, USA	44	50	Yermo Fire Station - CDMG
12092	7.3	0.42	1992	Landers, USA	27.965	300	Cool water - SCE
12101	6.9	0.53	1989	Loma Prieta ,USA	39.955	200	Capitola - CDMG
12102	6.9	0.56	1989	Loma Prieta ,USA	39.945	200	Gilroy Array #3 - CDMG
12111	7.4	0.51	1990	Manjil, Iran	53.52	50	Abbar - BHRC
12121	6.5	0.36	1987	Super. Hills ,USA	40	200	El Centro Imp. Co. - CDMG
12122	6.5	0.45	1987	Super. Hills, USA	22.3	100	Poe Road (temp) - USGS
12132	7	0.45	1992	Cape Mendocino,USA	36	50	Rio Dell Overpass - CDMG
12141	7.6	0.44	1999	Chi Chi, Taiwan	90	200	CHY101 - CWB
12142	7.6	0.51	1999	Chi Chi, Taiwan	90	200	TCU045 - CWB
12151	6.6	0.21	1971	San Fernando, USA	28	100	LA Hollywood Stor - CDMG
12171	6.5	0.35	1976	Friuli ,Italy	36.345	200	Tolmezzo

To reduce the computational effort, only the component with highest peak ground acceleration were used resulting in to 20 ground motions. Seven of these are graphical represented below. The remainder are illustrated in the appendix. These unscaled ground motions are applied at the base of the numerical models in both software’s as a uniform lateral excitation pattern. A selected few are presented below.

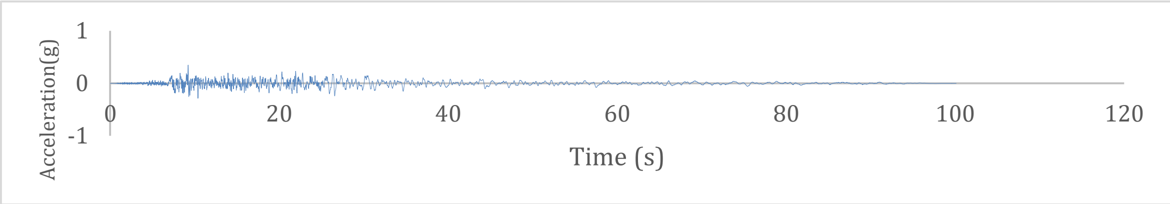

Figure 7-1 A EQ4 Imperial Valley PGA 0.35 g

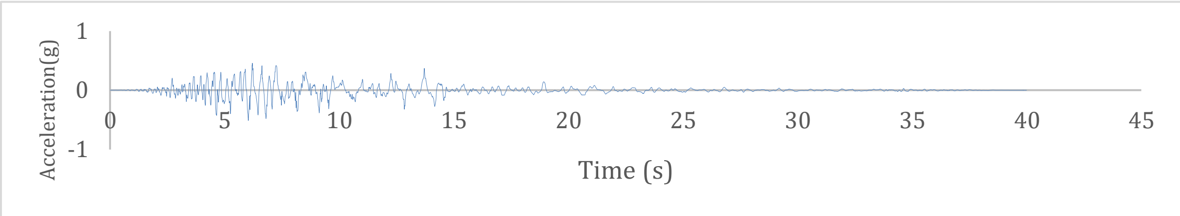

Figure 7-1 B EQ8 Loma Prieta PGA 0.511 g

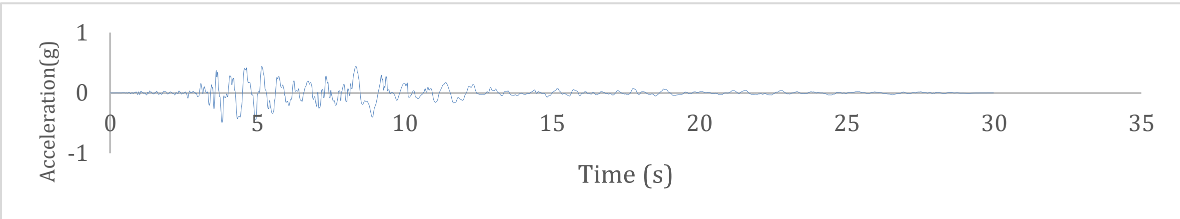

Figure 7 -1C EQ 12 Northridge PGA 0.49 g

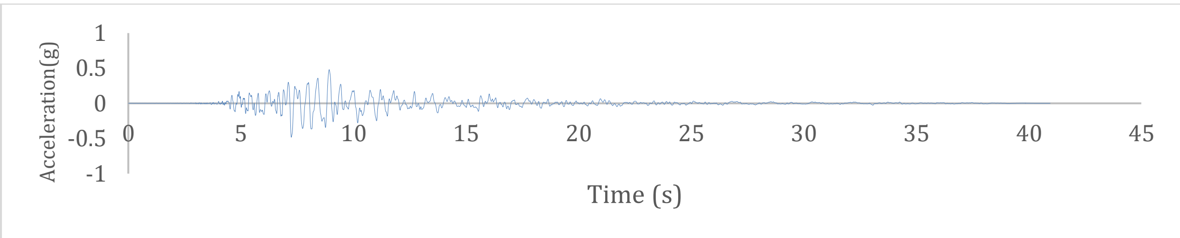

Figure 7 -1 D EQ 14 Kobe PGA 0.48 g

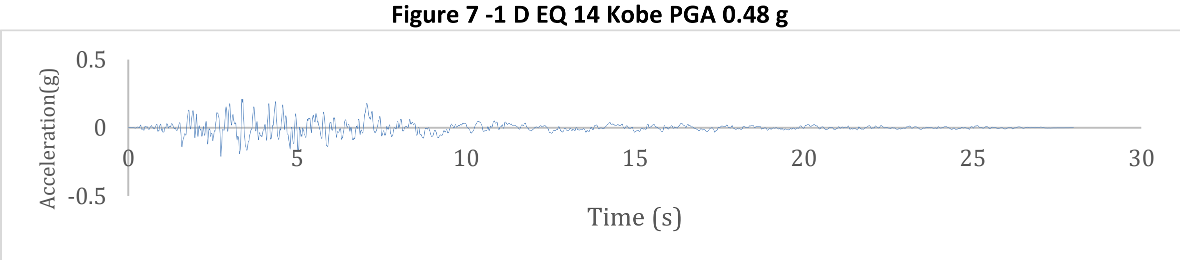

Figure 7-1E EQ 20 San Fernando PGA 0.20g

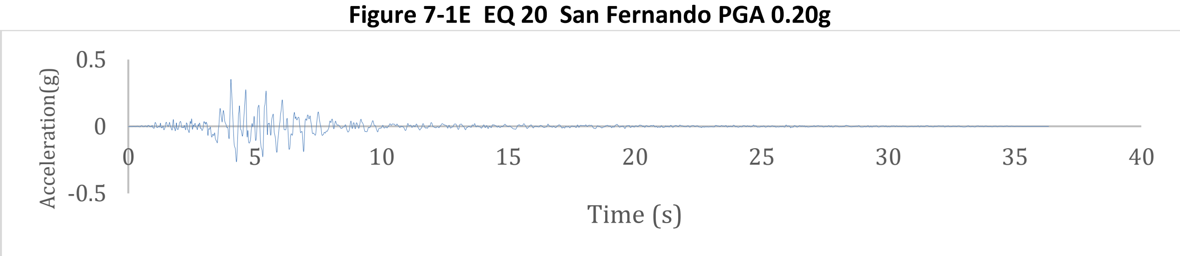

Figure 7- 1 F EQ 2 Friuli PGA 0.351 g

7.3 Scaling of time histories

Each record was scaled to distinct spectral acceleration (Sa) levels, ranging from 0.1g to 2.5g, in increments of 0.1g (a total of 25 analyses for each selected record). This therefore covers the entire range of structural response, from elasticity, to yielding and finally collapse. The spectral shape of mentioned ground motions was not a criterion in the selection process, as the FEMA P695 far-field ground motion set are independent of site hazard or structural type. According to (Nassirpour, D' and Ayala, 2017) these applied records are not reliant on period, any building-specific property of the structure and hazard disaggregation. The mean of the scaled accelerations is indicated by the solid black line.

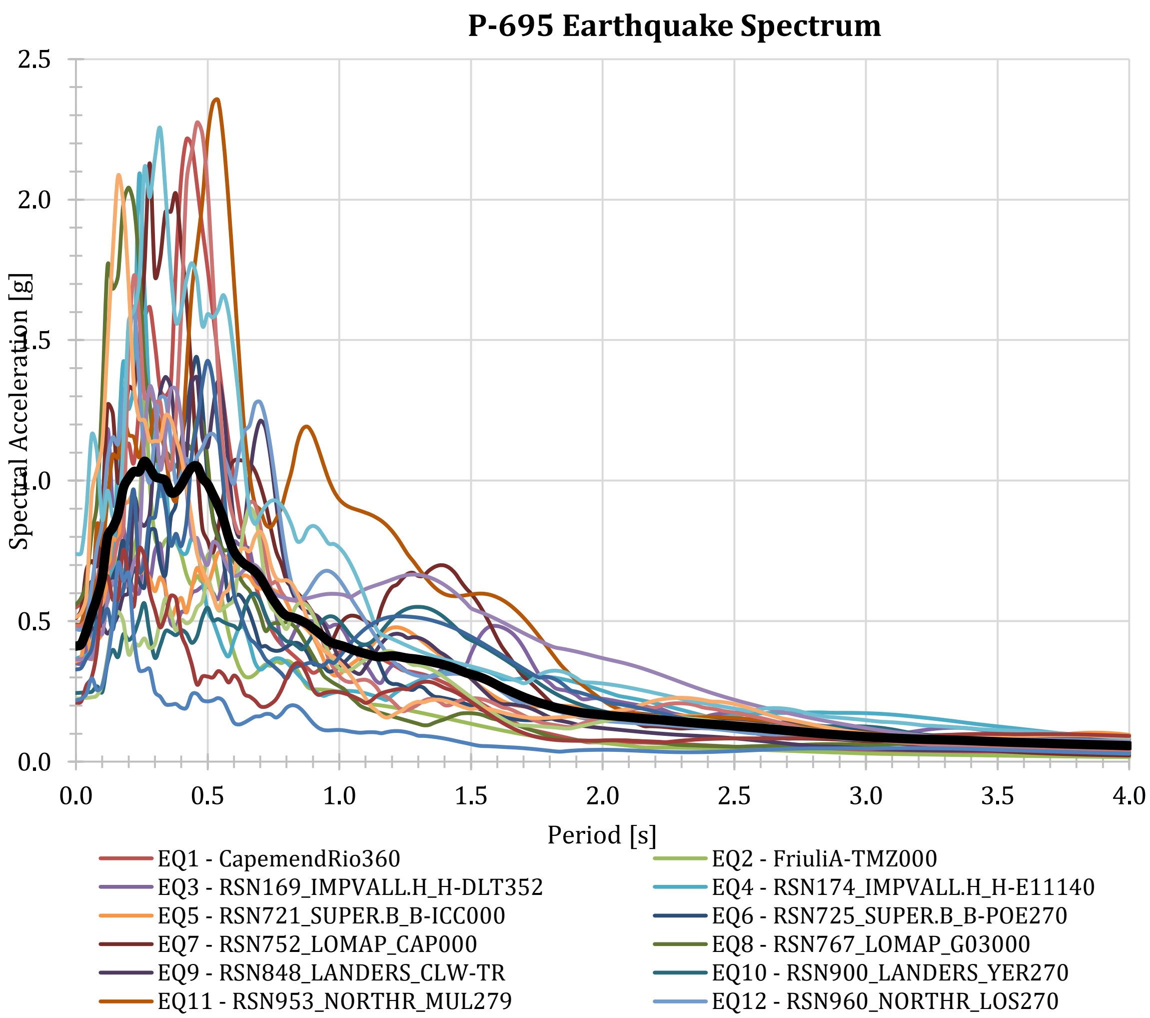

Figure 7-2: Showing scaled earthquakes (Nassirpour, D' and Ayala, 2017)

7.4 Nonlinear Responses

Frame 1

Similar to the pushover analysis, the control node at the roof in the nonlinear analysis was used to obtain the responses for roof displacement, roof drift and max inter-storey drift. A comparison of the final roof displacements is illustrated in figure 7.3 below. From figure 7.3 we can see that Seismostruct produced larger displacement values compared to Opensees. The time history records are also shown in figures 7.4 .It also shows the comparison between both software with the intention of revealing any inconsistencies among the software. From the time figures you can see that the frequency pattern of each response for both software matched showing that the structures are relative modelled accurately. It is observed in some instances that the peak response is achieved at different times along the time history for both programs. This can be due to non-linear behaviour and contribution from higher modes. This is shown for Imperial valley had roof displacement of 6.4 in at 31 secs for Seismostruct and 5 inches at 28.12 secs for Opensees, Northridge – 12 in at 10 .6 secs and 9 inches at 8.33 secs for Seismostruct and Opensees respectively and Kobe experiencing max displacements of 4 inches however at 16.8 secs and 16 .4 secs for Seismostruct and Opensees programs respectively. On the other hand the peak responses occurred in the same time step for the remaining illustrations below.i.e Loma Prieta, SanFernando and Friuli earthquakes. The maximum roof displacements for frame 1 in Seismostruct and Opensees was observed for EQ 16, Kocaeli and EQ12, Northridge earthquakes with a response of 12 inches and 9 inches respectively .See figure below for comparison of all max displacements.

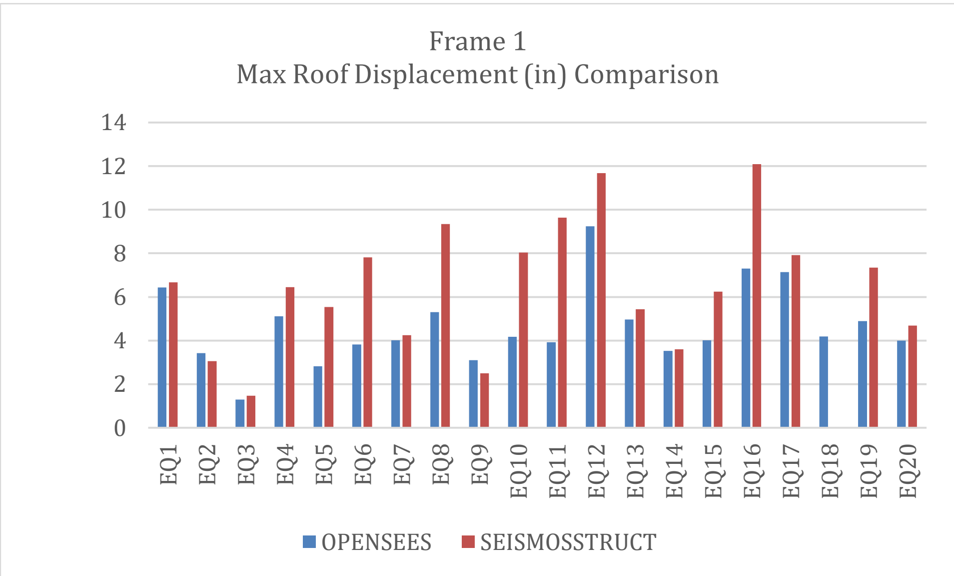

Figure 7-3 showing Max roof displacement software comparisons.

All maximum displacements occurred during the time ranges of high frequency for all earthquakes. At this point according to the hazus inter-storey drift ratio damage states for low-rise buildings, the building is able to achieve displacements beyond the threshold limits in hazus.

Frame 1

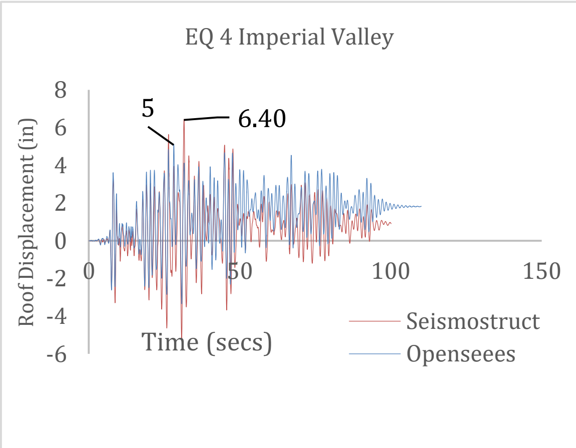

Figure 7.4 A Peak Displ. Frame 1 NLTHA, EQ 4

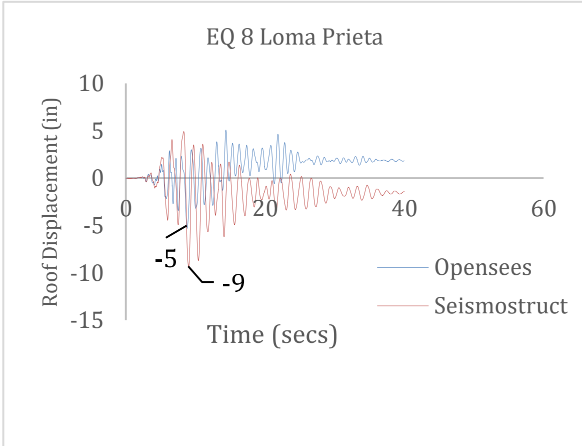

Figure 7.4B Peak Disp. Frame 1 NLTHA, EQ 8

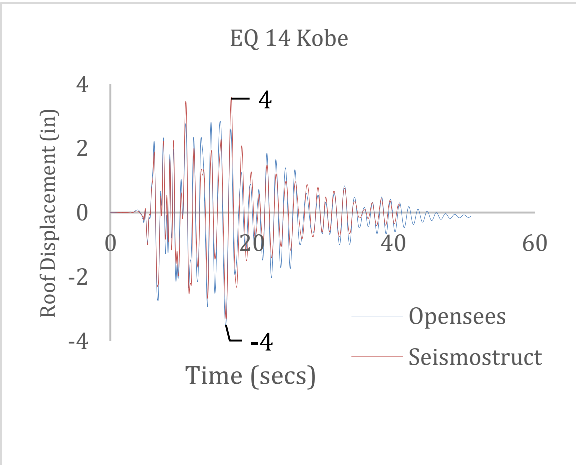

Figure 7.4C Peak Displ. Frame 1 NLTHA, EQ 14

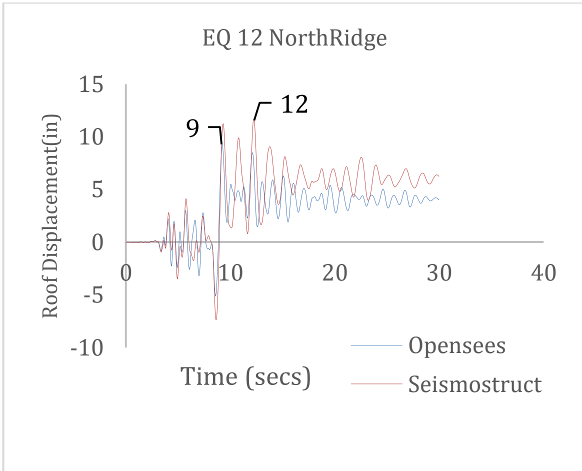

Figure 7.4D Peak Displ. Frame 1NLTHA, EQ 12

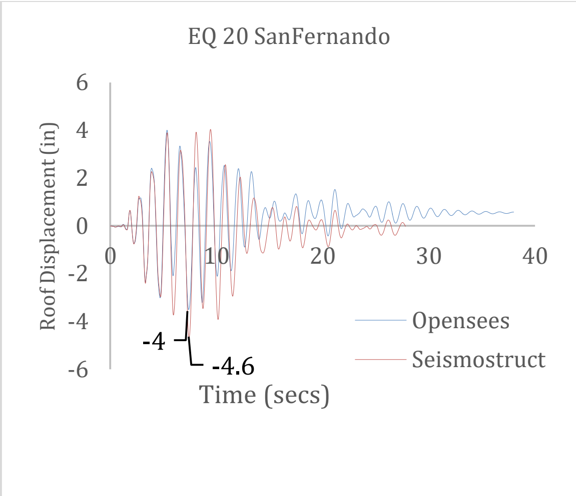

Figure 7.4 E FRAME 1 Peak Displ. Frame 1 NLTHA, 20

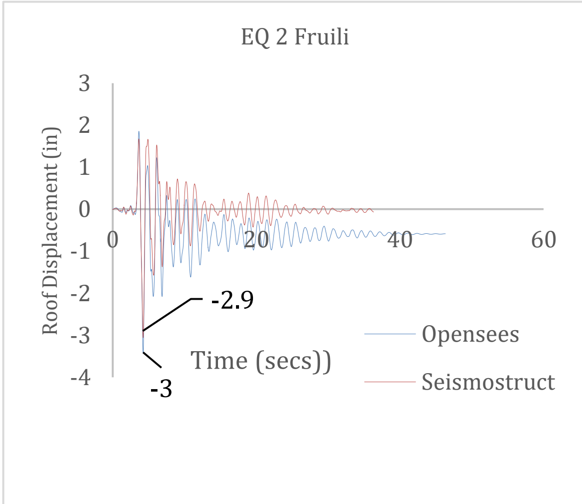

Figure 7.4F: Peak Displ. Frame 1 NLTHA, EQ 2

From the dynamic analysis, the maximum roof drifts and inter-storey drifts were also extracted for each earthquake for the different software's. A graphical representations comparing the responses are shown below. The maximum inter-storey drift ratios are representative of the response of the first storey for both programs. These were extrapolated because they were larger than those from the second storey and the failure of the structure would be due to soft storey action occurring.

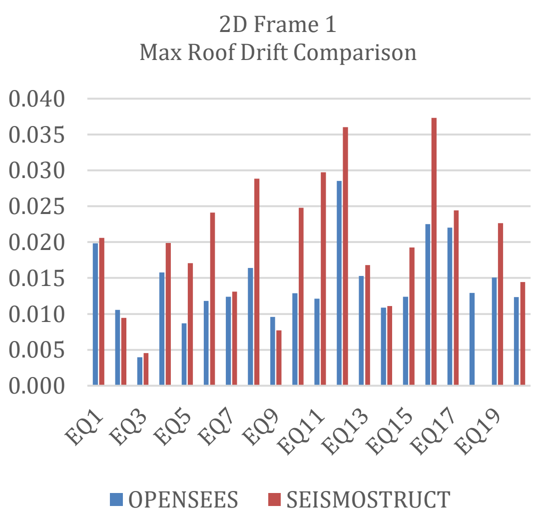

Figures 7.5A: Showing max roof drift comparison

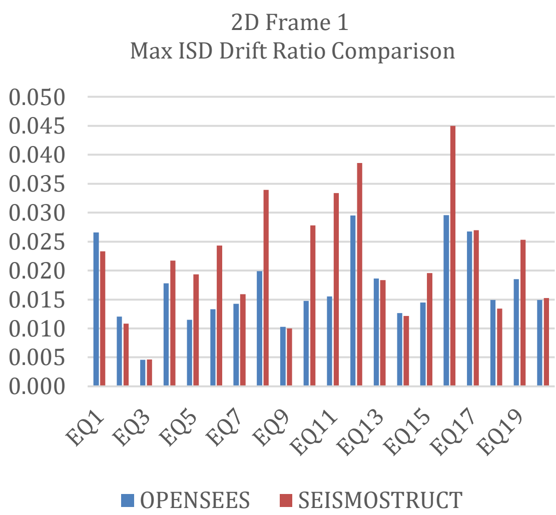

Figure 7.5 B Showing MISDR comparison

It can be seen that generally Seismostruct produced larger responses in both figures. Despite the Seismostruct producing larger values, the average of the differences between both programs for the max inter-storey drift ratio at second floor was found to be 0.005 in. However there were larger variations shown for Loma Prieta, Landers and Kocaeli. This can be due to the fact that these earthquakes have the largest peak ground acceleration values and Seismostruct interpretation of the ground motion recording caused the larger responses compared to Opensees.

Frame 2

The figures below show the response of frame 2 to ground motion records. Similar to Frame 1, the frequency patterns of each response match for both earthquakes, the peak responses occurred at different times during the analysis. However these differences in time step occurred for differently for the same earthquakes presented for frame1. From the earthquakes presented below, Frame 2 experienced peak responses simultaneously for Imperial Valley and Kobe earthquakes with roof displacements of 1.1 inches for Seismostruct and 2.82 inches for Opensees. The remaining earthquakes presented below resulted in peak roof displacements occurring different times during the analysis. Once completing the analysis for all 20 earthquakes, the maximum roof displacements for frame 2 in both software were observed for EQ 12, North Ridge. Seismostruct resulted in a peak response of 4.24 inches while Opensees resulted with the larger, being 4.74 inches. All maximum displacements occurred during the time ranges of high frequency for all earthquakes. Similar to frame 1 at this point according to the Hazus inter-storey drift ratio damage states for low rise buildings, the was able to go beyond the threshold limits. The figure below shows the distribution of the max displacements for all unscaled ground motion records.

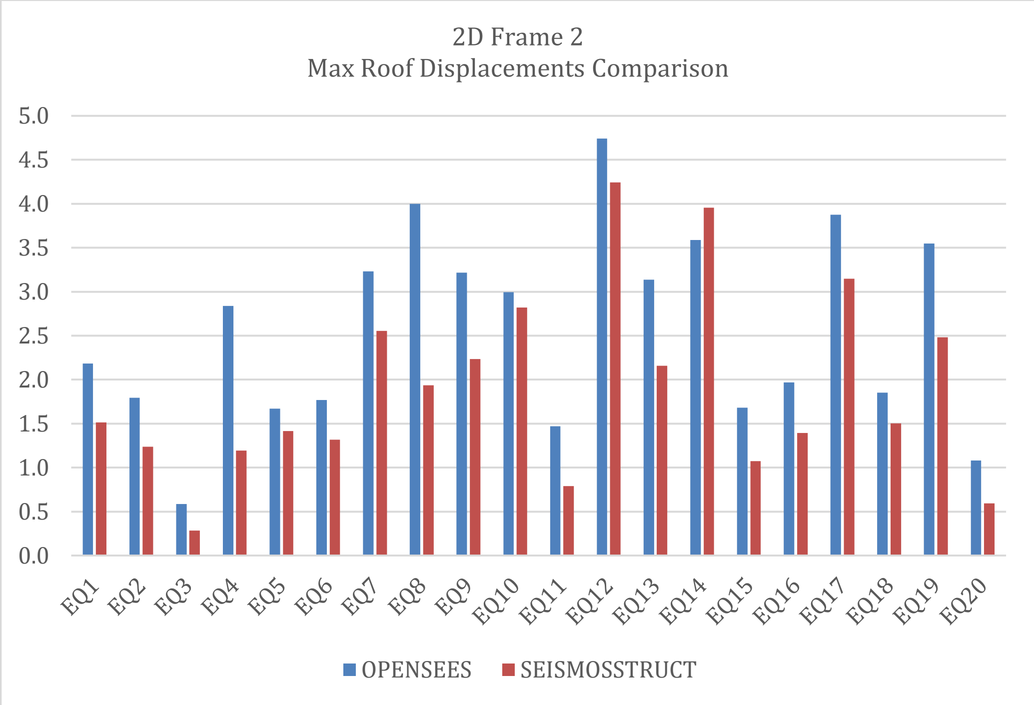

Figure 7.6: Showing max roof displacements for all ground motion records for frame 2

From the results, it is also observed that Opensees produced larger responses for frame 2, as opposed to the results obtained for frame 1.The reason for this will be discussed further in the discussion. The maximum roof drifts and inter-storey drift were also extracted and are displayed in figure 7.7 below, with the maximum inter-storey drift ratios are representative of the response of the first storey for both programs. It can be seen that generally Opensees produced larger responses in both figures. Despite this fact, the average of the differences between both programs for the max inter-storey drift ratio at second floor was found to be 0.002 inches. However, these values seem to show closer comparison compared to those presented in frame 1 where a few of the earthquakes generated larger responses in Seismostruct analysis.

FRAME 2 NLTHA RESULTS

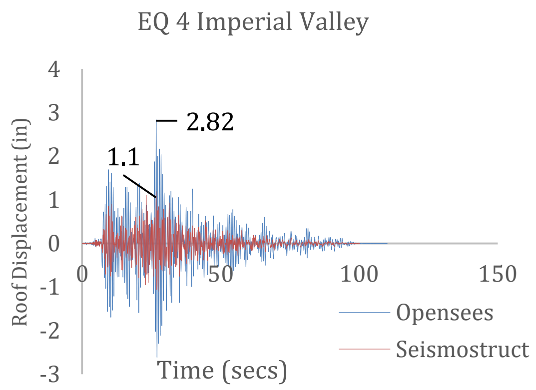

Figure7.7A: Peak response, frame 2, EQ4

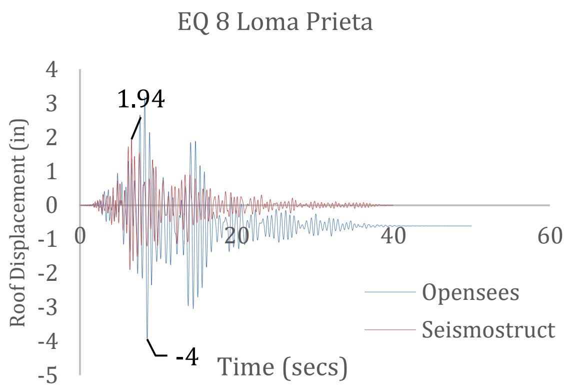

Figure7.7B: Peak response, frame 2, EQ8

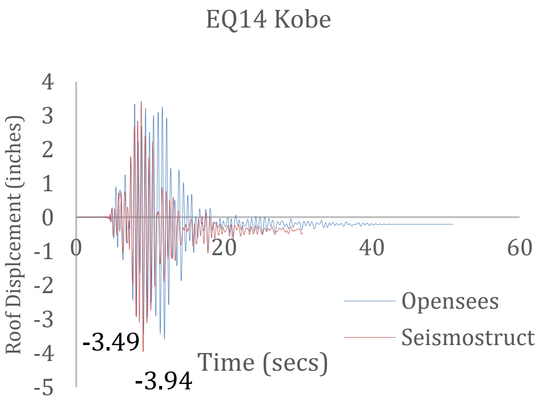

Figure7.7C: Peak response, frame 2, EQ14

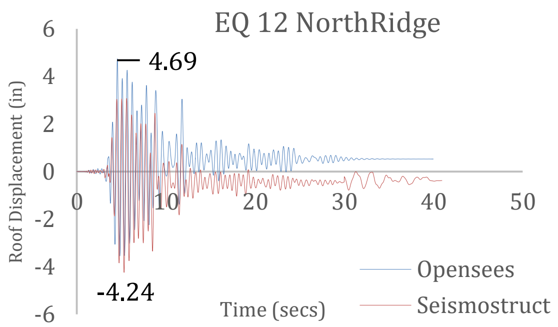

Figure7.7D: Peak response, frame 2, EQ12

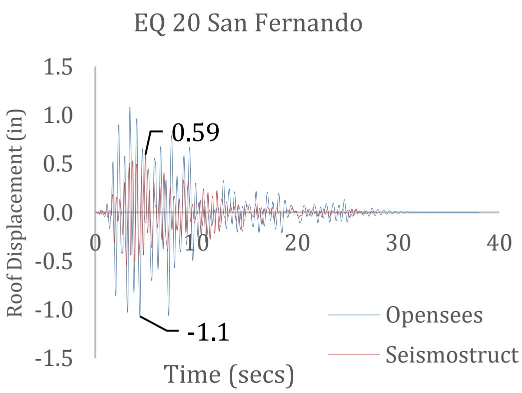

Figure7.7E: Peak response, frame 2, EQ20

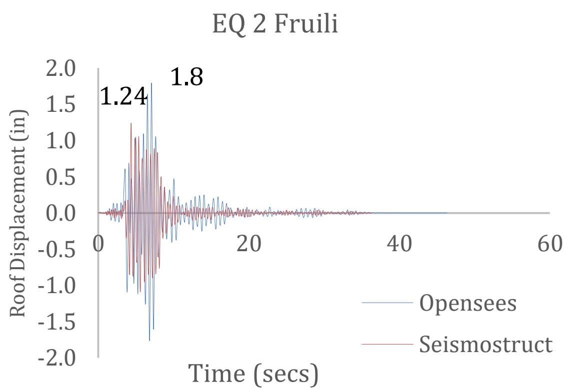

Figure7.7F: Peak response, frame 2, EQ2

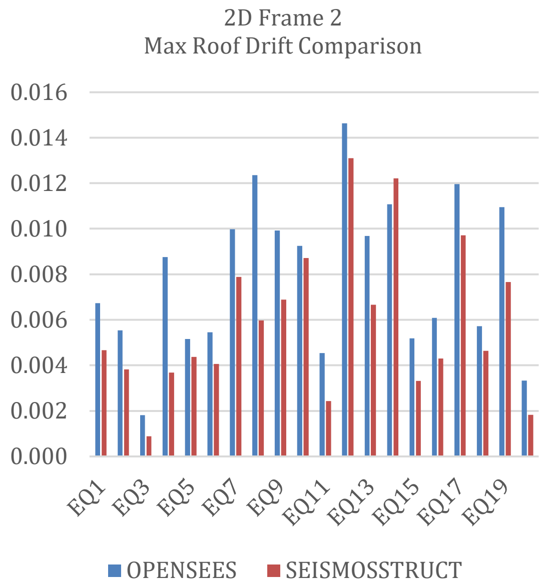

Figures 7.8: Showing max roof drift Frame 2

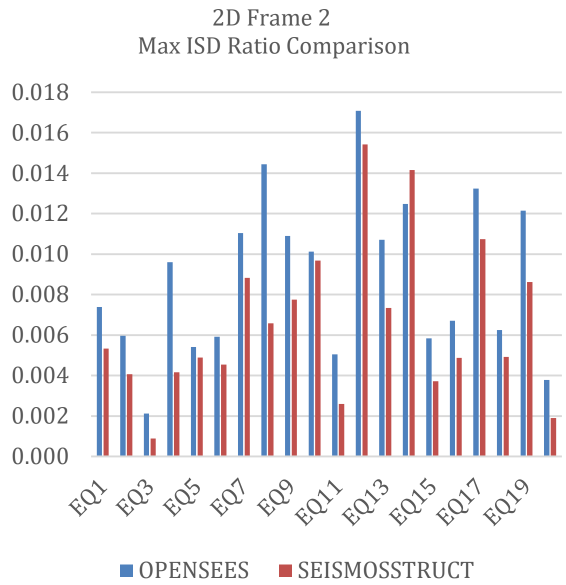

Figure 7.9: Showing max ISD ratio Frame 2

Frame 3

Frame 3 demonstrated a similar response to frame 1 where Seismostruct generally generated larger roof displacements. However these displacements are numerically smaller as frame 3 relatively has the largest cross section and strongest design. The response frequency from both programs are identical which indicate the model was generated with some accuracy. The max responses, similar to the previously discussed frames, occurred during the high frequency portion of the earthquake however not always occurring at the same time for both software. From the six response time histories presented below, Earthquake 2 resulted in max responses occurring simultaneously with magnitude of 0.7 inches and 0.4 inches for Seismostruct and Opensees programs respectively. The max responses for the remaining earthquakes occurs presented below occurred at varying times for both programs. The distribution of the max responses for all 20 earthquakes for both programs are illustrated in the figure 7.9 below. The maximum response occurred for Loma Prieta in Seismostruct with a magnitude of 1.89 inches and for Opensees a max response of 1.19 inches for earthquake 9 which is the same earthquake however recorded from a different station.

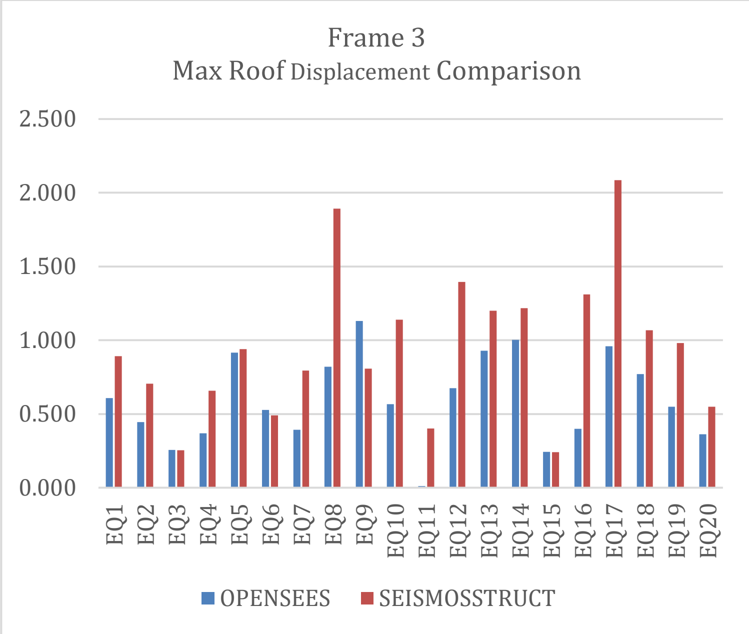

Figure 7.9 Showing max roof displacements for all 2 ground motion records for frame 3

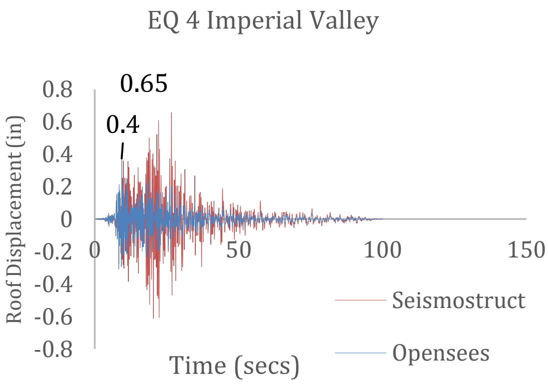

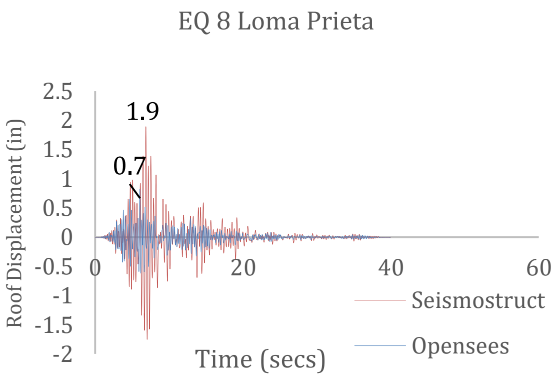

Figure 7.10 A: Peak Displ. Frame 3, EQ4

Figure 7.10B: Peak Displ. Frame 3, EQ8

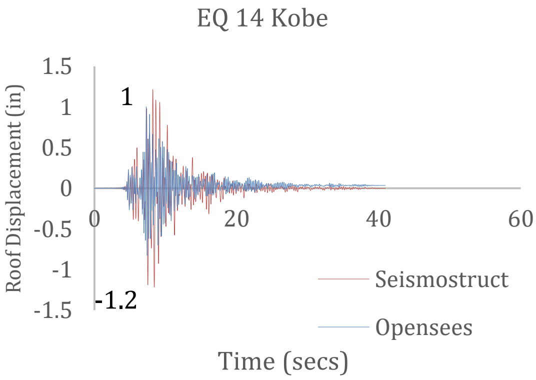

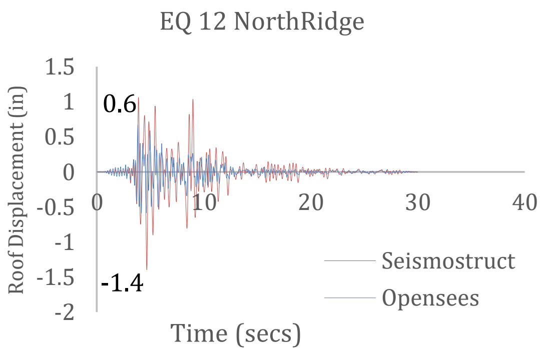

Figure 7.10 C: Peak Displ. Frame 3, EQ14

Figure 7.10 D: Peak Displ. Frame 3, EQ12

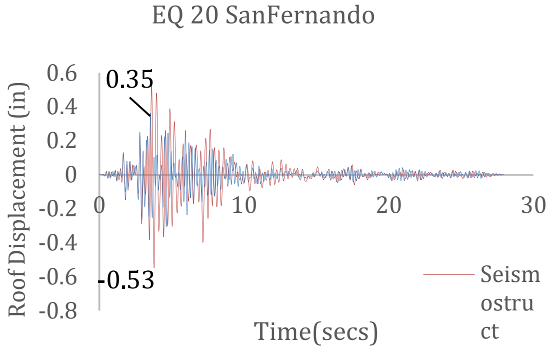

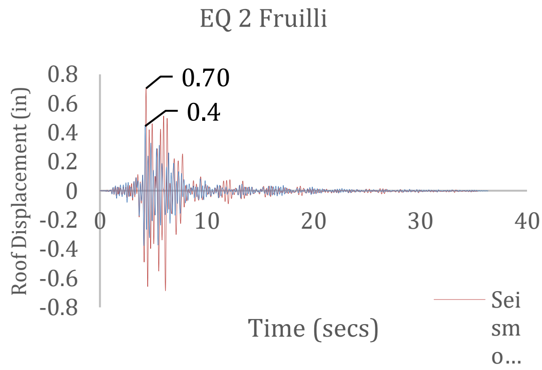

Figure 7.10 D: Peak Displ. Frame 3, EQ20

Figure 7.10 E: Peak Displ. Frame 3, EQ2

The maximum roof drifts and inter-storey drift were also extracted and are displayed in figure 7.11 below. Similar to frame 1, the response generated in Opensees for frame 3 were larger. The average differences between both programs for the max inter-storey drift ratio was found to be 0.0015 inches. When these values were compared to the hazus inter-storey drift ratio damage states for low rise buildings, it is observed that the building allow displacements pass the threshold.

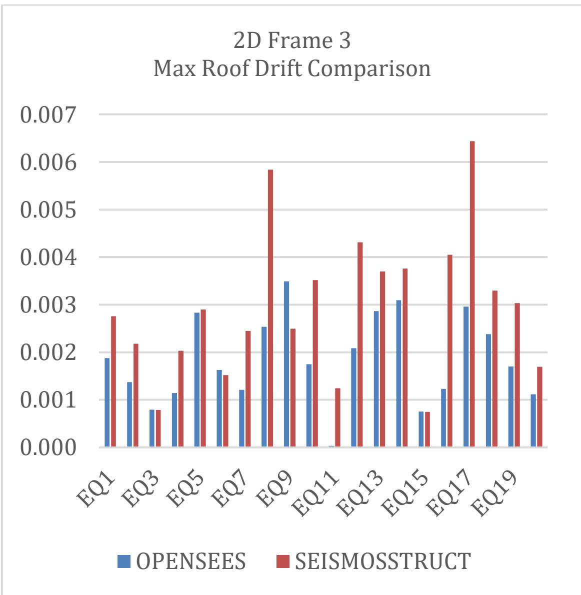

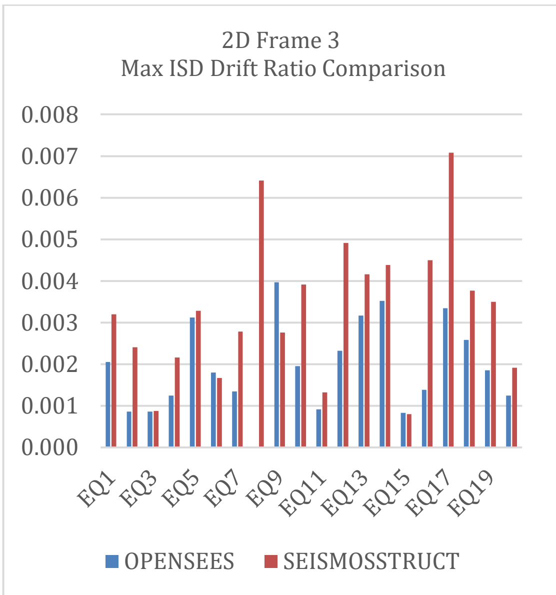

Figure 7.11: Showing max roof drift comparison

Figure 7.12 max ISD ratio comparison

7.5 Pushover Analysis vs Nonlinear Time History Response Analysis

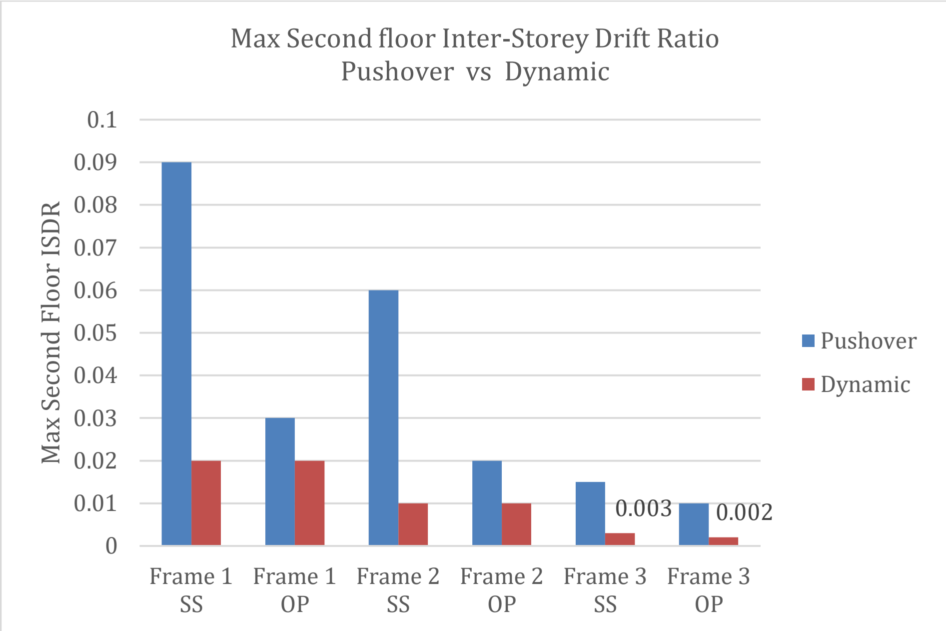

Figure 7.13: Showing summary of max second floor inter - storey drift ratio

The max roof inter-storey drifts were compared. From the figures above we can see the same trend where Opensees produced conservative results. As compared to Seismostruct with frame 2 showing a similar trend in results. They show a difference of average a 0.0023 inches for frame 2, 0.0014 inches for frame 3 and 0.00496 inches in frame one.

The inter-story drifts from the nonlinear time history analysis was then compared to push over analysis values at second floor for all frame .For frame 1, Opensees produced similar values in both analysis having values of 0.03 inches in push over analysis and 0.02 inches in nonlinear time history analysis with a 0.01 difference. For the same frame Siesmostruct produced drift values of 0.09 inches for the pushover analysis and 0.02 for the nonlinear time history analysis. These show a difference of 0.07 inches. In frame 2 Opensees had results 0.01 for nonlinear time history analysis and 0.02 push over analysis. While Seismostruct produced 0.06 pushover and 0.01 nonlinear time history analysis. For frame 3, 0.002 (NLTHA) and 0.01 pushover analysis, and Seismostruct 0.015 in pushover analysis and 0.003 nonlinear time history analysis.

From these results we see the Opensees showed similar values in both analysis compared to Seismostruct which relatively had greater difference in values. However in frame three Seismostruct and Opensees produced similar values. This is may be due to Seismostruct not able to produce results for cross sections frames. However Opensees was able to produce results despite the size of the cross section.

The table below provide a summary of the information presented above in a tabulated format. They also highlight the peak ground accelerations and spectral accelerations generated from the scaled earthquake based on the first period of the each frame. Further explanation of the use of these intensity measures is done below.

Table 7-2: Showing intensity measure, max roof displacement and max roof drift Frame 1

Earthquake ID	PGA (g)	Sa (T1)g	SEISMOSSTRUCT		OPENSEES	
			Max Displacement (in)	Max Roof Drift	Max Displacement (in	Max Roof Drift
EQ1	0.54893	0.346	6.66557	0.0206	6.43227	0.020
EQ2	0.35133	0.2564	3.05522	0.0094	3.42326	0.011
EQ3	0.3497	0.1131	1.47661	0.0046	1.28879	0.004
EQ4	0.36681	0.499	6.4434	0.0199	5.11902	0.016
EQ5	0.35726	0.2344	5.5341	0.0171	2.8204	0.009
EQ6	0.47498	0.3646	7.81156	0.0241	3.81898	0.012
EQ7	0.51113	0.3373	4.2491	0.0131	4.01543	0.012
EQ8	0.55912	0.4498	9.34313	0.0288	5.31013	0.016
EQ9	0.4172	0.3074	2.50208	0.0077	3.10808	0.010
EQ10	0.24452	0.4911	8.0306	0.0248	4.17684	0.013
EQ11	0.48796	0.5059	9.6364	0.0297	3.92061	0.012
EQ12	0.47163	1.0516	11.67356	0.0360	9.24603	0.029
EQ13	0.48323	0.6771	5.44037	0.0168	4.95939	0.015
EQ14	0.225	0.4212	3.60043	0.0111	3.52511	0.011
EQ15	0.36418	0.4324	6.2419	0.0193	4.01732	0.012
EQ16	0.73925	0.5951	12.09336	0.0373	7.29806	0.023
EQ17	0.51456	0.8028	7.91393	0.0244	7.13443	0.022
EQ18	0.32819	0.3973	0.00542419	0.0000	4.18537	0.013
EQ19	0.20988	0.3427	7.34368	0.0227	4.88623	0.015
EQ20	0.21884	0.2438	4.68385	0.0145	4.00079	0.012

7.6 DISCUSSION

Seismostruct is able to provide the relative displacements therefore to determine the drifts at each floor or roof drift we have to divide by the height of the floor for the floor drift to by the height of the building for the roof drift. The plots above for the roof displacement show that Seismostruct generally provided larger displacements. However, Frame 2 generated results with the values from Seismostruct being conservative compared to Opensees. This result may not be fully accurate because from the push over analysis of frame 2, Siesmostruct encountered convergence problems resulting in the target displacement not being reached. As shown in the push over analysis of frame a second plot is shown attempting to rectify the issue of the first plot. This was done however when conducting the nonlinear analysis, Seismostruct encountered more errors. Therefore the choice was made to use the first pushover curve to run the dynamic analysis. We saw that the displacements reached I the push over analysis were less compared to those in Opensees and a similar trend is seen in the dynamic analysis. If Seismostruct was able to carry out the analysis to the target displacement without any errors, the nonlinear time history analysis would have resulting in Opensees providing conservative results. Also based in the results the reason why Seimostruct produced such larger responses may be due to the use of the bilinear steel element used for the analysis. Even though it models the nonlinear behaviour similar to that of the rotational spring, however according to seism soft (2016) if used in heavy seismic loading analysis the results would not be a good estimate of the occurs in real life. In this analysis the records used had complex loading histories therefore this can be the reason for the responses.

Chapter 8.0

Fragility Curves

The vulnerability of a structure exposed to seismic actions is usually expressed using vulnerability and fragility functions. These functions express the relationship between the levels of ground shaking expected at a site due to the probability damage. Fragility curves incorporate these functions which are used to describe graphically, the probability that specified structures will reach or exceed specified damage states for certain levels of intensity earthquakes. Fragility functions are usually expressed in the form:

$P\ (DS \geq ds_i\ |IM)$ for $IM_{min} \leq IM \leq IM_{max}$

Where; DS is the damage state of the building class being assessed, ds_i is a predetermined damage state and IM which represents the intensity measure expressing the ground motion damage potential, with respect to the specified building.(Rossetto et al. 2016)

8.1 Fracas methodology

The fragility curves in the research will be generated using the fragility through capacity spectrum assessment (FRACAS).This procedure builds and expands on a modified capacity spectrum method initially developed by (Rossetto and Elanashai, 2005). FRACAS applies the said methodology but improves it, allowing for a more sophisticated capacity curve idealizations, the use of various hysteretic models for SDOF in the inelastic demand calculation, and the construction of fragility functions through numerous statistical model fitting techniques. This method is efficient allowing the fragility curves to be generated from the analysis of a specific structure subjected to a number of acceleration time histories with distinct characteristics. The variation in seismic input and structural characteristics on the damage statistics for the modelled building class are also accounted for in this method along with the uncertainty in the prediction is evaluated.

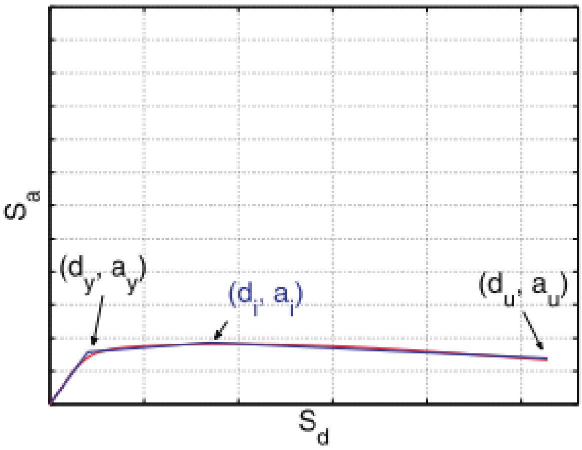

Figure 8.1 A Capacity Curve Idealisation

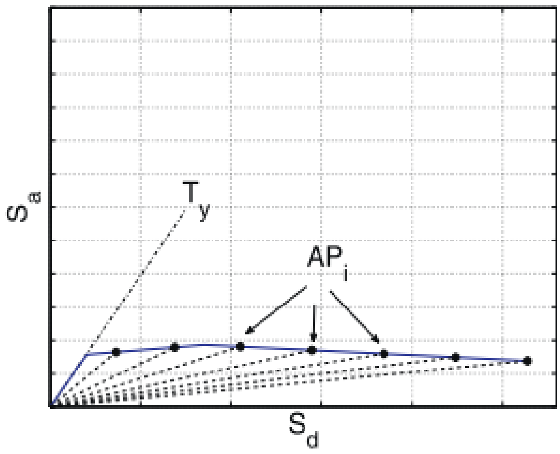

Figure 8.1B :Discretization into post yield periods

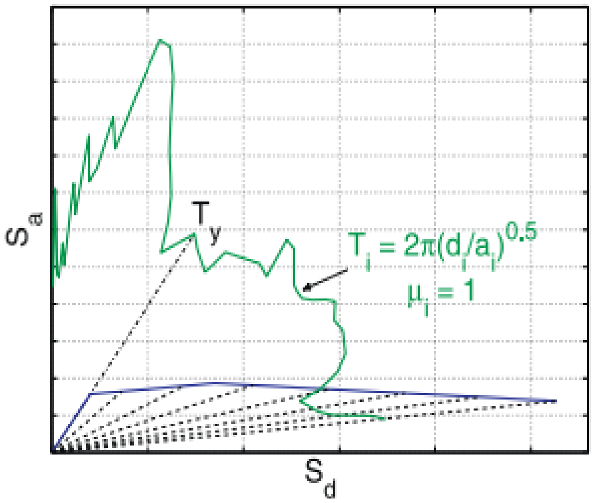

Figure 8.1 C Elastic Response Period

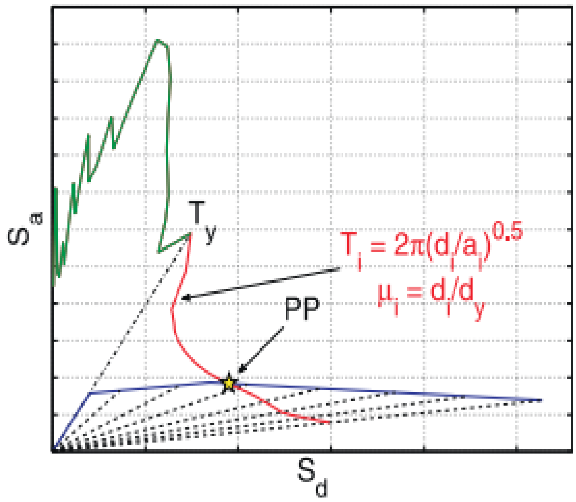

Figure 8.1D : Inelastic Response Spectrum & PP

The figures above illustrate the steps involved in developing the perfomance point , (Rossetto et al. 2016)

The procedure used to determine the performance point is summarised below.

1. The first step involves converting the force – displacement curve into a capacity curve relating to a single degree of freedom model. This process utilizes the floor masses and inter-storey displacements generated from the push over analysis.

2. The second step involves idealisation of the capacity curve which can be modelled using different idealisation models, yielding point, hardening and ultimate point This curve is represented using various nonlinear characteristics, point of yielding, hardening characteristics and structures capacity.

3. The third step divides the capacity curve into a number of points along with respective pre- and post-yield periods.

4. The forth step consist of utilizing the input ground motions to generate an elastic response spectrum where the demand is determined up to the yielding

5. The fifth step entails computing the inelastic demand of the equivalent single degree of freedom relating to the specified post-yield periods.

6. The final step defines the performance point. This is defined as the point where the capacity curve is intersected by the demand curve. The equivalent engineering demand parameters can be determined by back calculating the performance point to the force-displacement representation.

The fragility analysis was conducted for the frame 1 and 2 in both programs presenting the sensitivity of each model has on the risk assessment.

Table 8-1 Showing parameters for frames OP 1

Damage State	Opensees Frame 1	
	Median	Dispersion
Slight	1.36	0.54
Moderate	3.25	0.54
Complete	21.51	0.70

Table 8-2 Showing parameters curves for SS frames 1

Damage State	Seismostruct Frame 1	
	Median	Dispersion
Slight	2.65	0.61
Moderate	15.47	0.72
Complete	0	-2.64E+13

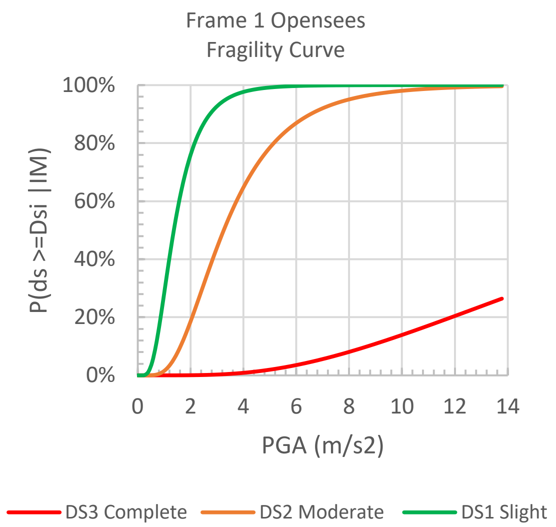

Figure 8.2: Showing Fragility curves frame 1OP

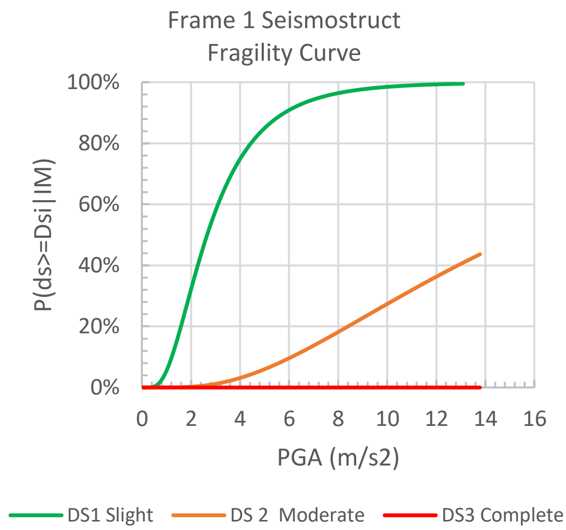

Figure 8.3: Showing Fragility curves frame 1SS

Damage State	Opensees Frame 2	
	Median	Dispersion
Slight	3.00	0.37
Moderate	14.14	0.37
Complete	0.00	-2.64E+13

Damage State	Seismostruct Frame 2	
	median	dispersion
Slight	4.08	0.31
Moderate	0	-2.63E+13
Complete	0	-2.63E+13

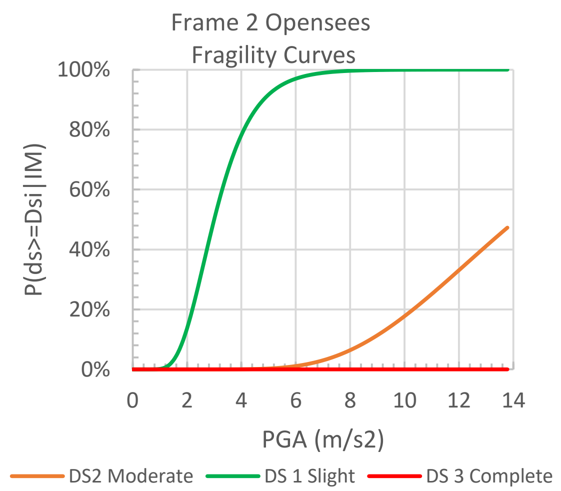

Figure 8.4: Showing Fragility curves frame 2, OP

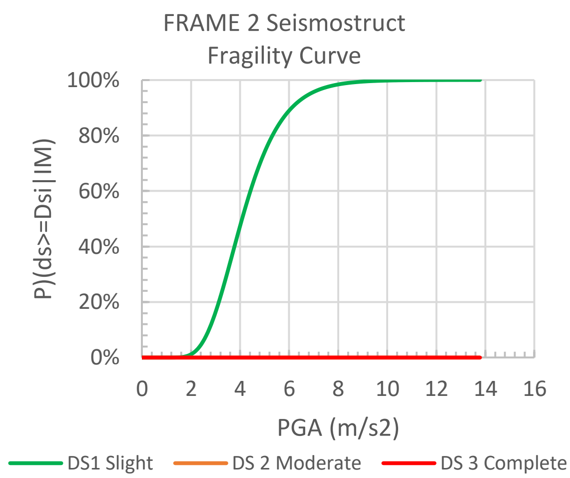

Figure 8.5: Showing Fragility curves frame 2, SS

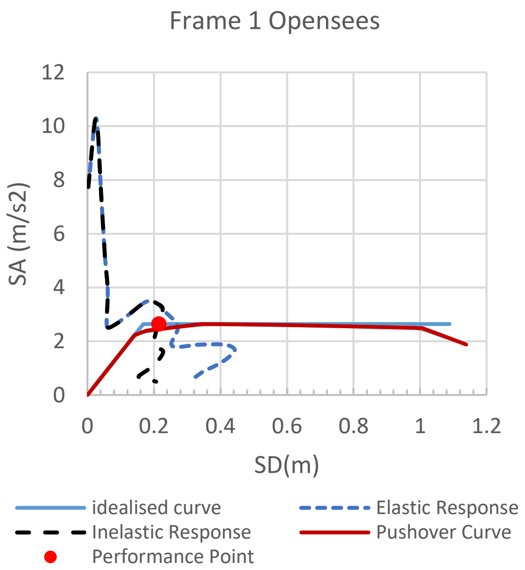

Figure 8.6A: Showing PP for frame 1 in Opensees

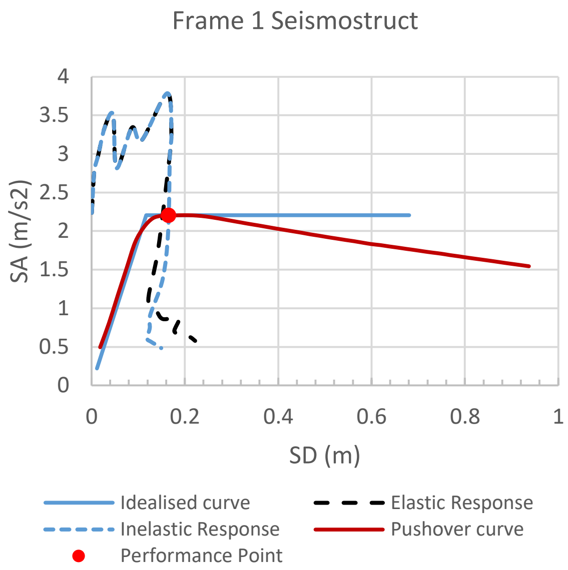

Figure 8.6 B: Showing PP for frame 1 in Seismostruct

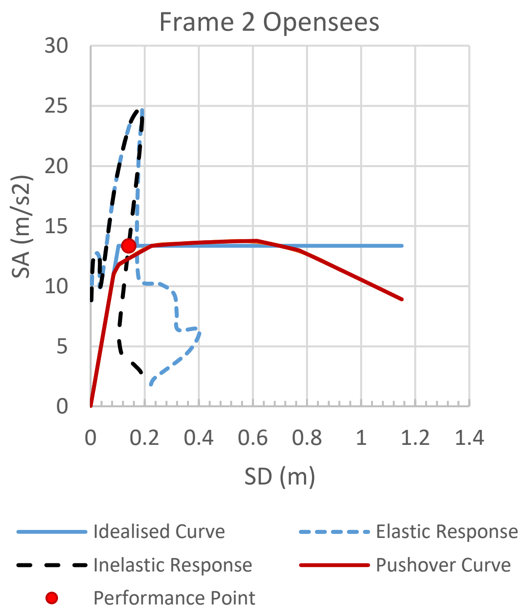

Figure 8.6 C: Showing PP for frame 2 in Opensees

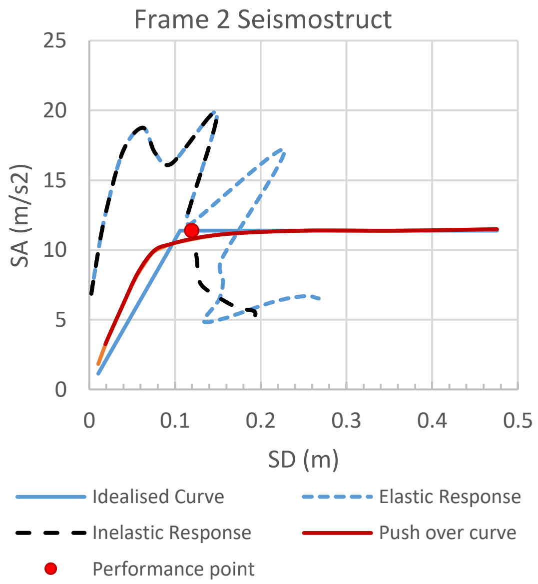

Figure 8.6 D: Showing PP for frame 2 in Seismostruct

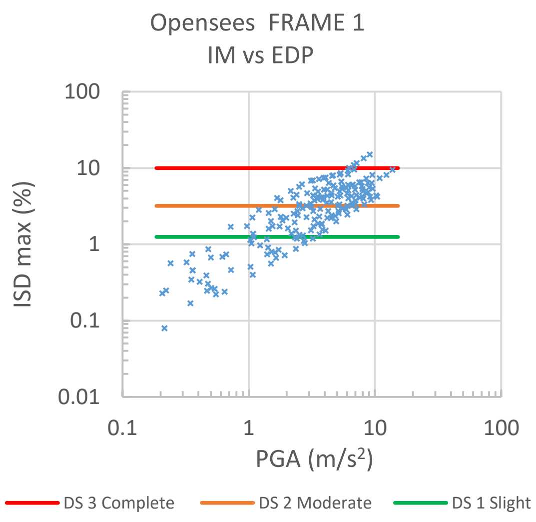

Figure 8.7 A: Showing IM and EDP plot frame 1, O.P

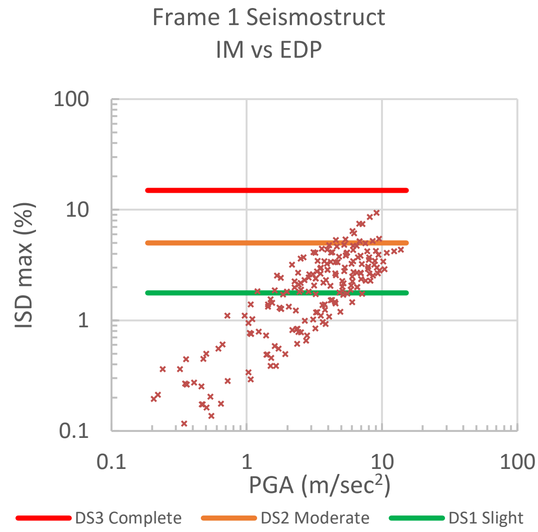

Figure 8.7 B: Showing IM and EDP plot frame 1, S.S

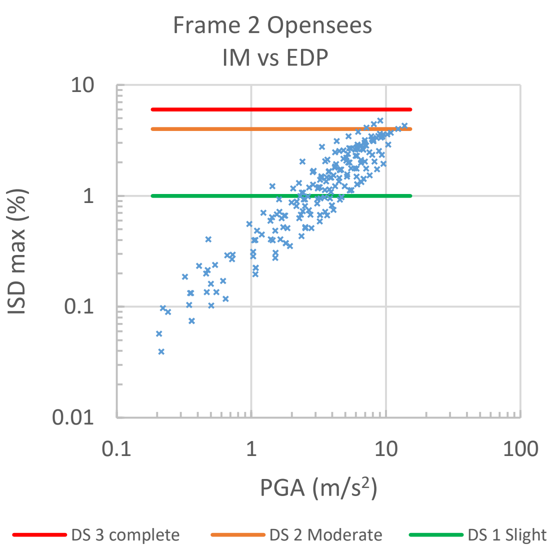

Figure 8.7C: Showing IM and EDP plot frame 2, O.P

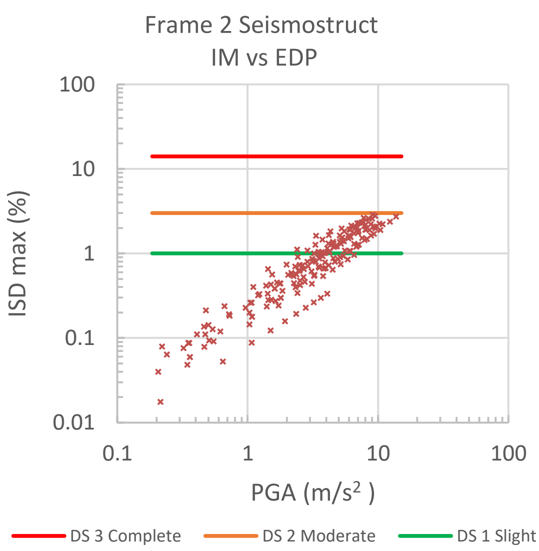

Figure 8.7 D: Showing IM and EDP plot frame 2, SS

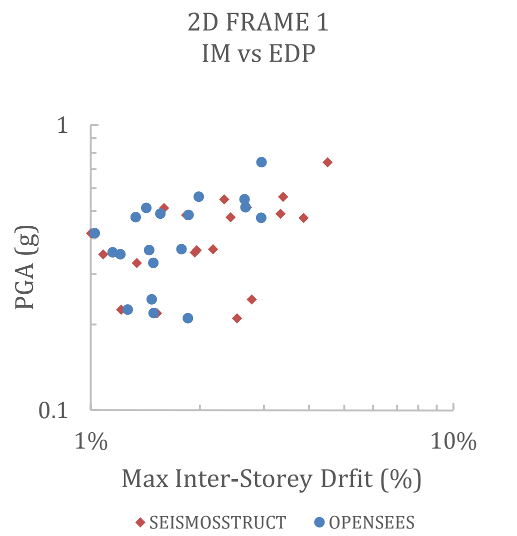

Figure 8.8 A showing IM and EDP comparison, frame 1

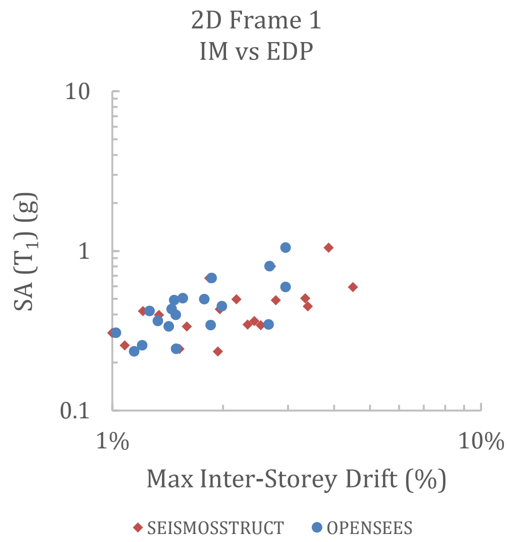

Figure 8.8 B showing IM and EDP comparison, frame 1

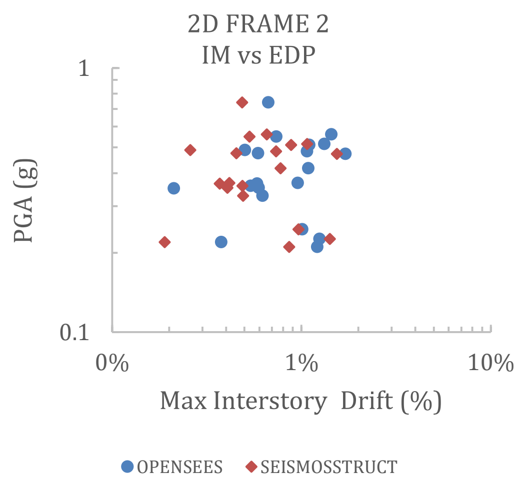

Figure 8.8 C showing IM and EDP comparison, frame 2

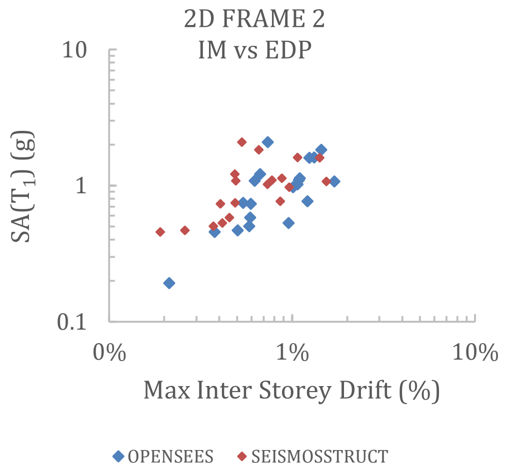

Figure 8.8 D showing IM and EDP comparison, frame 2

9.0 FURTHER ANALYSIS

Opensees Fibre based elements vs Seismostruct forced based concentrated plasticity and displacement based inelasticity.

The figure below shows the pushover curves a reinforced concrete 3D building. The plot shows the comparison of pushover curves using fibre section distributed plasticity element in Opensees, force based concentrated plasticity in Seismostruct and Displacement base distributed plasticity. The results show the initial elastic stiffness is the same for all curves however the Opensees had a slight reduction. This could be due to the material characteristics in the different programs having minor differences. The distributed plasticity in Opensees tend to be a conservative and while the displacement based plasticity in Seismostruct produced high demands.

Table 9 .1Showing Eigen analysis results for 3d building

Seismostruct	
Mode 1 ,T1	Mode 2 ,T2
0.43 s	0.34 s
Opensees	
Mode 1, T 1	**Mode 2, T 2**
0.40 s	0.40 s

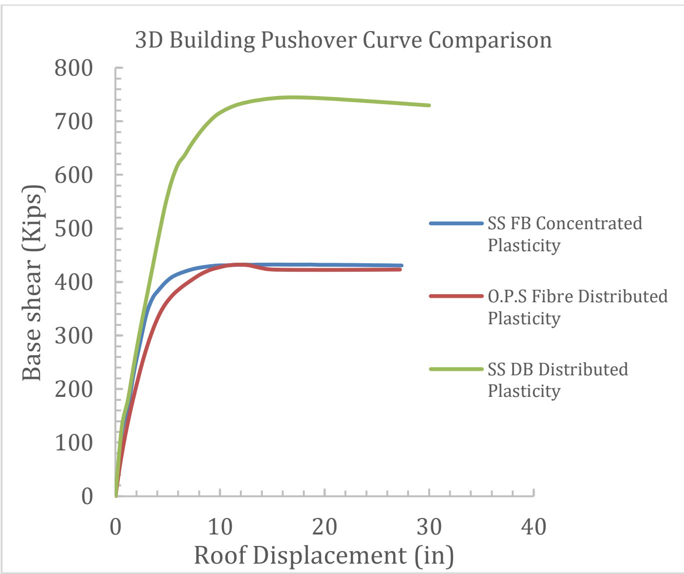

Figure 9.1: Showing pushover curves for 3d building

9.1 Future Works

To gain further insight into understanding the inconsistencies with both modelling techniques used I would suggest the following:

1) Conduct the same analysis using the IMK springs in Opensees in a 3 dimensional real life earthquake resistant structure and model the same structure in Seismostruct and compare the response of the structure via Nonlinear Static push over analysis and Nonlinear Time history Analysis. This would further allow us to understand if the results would follow the similar pattern observed in the 2d frame above. Also, varying the heights and bays of the 2 d frames to get an understanding of how varying stiffness along the height would produce any changes in the previous results.
2) Continuing from the 3d building analysis, conduct nonlinear time history analysis using the three element types of the 3 dimensional building presented previously to determine which elements type responses match.

Chapter 10.0

CONCLUSION

10.1 Nonlinear analysis

The investigation first examined the effects of modelling assumptions and two different computer programs on nonlinear response of 2 dimensional buildings. It was found that modelling assumptions significantly affected the pushover curves. From the nonlinear pushover analysis, it was found that Seismostruct reproduced conservative base shear displacement results compared to Opensees. The results from the nonlinear time history analysis showed that Seismostruct produced larger peak displacements compared to Opensees. The main reason this could have happened is due to the steel material models not being able to be used in complex loading situations.

11.0 References

1. ACI Committee 318 (2008) *Building Code Requirements for Structural Concrete (ACI 318-08), American Concrete Institute*. doi: 10.1016/0262-5075(85)90032-6.
2. Adam, C. and Jäger, C. (2012) 'Simplified collapse capacity assessment of earthquake excited regular frame structures vulnerable to P-delta', *Engineering Structures*. Elsevier Ltd, 44, pp. 159–173. doi: 10.1016/j.engstruct.2012.05.036.

3. Almeida, J. P., Tarquini, D. and Beyer, K. (2016) 'Modelling Approaches for Inelastic Behaviour of RC Walls: Multi-level Assessment and Dependability of Results', *Archives of Computational Methods in Engineering*. Springer Netherlands, 23(1), pp. 69–100. doi: 10.1007/s11831-014-9131-y.

4. Applied Technology Council (2017) 'Guidelines for Nonlinear Structural Analysis for Design of Buildings; Part IIb – Reinforced Concrete Moment Frames', *NIST GCR 17-917-46v3,* p. 135. doi: 10.6028/NIST.GCR.17-917-46v2.

5. Arnold, C. (2006) 'Earthquake Effects on Buildings', *Designing for Earthquakes, A Manual for Architects,* (December), p. 4.1-4.27.

6. Asce (2005) 'Seismic Design Requirements for Building Structures', 12, p. Chapter 12.
7. ATC (2009) 'Quantification of building seismic performance factors', *Fema P695,* (June), p. 421.
8. Berry, M., Parrish, M. and Eberhard, M. (2004) 'PEER Structural Performance Database User's Manual', (Version. 1.0), p. 38. Available at: https://nisee.berkeley.edu/spd/.

9. Calabrese, A., Almeida, J. P. and Pinho, R. (2010) *Numerical issues in distributed inelasticity modeling of RC frame elements for seismic analysis*, *Journal of Earthquake Engineering*. doi: 10.1080/13632461003651869.

10. Carr, A. J. 'Wit.carr.0001b.1', pp. 1–355.
11. Category, S. D. (2012) 'Seismic Loads Based on IBC 2012 / ASCE 7-10', pp. 160–179.

12. Celik, O. C. and Ellingwood, B. R. (2007) 'Probabilistic Assessment of Non-Ductile Reinforced Concrete Frames Susceptible to Mid-America Ground Motions', *School of Civil and Environmental Engineering,* Ph.D.(August).

13. Charney, F. a. (2008) ‘Unintended Consequences of Modeling Damping in Structures’, *Journal of Structural Engineering*, 134(4), pp. 581–592. doi: 10.1061/(ASCE)0733-9445(2008)134:4(581).

14. D’ARAGONA, M. G. (2015) ‘Post-Earthquake Assessment of Damaged Non-Ductile Buildings: Detailed Evaluation for Rational Reparability Decisions’.

15. Deierlein, G. G., Reinhorn, A. M. and Willford, M. R. (2010) ‘Nonlinear Structural Analysis For Seismic Design: A Guide for Practicing Engineers’, *NEHRP Seismic Design Technical Brief No. 4*, (4), p. 36.

16. Denavit, M. D. and Hajjar, J. F. (2013) ‘Description of geometric nonlinearity for beam-column analysis in OpenSees’, *Department of Civil and Environment Engieering Reports*. Available at: http://hdl.handle.net/2047/d20003280.

17. Dimitrios, L. (2013) ‘Sidesway collapse of deteriorating structural systems under seismic excitations’, *PhD thesis*, 53(9), pp. 1689–1699. doi: 10.1017/CBO9781107415324.004.

18. Sang-Hyun, Kyung-Won Min, Lan Chung, Sung-Kyung Lee, Myoung-Kyu Lee, Jae-Seung Hwang, Seung-Bok Choi, and H.-G. L. (2007) ‘Distributed and Concentrated Inelasticity Beam-Column Elements used in Earthquake Engineering’, *Journal of Intelligent Material Systems and Structures*, 18(19), p. 1111–1120.

19. Esmaili, O., Zareian, F. and Ludwig, L. G. (2012) ‘Seismic Performance of Modern Commercial Low - rise Reinforced Concrete Frame Buildings in Los Angeles County’, *15th World Conference on Earthquake Engineering, Lisbon Portugal*.

20. European Commitee for Standardization (2004) ‘Eurocode 8: Design of structures for earthquake resistance - Part 1 : General rules, seismic actions and rules for buildings’, *European Committee for Standardization*, 1(English), p. 231. doi: [Authority: The European Union per Regulation 305/2011, Directive 98/34/EC, Directive 2004/18/EC].

21. Fajfar, P. and Krawinkler, H. (2004) ‘Performance-based seismic design concepts and implementation’, (September), pp. 89–100.

22. Fedak, L. K. (2012) ‘Evaluation of Plastic Hinge Models and Inelastic Analysis Tools for

Performance-Based Seismic Design of Rc Bridge Columns', p. 157.

23. Hardyniec, A. B., Moen, C. D. and West, R. L. (2014) 'An Investigation of the Behavior of Structural Systems with Modeling Uncertainties An Investigation of the Behavior of Structural Systems with Modeling Uncertainties'.

24. Haselton, C. B. and Deierlein, G. G. (2008) 'Assessing Seismic Collapse Safety of Modern Reinforced Concrete Moment-Frame Buildings', *Civil Engineering*, 137(February), pp. 481–491. doi: 10.1061/(ASCE)ST.1943-541X.0000318.

25. Haselton, C. B., Goulet, C. A., Mitrani-reiser, J., Beck, J. L., Deierlein, G. G., Porter, K. A. and Stewart, J. P. (2008) 'PACIFIC EARTHQUAKE ENGINEERING An Assessment to Benchmark the Seismic Performance of a Code-Conforming Reinforced Concrete Moment-Frame Building An Assessment to Benchmark the Seismic Performance of a Code-Conforming Reinforced Concrete Moment-Frame Build', (August 2008), pp. 1–360.

26. Haselton, C. B., Liel, A. B., Dean, B. S., Chou, J. H. and Deierlein, G. G. (2007) 'Seismic Collapse Safety and Behavior of Modern Reinforced Concrete Moment Frame Buildings', *Structural Engineering Research Frontiers*, pp. 1–14. doi: 10.1061/40944(249)22.

27. Haselton, C. B., Liel, A. B. and Deierlein, G. G. (2009) 'Simulating structural collapse due to earthquakes: model idealization, model calibration, and numerical solution algorithms', *Computational Methods in Structural Dynamics and Earthquake Engineering (COMPDYN)*.

28. Haselton, C. B., Liel, A. B., Deierlein, G. G., Dean, B. S. and Chou, J. H. (2011) 'Seismic Collapse Saefty of Reinforced Concrete Buildings. 1: Assessment of Ductile Moment Frames', *Journal of Civil Engineering*, 137(February), pp. 481–491. doi: 10.1061/(ASCE)ST.1943-541X.0000318.

29. Haselton, C. B., Liel, A. B. and Lange, S. T. (2008) 'Beam-Column Element Model Calibrated for Predicting Flexural Response Leading to Global Collapse of RC Frame Buildings', *Peer 2007*, 3(May).

30. Hashemi, M. J., Mosqueda, G., Lignos, D. G., Medina, R. A. and Miranda, E. (2016)

31. 'Assessment of Numerical and Experimental Errors in Hybrid Simulation of Framed Structural Systems through Collapse', *Journal of Earthquake Engineering*, 20(6), pp. 885–909. doi:

10.1080/13632469.2015.1110066.

32. Hsu, T. T. C. and Mo, Y. L. (2010) *Unified Theory of Concrete Structures*, *Unified Theory of Concrete Structures*. doi: 10.1002/9780470688892.

33. Ibarra, L. F. and Krawinkler, H. (2005) 'Global Collapse of Frame Structures under Seismic Excitations', *Evaluation*, (152), pp. 1–301. doi: 10.1002/eqe.

34. Ibarra, L. F., Medina, R. A. and Krawinkler, H. (2005) 'Hysteretic models that incorporate strength and stiffness deterioration', *Earthquake Engineering and Structural Dynamics*, 34(12), pp. 1489–1511. doi: 10.1002/eqe.495.

35. Infilled, M., Frame, S. and Curves, F. (2012) 'Keywords: Seismic Loss Estimation, Masonry Infilled Steel Frame, Incremental Dynamic Analysis (IDA), Fragility Curves 1.', pp. 1–16.

36. Krawinkler, H. and Miranda, E. (2004) 'Chapter 9 PERFORMANCE-BASED EARTHQUAKE ENGINEERING', pp. 1–41.

37. Ladjinovic, D., Raseta, A., Radujkovic, A. and Folic, R. (2012) 'Comparison of Structural Models for Seismic Analysis of Multi-Storey Frame Buildings', *15th World Conference on Earthquake Engineering, Lisbon Portugal*.

38. Lignos, D. G. and Krawinkler, H. (2013) 'Development and Utilization of Structural Component Databases for Performance-Based Earthquake Engineering', *Journal of Structural Engineering*, 139(8), pp. 1382–1394. doi: 10.1061/(ASCE)ST.1943-541X.0000646.

39. Mashaly, E. S., El-Heweity, M., Abou-Elfath, H. and Ramadan, M. (2011) 'A new beam-column model for seismic analysis of RC frames - Part I: Model derivation', *Alexandria Engineering Journal*. Faculty of Engineering, Alexandria University, 50(4), pp. 313–320. doi: 10.1016/j.aej.2012.01.003.

40. Mazzoni, S., McKenna, F., Scott, M. H. and Fenves, G. L. (2007) 'OpenSees command language manual', *Pacific Earthquake Engineering Research (PEER) Center*, p. 451. Available at:http://opensees.berkeley.edu/OpenSees/manuals/usermanual/OpenSeesCommandLanguageManual.pdf.

41. Melo, J., Varum, H. and Rossetto, T. (2014) 'Nonlinear Modelling of Rc Elements Built With Plain Reinforcing Bars', *2Ecees*, (August), pp. 3–4.

42. NEHRP Consultants Joint Venture (2013) ‘Nonlinear Analysis Research and Development Program for Performance Based Seismic Engineering’, *Nist Gcr 14-917-27*.

43. McKenna, F. (2011). OpenSees: A Framework for Earthquake Engineering Simulation. *Computing in Science & Engineering*, 13(4), pp.58-66.

44. Framework, A. C. and Assessment, E. P. (2004) ‘Performance-Based Seismic Design – Concepts and Implementation . P . Fajfar and H . Krawinkler , Editors , PEER Special Publication ’, (September), pp. 1–12.

45. Paspuleti, C. (2002) ‘Seismic Analysis of an Older Reinforced Concrete Frame Structure’.

46. Pioldi, F. and Rizzi, E. (2015) ‘On modal identification of structures from earthquake response signals by a refined Frequency Domain Decomposition approach’, (December).

47. Rahaie, A. R. and Fallah Nafari, S. (2013) ‘A comparison between lumped and distributed plasticity approaches in the pushover analysis results of a pc frame bridge’, *International Journal of Civil Engineering*, 11(4 A), pp. 217–225.

48. Reshotkina, S. and Lau, D. (2012) ‘Damage-Based Degradations in Stiffness and Strength in the Post-Peak Behaviour in Seismic Progressive Collapse of Reinforced Concrete Structures’, *15th World*

49. Restrepo, J. I. (2018) ‘Advanced Seismic Design of Structures’, pp. 1–7.

50. Rodrigues, H., Varum, H., Arêde, A. and Costa, A. (2012) ‘Comparative efficiency analysis of different nonlinear modelling strategies to simulate the biaxial response of RC columns’, *Earthquake Engineering and Engineering Vibration*, 11(4), pp. 553–566. doi: 10.1007/s11803-012-0141-1.

51. Roh, H., Reinhorn, A. M. and Lee, J. S. (2012) ‘Power spread plasticity model for inelastic analysis of reinforced concrete structures’, *Engineering Structures*. Elsevier Ltd, 39, pp. 148–161. doi: 10.1016/j.engstruct.2012.01.019.

52. Rossetto, T., Gehl, P., Minas, S., Galasso, C., Duffour, P., Douglas, J. and Cook, O. (2016) ‘FRACAS: A capacity spectrum approach for seismic fragility assessment including record-to-record variability’, *Engineering Structures*. The Authors, 125, pp. 337–348 d. oi:10.1016/j.engstruct.2016.06.043 ‘S0141029612000703’.

53. Schotanus, M. I. (2002) ‘Fragility analysis of reinforced concrete structures using a response surface approach’, pp. 1–86.

54. Segura, C. L. (2011) ‘Implementation of Lumped Plasticity Models and Developments in an Object Oriented Nonlinear Finite Element Code’, p. 165.

55. Seismosoft Ltd. (2016) ‘SeismoStruct User Manual 2016’.

56. SeismoSoft, S. (2010). SeismoStruct is a FEM-program developed for the analytical assessment of structures subjected to earthquake strong motion. Seismosoft Ltd, Version 7.0.6, 2016

57. Semere, S. A. (2016) ‘Investigation of RC Structural Behaviour of Wall-Equivalent Dual System through Non-Linear Analyses.’, (June).

58. Sudret, B., Mai, C. and Konakli, K. (2014) ‘Assessment of the lognormality assumption of seismic fragility curves using non-parametric representations’, (March 2012), pp. 25–41. doi: 10.1002/eqe.

59. Taucer, F. F., Spacone, E. and Filippou, F. C. (1991) ‘A Fiber Beam-Column Element for Seismic Response Analysis of Reinforced Concrete Structures’, *Ucb/Eerc-91/17*, (December 1991), p. 138. Available at: www.ce.berkeley.edu/~filippou/Research/.../Reports/EERC91-17.pdf.

60. Zareian, F. (2006) ‘Simplified performance-based earthquake engineering’, *ProQuest Dissertations and Theses*, (169), p. 338.

61. Zareian, F. and Medina, R. A. (2010) ‘A practical method for proper modeling of structural damping in inelastic plane structural systems’, *Computers and Structures*. Elsevier Ltd, 88(1–2), pp. 45–53. doi: 10.1016/j.compstruc.2009.08.001.

62. Zendaoui, A., Kadid, A. and Yahiaoui, D. (2016) ‘Comparison of Different Numerical Models of RC Elements for Predicting the Seismic Performance of Structures’, *International Journal of Concrete Structures and Materials*. Springer Netherlands, 10(4), pp. 461–478. doi:

12.0 APPENDIX A

```
Cory George, University College London, 2017-2018
# Dissertation - Seismic Analysis and Fragility Assessment of RC
Structures
# 2-Story Reinforced Concrete Frame with Concentrated Plasticity
# Centre line Model with Concentrated Plastic Hinges at Beam-Column
Joint
# Units: kips, inches, seconds
#This script was modified from the script produced by Laura Eads (2013)
# Element and Node ID conventions:
#     1xy = frame columns with springs at both ends
#     2xy = frame beams with springs at both ends
#     6xy = trusses linking frame and P-delta column
#     7xy = P-delta columns
#     3,xya = frame column rotational springs
#     4,xya = frame beam rotational springs
#     5,xya = P-delta column rotational springs
#     where:
#           x = Pier or Bay #
#           y = Floor or Story #
#           a = an integer describing the location relative to beam-
column joint (see description where elements and nodes are defined)

#####################################################################
#          Set Up & Source Definition
#######################################################################
wipe all;
# clear memory of past model definitions
model BasicBuilder -ndm 2 -ndf 3;# Define the model builder, ndm =
#dimension, ndf = #dofs
source DisplayModel2D.tcl;# procedure for displaying a 2D perspective
of model
source DisplayPlane.tcl;# procedure for displaying a plane in a model
source rotSpring2DModIKModel.tcl;  # procedure for defining a rotational
spring (zero-length element)
source rotLeaningCol.tcl;# procedure for defining a rotational spring
(zero-length element) with very small stiffness

# define UNITS ----------------------------------------------------------
set in 1.;                       # define basic units -- output units
set kip 1.;                      # define basic units -- output units
set sec 1.;                      # define basic units -- output units
set LunitTXT "inch";             # define basic-unit text for output
set FunitTXT "kip";              # define basic-unit text for output
set TunitTXT "sec";              # define basic-unit text for output
set ft [expr 12.*$in];           # define engineering units
set ksi [expr $kip/pow($in,2)];
set psi [expr $ksi/1000.];
set lbf [expr $psi*$in*$in];                    # pounds force
set pcf [expr $lbf/pow($ft,3)];                 # pounds per cubic foot
set psf [expr $lbf/pow($ft,3)];                 # pounds per square foot
set in2 [expr $in*$in];                         # inch^2
set in4 [expr $in*$in*$in*$in];                 # inch^4
set cm [expr $in/2.54];  # centimeter, needed for displacement input in
MultipleSupport excitation
```

```
set PI [expr 2*asin(1.0)];                        # define constants
set g [expr 32.2*$ft/pow($sec,2)];              # gravitational
acceleration
set Ubig 1.e10;                                  # a really large number
set Usmall [expr 1/$Ubig];                       # a really small number

########################################################################
#          Define Analysis Type
#######################################################################
# Define type of analysis:  "pushover" = pushover;  "dynamic" = dynamic
set analysisType "dynamic";

if {$analysisType == "pushover"} {
set dataDir Concentrated-Pushover-Output;# name of output folder
file mkdir $dataDir;  create output folder
}
if {$analysisType == "dynamic"} {
set dataDir Concentrated-Dynamic-Output;# name of output folder
file mkdir $dataDir;# create output folder
}

########################################################################
#          Define Building Geometry, Nodes, and Constraints
#######################################################################
# define structure-geometry parameters
set NStories 2;              # number of stories
set NBays 1;        # number of frame bays (not including bay for P-
delta column)
set WBay      [expr 16.4*12.0]; # bay width in inches
set HStory1   [expr 15.0*12.0]; # 1st story height in inches
set HStoryTyp [expr 12.0*12.0]; #story height of other stories (inches)
set HBuilding [expr $HStory1 + ($NStories-1)*$HStoryTyp];# Total height
of frame

# calculate locations of beam/column joints:
set Pier1  0.0;   # leftmost column line ,see figure.
set Pier2  [expr $Pier1 + $WBay];
set Pier3  [expr $Pier2 + $WBay];    # P-delta column line
set Floor1 0.0;                     # ground floor
set Floor2 [expr $Floor1 + $HStory1];
set Floor3 [expr $Floor2 + $HStoryTyp];

# calculate joint offset distance for beam plastic hinges
set phlat23 [expr 0.0];                                        #
lateral dist from beam-col joint to loc of hinge on Floor 2
#number of modes
set numModes 5                     #Command stating how many eigen
values to want as output

# calculate nodal masses -- lump floor masses at frame nodes
set g 386.2;      # acceleration due to gravity in/sec2
set Floor2Weight 21.3;  # weight of Floor 2 in kips
set Floor3Weight 16.2;# weight of Floor 3 in kips
set WBuilding  [expr $Floor2Weight + $Floor3Weight] # total building
weight
set NodalMass2 [expr ($Floor2Weight/$g) / (2.0)];# mass at each node on
Floor 2
```

```
set NodalMass3 [expr ($Floor3Weight/$g) / (2.0); # mass at each node on
Floor 3
set Negligible 1e-9 # a very small no. to avoid problems with zero

# define nodes and assign masses to beam-column intersections of frame
# command:  node nodeID xcoord ycoord -mass mass_dof1 mass_dof2
mass_dof3
# nodeID convention:  "xy" where x = Pier # and y = Floor #
node 11 $Pier1 $Floor1;
node 21 $Pier2 $Floor1;
node 31 $Pier3 $Floor1;
node 12 $Pier1 $Floor2 -mass $NodalMass2 $Negligible $Negligible;
node 22 $Pier2 $Floor2 -mass $NodalMass2 $Negligible $Negligible;
node 32 $Pier3 $Floor2;
node 13 $Pier1 $Floor3 -mass $NodalMass3 $Negligible $Negligible;
node 23 $Pier2 $Floor3 -mass $NodalMass3 $Negligible $Negligible;
node 33 $Pier3 $Floor3;

# define extra nodes for plastic hinge rotational springs
# nodeID convention:  "xya" where x = Pier #, y = Floor #, a = location
relative to beam-column joint
# "a" convention: 1 = left,outer; 2 = left,inner; 3 = right,inner; 4 =
right,outer
# "a" convention: 5 = down,outer; 6 = down,inner; 7 = up,inner; 8 =
up,outer
# column hinges at bottom of Story 1 (base)
node 117 $Pier1 $Floor1;
node 217 $Pier2 $Floor1;
# column hinges at top of Story 1
node 126 $Pier1 $Floor2;
node 226 $Pier2 $Floor2;
node 326 $Pier3 $Floor2; # zero-stiffness spring will be used on p-
delta column
# column hinges at bottom of Story 2
node 127 $Pier1 $Floor2;
node 227 $Pier2 $Floor2;
node 327 $Pier3 $Floor2;# zero-stiffness spring will be used on p-delta
column
# column hinges at top of Story 2
node 136 $Pier1 $Floor3;
node 236 $Pier2 $Floor3;
node 336 $Pier3 $Floor3; # zero-stiffness spring will be used on p-
delta column

# beam hinges at Floor 2
node 122 [expr $Pier1 + $phlat23] $Floor2;
node 223 [expr $Pier2 - $phlat23] $Floor2;
# beam hinges at Floor 3
node 132 [expr $Pier1 + $phlat23] $Floor3;
node 233 [expr $Pier2 - $phlat23] $Floor3;

# constrain beam-column joints in a floor to have the same lateral
displacement using the "equalDOF" command
# command: equalDOF $MasterNodeID $SlaveNodeID $dof1 $dof2...
set dof1 1; # constrain movement in dof 1 (x-direction)
equalDOF 12 22 $dof1;  # Floor 2:  Pier 1 to Pier 2
equalDOF 12 32 $dof1;  # Floor 2:  Pier 1 to Pier 3
equalDOF 13 23 $dof1;  # Floor 3:  Pier 1 to Pier 2
```

```
equalDOF 13 33 $dof1;  # Floor 3:  Pier 1 to Pier 3

# assign boundary condidtions with "fix" command:  fix nodeID dxFixity
dyFixity rzFixity
# fixity values: 1 = constrained; 0 = unconstrained
# fix the base of the building; pin P-delta column at base
fix 11 1 1 1;
fix 21 1 1 1;
fix 31 1 1 0;                # P-delta column is pinned

########################################################################
#          Define Section Properties and Elements
#######################################################################
# define material properties
set fc 5699.98*psi; # characteristic concrete compressive strength
set Es [expr 57*$ksi*pow($fc/$psi,0.5);# concrete Young's Modulus
puts "Es [expr 57*$ksi*pow($fc/$psi,0.5)]"

# Section Properties:
set HCol [expr 17.96*$in];# square-Column width
set BCol $HCol;
set HBeam [expr 17.96*$in];# Beam depth -- perpendicular to bending
axis
set BBeam [expr 17.96*$in];# Beam width -- parallel to bending axis

# column section properties:
set Acol_12 [expr $HCol*$BCol]; # cross-sectional area
puts "Acol_12 [expr $HCol*$BCol]"
set Icol_12 [expr 1./12*$BCol*pow($HCol,3)];# about-local-z Rect-Column
gross moment of inertial
puts "Icol_12 [expr 1./12*$BCol*pow($HCol,3)]"

# define RC column section for Story 1 & 2
#set Acol_12  69;      # cross-sectional area
#set Icol_12  319;     # moment of inertia
set Mycol_12 3100;     # yield moment,input from hasselton et al.(2007)
database
# beam sections properties:
set Abeam_23 [expr $HBeam*$BBeam];# rectuangular-Beam cross-sectional
area
puts "Abeam_23 [expr $HBeam*$BBeam]"
set Ibeam_23 [expr 1./12*$BBeam*pow($HBeam,3)];# about-local-z Rect-
Beam moment of inertia
puts "Ibeam_23 [expr 1./12*$BBeam*pow($HBeam,3)]"



# define RC beam section for Floor 2 & 3
#set Abeam_23  69;# cross-sectional area (full section properties)
#set Ibeam_23  319; # moment of inertia  (full section properties)
set Mybeam_23  3100;# yield moment at plastic hinge location ,from
Hasselton et al.(2007) database

# note: Hinges are formed right at the beam-column joint

# determine stiffness modifications to equate the stiffness of the
spring-elastic element-spring subassembly to the stiffness of the
actual frame member
```

```
# Reference:  Ibarra, L. F., and Krawinkler, H. (2005). "Global
collapse of frame structures under seismic excitations," Technical
Report 152,
#             The John A. Blume Earthquake Engineering Research Center,
Department of Civil Engineering, Stanford University, Stanford, CA.
# calculate modified section properties to account for spring stiffness
being in series with the elastic element stiffness
set n 10.0;      # stiffness multiplier for rotational spring

# calculate modified moment of inertia for elastic elements
set Icol_12mod  [expr $Icol_12*($n+1.0)/$n]; # modified moment of
inertia for columns in Story 1 & 2
set Ibeam_23mod [expr $Ibeam_23*($n+1.0)/$n];# modified moment of
inertia for beams in Floor 2 & 3

# calculate modified rotational stiffness for plastic hinge springs

set Ks_col_1   [expr $n*6.0*$Es*$Icol_12mod/$HStory1];# rotational
stiffness of Story 1 column springs
set Ks_col_2   [expr $n*6.0*$Es*$Icol_12mod/$HStoryTyp];# rotational
stiffness of Story 2 column springs
set Ks_beam_23 [expr $n*6.0*$Es*$Ibeam_23mod/$WBay];
# rotational stiffness of Floor 2 & 3 beam springs

# set up geometric transformations of element
set PDeltaTransf 1;
geomTransf PDelta $PDeltaTransf;                                  #
PDelta transformation

# define elastic column elements using "element" command
# command: element elasticBeamColumn $eleID $iNode $jNode $A $E $I
$transfID
# eleID convention:  "1xy" where 1 = col, x = Pier #, y = Story #
# Columns Story 1
element elasticBeamColumn  111  117 126 $Acol_12 $Es $Icol_12mod
$PDeltaTransf;   # Pier 1
element elasticBeamColumn  121  217 226 $Acol_12 $Es $Icol_12mod
$PDeltaTransf;   # Pier 2
# Columns Story 2
element elasticBeamColumn  112  127 136 $Acol_12 $Es $Icol_12mod
$PDeltaTransf;   # Pier 1
element elasticBeamColumn  122  227 236 $Acol_12 $Es $Icol_12mod
$PDeltaTransf;   # Pier 2

# define elastic beam elements
# eleID convention:  "2xy" where 2 = beam, x = Bay #, y = Floor #
# Beams Story 1
element elasticBeamColumn  212  122 223 $Abeam_23 $Es $Ibeam_23mod
$PDeltaTransf;
# Beams Story 2
element elasticBeamColumn  222  132 233 $Abeam_23 $Es $Ibeam_23mod
$PDeltaTransf;

# define p-delta columns and rigid links
# command: element truss $eleID $iNode $jNode $A $materialID
set TrussMatID 600; # define a material ID
set Arigid 10000.0; # define area of truss section (make much larger
than A of frame elements)
```

```
set Irigid 100000.0;# moment of inertia for p-delta columns  (make much
larger than I of frame elements)
uniaxialMaterial Elastic $TrussMatID $Es;# define truss material
# rigid links
# eleID convention:  6xy, 6 = truss link, x = Bay #, y = Floor #
element truss  622 22 32 $Arigid $TrussMatID; # Floor 2
element truss  623 23 33 $Arigid $TrussMatID; # Floor 3
# p-delta columns
# eleID convention:  7xy, 7 = p-delta columns, x = Pier #, y = Story #
element elasticBeamColumn  731  31  326 $Arigid $Es $Irigid
$PDeltaTransf;   # Story 1
element elasticBeamColumn  732  327 336 $Arigid $Es $Irigid
$PDeltaTransf;   # Story 2

# display the model with the node numbers
DisplayModel2D NodeNumbers

########################################################################
#          Define Rotational Springs for Plastic Hinges
########################################################################
# define rotational spring properties and create spring elements using
"rotSpring2DModIKModel" procedure
# rotSpring2DModIKModel creates a uniaxial material spring with a
bilinear response based on Modified Ibarra Krawinkler Deterioration
Model
# references provided in rotSpring2DModIKModel.tcl
# command: rotSpring2DModIKModel  id    ndR  ndC     K   asPos  asNeg
MyPos      MyNeg      LS    LK    LA    LD   cS   cK   cA   cD  th_p+
th_p-   th_pc+   th_pc-  Res+   Res-   th_u+   th_u-    D+     D-

# input values for Story 1 column springs
set McMy 1.3;                 # ratio of capping moment to yield moment,
Mc / My
set LS 1000.0;                # basic strength deterioration (a very
large # = no cyclic deterioration)
set LK 1000.0;                # unloading stiffness deterioration (a very
large # = no cyclic deterioration)
set LA 1000.0;                # accelerated reloading stiffness
deterioration (a very large # = no cyclic deterioration)
set LD 1000.0;                # post-capping strength deterioration (a
very large # = no deterioration)
set cS 1.0;                   # exponent for basic strength deterioration
(c = 1.0 for no deterioration)
set cK 1.0;                   # exponent for unloading stiffness
deterioration (c = 1.0 for no deterioration)
set cA 1.0;                   # exponent for accelerated reloading
stiffness deterioration (c = 1.0 for no deterioration)
set cD 1.0;                   # exponent for post-capping strength
deterioration (c = 1.0 for no deterioration)
set th_pP 0.025;        # plastic rot capacity for pos loading
set th_pN 0.025;        # plastic rot capacity for neg loading
set th_pcP 0.15;              # post-capping rot capacity for pos loading
set th_pcN 0.15;              # post-capping rot capacity for neg loading
set ResP 0.4;                 # residual strength ratio for pos loading
set ResN 0.4;                 # residual strength ratio for neg loading
set th_uP 0.4;                # ultimate rot capacity for pos loading
set th_uN 0.4;                # ultimate rot capacity for neg loading
```

```
set DP 1.0;                   # rate of cyclic deterioration for pos
loading
set DN 1.0;                   # rate of cyclic deterioration for neg
loading
set a_mem [expr ($n+1.0)*($Mycol_12*($McMy-1.0)) / ($Ks_col_1*$th_pP)];
                  # strain hardening ratio of spring
set b [expr ($a_mem)/(1.0+$n*(1.0-$a_mem))];
            # modified strain hardening ratio of spring (Ibarra &
Krawinkler 2005, note: Eqn B.5 is incorrect)

# define column springs
# Spring ID: "3xya", where 3 = col spring, x = Pier #, y = Story #, a =
location in story
# "a" convention: 1 = bottom of story, 2 = top of story
# col springs @ bottom of Story 1 (at base)
rotSpring2DModIKModel 3111 11 117 $Ks_col_1 $b $b $Mycol_12 [expr -
$Mycol_12] $LS $LK $LA $LD $cS $cK $cA $cD $th_pP $th_pN $th_pcP
$th_pcN $ResP $ResN $th_uP $th_uN $DP $DN;
rotSpring2DModIKModel 3211 21 217 $Ks_col_1 $b $b $Mycol_12 [expr -
$Mycol_12] $LS $LK $LA $LD $cS $cK $cA $cD $th_pP $th_pN $th_pcP
$th_pcN $ResP $ResN $th_uP $th_uN $DP $DN;
#col springs @ top of Story 1 (below Floor 2)
rotSpring2DModIKModel 3112 12 126 $Ks_col_1 $b $b $Mycol_12 [expr -
$Mycol_12] $LS $LK $LA $LD $cS $cK $cA $cD $th_pP $th_pN $th_pcP
$th_pcN $ResP $ResN $th_uP $th_uN $DP $DN;
rotSpring2DModIKModel 3212 22 226 $Ks_col_1 $b $b $Mycol_12 [expr -
$Mycol_12] $LS $LK $LA $LD $cS $cK $cA $cD $th_pP $th_pN $th_pcP
$th_pcN $ResP $ResN $th_uP $th_uN $DP $DN;

# recompute strain hardening since Story 2 is not the same height as
Story 1
set a_mem [expr ($n+1.0)*($Mycol_12*($McMy-1.0)) / ($Ks_col_2*$th_pP)];
      # strain hardening ratio of spring
set b [expr ($a_mem)/(1.0+$n*(1.0-$a_mem))];
            # modified strain hardening ratio of spring (Ibarra &
Krawinkler 2005, note: there is mistake in Eqn B.5)
# col springs @ bottom of Story 2 (above Floor 2)
rotSpring2DModIKModel 3121 12 127 $Ks_col_2 $b $b $Mycol_12 [expr -
$Mycol_12] $LS $LK $LA $LD $cS $cK $cA $cD $th_pP $th_pN $th_pcP
$th_pcN $ResP $ResN $th_uP $th_uN $DP $DN;
rotSpring2DModIKModel 3221 22 227 $Ks_col_2 $b $b $Mycol_12 [expr -
$Mycol_12] $LS $LK $LA $LD $cS $cK $cA $cD $th_pP $th_pN $th_pcP
$th_pcN $ResP $ResN $th_uP $th_uN $DP $DN;
#col springs @ top of Story 2 (below Floor 3)
rotSpring2DModIKModel 3122 13 136 $Ks_col_2 $b $b $Mycol_12 [expr -
$Mycol_12] $LS $LK $LA $LD $cS $cK $cA $cD $th_pP $th_pN $th_pcP
$th_pcN $ResP $ResN $th_uP $th_uN $DP $DN;
rotSpring2DModIKModel 3222 23 236 $Ks_col_2 $b $b $Mycol_12 [expr -
$Mycol_12] $LS $LK $LA $LD $cS $cK $cA $cD $th_pP $th_pN $th_pcP
$th_pcN $ResP $ResN $th_uP $th_uN $DP $DN;

# create region for frame column springs
region 1 -ele 3111 3211 3112 3212 3121 3221 3122 3222;

# define beam springs
# Spring ID: "4xya", where 4 = beam spring, x = Bay #, y = Floor #, a =
location in bay
# "a" convention: 1 = left end, 2 = right end
```

```
# redefine the rotations since they are not the same
set th_pP 0.025;
set th_pN 0.025;
set th_pcP 0.15;
set th_pcN 0.15;
set a_mem [expr ($n+1.0)*($Mybeam_23*($McMy-1.0)) /
($Ks_beam_23*$th_pP)]; # strain hardening ratio of spring
set b [expr ($a_mem)/(1.0+$n*(1.0-$a_mem))];
                 # modified strain hardening ratio of spring (Ibarra &
Krawinkler 2005, note: there is mistake in Eqn B.5)
#beam springs at Floor 2
rotSpring2DModIKModel 4121 12 122 $Ks_beam_23 $b $b $Mybeam_23 [expr -
$Mybeam_23] $LS $LK $LA $LD $cS $cK $cA $cD $th_pP $th_pN $th_pcP
$th_pcN $ResP $ResN $th_uP $th_uN $DP $DN;
rotSpring2DModIKModel 4122 22 223 $Ks_beam_23 $b $b $Mybeam_23 [expr -
$Mybeam_23] $LS $LK $LA $LD $cS $cK $cA $cD $th_pP $th_pN $th_pcP
$th_pcN $ResP $ResN $th_uP $th_uN $DP $DN;
#beam springs at Floor 3
rotSpring2DModIKModel 4131 13 132 $Ks_beam_23 $b $b $Mybeam_23 [expr -
$Mybeam_23] $LS $LK $LA $LD $cS $cK $cA $cD $th_pP $th_pN $th_pcP
$th_pcN $ResP $ResN $th_uP $th_uN $DP $DN;
rotSpring2DModIKModel 4132 23 233 $Ks_beam_23 $b $b $Mybeam_23 [expr -
$Mybeam_23] $LS $LK $LA $LD $cS $cK $cA $cD $th_pP $th_pN $th_pcP
$th_pcN $ResP $ResN $th_uP $th_uN $DP $DN;

# create region for beam springs
region 2 -ele 4121 4122 4131 4132;

# define p-delta column spring: zero-stiffness elastic spring
#Spring ID: "5xya" where 5 = leaning column spring, x = Pier #, y =
Story #, a = location in story
# "a" convention: 1 = bottom of story, 2 = top of story
#           ElemID ndR ndC
rotLeaningCol 5312 32 326;   # top of Story 1
rotLeaningCol 5321 32 327;   # bottom of Story 2
rotLeaningCol 5322 33 336;   # top of Story 2

# create region for P-Delta column springs
region 3 -ele 5312 5321 5322;

######################################################################
#                        Eigenvalue Analysis
#######################################################################
#set lambda [eigen  $numModes];

# calculate frequencies and periods of the structure
#---------------------------------------------------
#set omega {}
#set f {}
#set T {}
#set pi 3.141593

#foreach lam $lambda {
#lappend omega [expr sqrt($lam)]
#lappend f [expr sqrt($lam)/(2*$pi)]
#lappend T [expr (2*$pi)/sqrt($lam)]
#}
```

```
#puts "periods are $T"

#######################################################################
#                        Eigenvalue Analysis
########################################################################
set pi [expr 2.0*asin(1.0)];                             # Definition
of pi
set nEigenI 1;                                                      #
mode i = 1
set nEigenJ 2;                                                      #
mode j = 2
set lambdaN [eigen [expr $nEigenJ]];                     # eigenvalue
analysis for nEigenJ modes
set lambdaI [lindex $lambdaN [expr 0]];                  # eigenvalue
mode i = 1
set lambdaJ [lindex $lambdaN [expr $nEigenJ-1]];         # eigenvalue
mode j = 2
set w1 [expr pow($lambdaI,0.5)];                         # w1 (1st mode
circular frequency)
set w2 [expr pow($lambdaJ,0.5)];                         # w2 (2nd mode
circular frequency)
set T1 [expr 2.0*$pi/$w1];                                     # 1st
mode period of the structure
set T2 [expr 2.0*$pi/$w2];                                     # 2nd
mode period of the structure
puts "T1 = $T1 s"
puts "T2 = $T2 s"

#######################################################################
#               Gravity Loads & Gravity Analysis
########################################################################
# apply gravity loads
pattern Plain 101 Constant {

# point loads on leaning column nodes
set P_PD2 [expr -17.9];           # Floor 2 gravity columns
set P_PD3 [expr -12.9];           # Floor 3 gravity columns
load 32 0.0 $P_PD2 0.0;           # Floor 2
load 33 0.0 $P_PD3 0.0;           # Floor 3

# point loads on frame column nodes
set P_F2 [expr 0.5*(-1.0*$Floor2Weight-$P_PD2)];   # load on each frame
node in Floor 2
set P_F3 [expr 0.5*(-1.0*$Floor3Weight-$P_PD3)];   # load on each frame
node in Floor 3
# Floor 2 loads
load 12 0.0 $P_F2 0.0;
load 22 0.0 $P_F2 0.0;
# Floor 3 loads
load 13 0.0 $P_F3 0.0;
load 23 0.0 $P_F3 0.0;
}
# Gravity-analysis: load-controlled static analysis
set Tol 1.0e-6;                                    # convergence
tolerance for test
variable constraintsTypeGravity Plain;             # default
constraints $constraintsTypeGravity;               # how it handles
boundary conditions
```

```
numberer RCM;                                          # renumber dof's to
minimize band-width (optimization), if you want to
system BandGeneral;                                    # how to store and
solve the system of equations in the analysis (large model: try
UmfPack)
test NormDispIncr $Tol 6;                              # determine if
convergence has been achieved at the end of an iteration step
algorithm Newton;                                      # use Newton's
solution algorithm: updates tangent stiffness at every iteration
set NstepGravity 10;                                   # apply gravity in
10 steps
set DGravity [expr 1.0/$NstepGravity];                 # load increment
integrator LoadControl $DGravity;                      # determine the
next time step for an analysis
analysis Static;                                       # define type of
analysis static or transient
analyze $NstepGravity;                                 # apply gravity

# maintain constant gravity loads and reset time to zero
loadConst -time 0.0
puts "Model Built"

########################################################################
#              Recorders
########################################################################
# record drift histories
recorder Drift -file $dataDir/Drift-Story1.out -time -iNode 11 -jNode
12 -dof 1 -perpDirn 2; #interstory drift between 1s and ground floor
recorder Drift -file $dataDir/Drift-Story2.out -time -iNode 12 -jNode
13 -dof 1 -perpDirn 2; # interstory drift between 1st and 2nd floor
recorder Drift -file $dataDir/Drift-Roof.out -time -iNode 11 -jNode 13
-dof 1 -perpDirn 2;  # roof drift with control node 13
recorder Node -file $dataDir/Displ.out -time -node 12 13 -dof 1 disp;
#roof displacement time time history of node 13
recorder Node -file $dataDir/Accel.out -time -node 13 -dof 1 disp;
#accleration time history at node 13
# record base shear history
recorder Node -file $dataDir/Vbase.out -time -node 117 217 31 -dof 1
reaction;  # base shear recorded at rotational spring elements at
original frame bases
# record response history of all frame column springs (one file for
moment, one for rotation)
recorder Element -file $dataDir/MRFcol-Mom-Hist.out -time -region 1
force;   # moment recorded at for the rotational springs connected to
columns in original frame
recorder Element -file $dataDir/MRFcol-Rot-Hist.out -time -region 1
deformation; # rotation of rotational springs connected to cols in
original frame
# record response history of all frame beam springs (one file for
moment, one for rotation)
recorder Element -file $dataDir/MRFbeam-Mom-Hist.out -time -region 2
force;   # same as columns
recorder Element -file $dataDir/MRFbeam-Rot-Hist.out -time -region 2
deformation; # same as columns

# record response history of all P-Delta column springs (one file for
moment, one for rotation)
```

```
recorder Element -file $dataDir/PDcol-Mom-Hist.out -time -region 3
force; # same as columns
recorder Element -file $dataDir/PDcol-Rot-Hist.out -time -region 3
deformation; # same as columns

###################################################################
#                              Analysis Section
#######################################################################
Pushover Analysis
#######################################################################
if {$analysisType == "pushover"} {
puts "Running Pushover..."
# displacement parameters
set IDctrlNode 13;                           # node where displacement
is read for disp control
set IDctrlDOF 1;                             # degree of freedom (1)
of disp read for disp control
set Dmax [expr 0.1*$HBuilding];              # maximum displacement of
pushover: 10% roof drift
set Dincr [expr 0.01];                       # displacement increment

# calculate the lateral loads and create load pattern:  distribute
proportional to floor weight and height
set W2H2 [expr $Floor2Weight*$Floor2];
set W3H3 [expr $Floor3Weight*$Floor3];
set sumWiHi [expr $W2H2 + $W3H3];
set lat2 [expr 1.0/($NBays+1.0) * $WBuilding * $W2H2/$sumWiHi];
      # force on each frame node in Floor 2
set lat3 [expr 1.0/($NBays+1.0) * $WBuilding * $W3H3/$sumWiHi];     #
force on each frame node in Floor 3
pattern Plain 200 Linear {
load 12 $lat2 0.0 0.0;
load 13 $lat2 0.0 0.0;
load 22 $lat3 0.0 0.0;
load 23 $lat3 0.0 0.0;
}
puts " lat2 [expr 1.0/($NBays+1.0) * $WBuilding * $W2H2/$sumWiHi]"
puts " lat3 [expr 1.0/($NBays+1.0) * $WBuilding * $W3H3/$sumWiHi]"
# display deformed shape:
set ViewScale 5;
DisplayModel2D DeformedShape $ViewScale ;      # display deformed shape,
the scaling factor needs to be adjusted for each model

# analysis commands
constraints Plain;
numberer RCM;
system BandGeneral;
test NormUnbalance 1.0e-6 400;              #tolerance, max iterations
algorithm Newton;
integrator DisplacementControl  $IDctrlNode   $IDctrlDOF $Dincr;
analysis Static;
set Nsteps [expr int($Dmax/$Dincr)];         # number of pushover
analysis steps
set ok [analyze $Nsteps];                       # this will return zero
if no convergence problems were encountered
puts "Pushover complete"
}
#######################################################################
```

```
#   Time History/Dynamic Analysis
######################################################################
if {$analysisType == "dynamic"} {
puts "Running dynamic analysis..."
# display deformed shape:
set ViewScale 5;                          # amplify display of deformed
shape
DisplayModel2D DeformedShape $ViewScale;      # display deformed shape,
the scaling factor needs to be adjusted for each model

# Rayleigh Damping
# calculate damping parameters
set zeta 0.05;          # percentage of critical damping
set a0 [expr $zeta*2.0*$w1*$w2/($w1 + $w2)];        # mass damping
coefficient based on first and third modes
set a1 [expr $zeta*2.0/($w1 + $w2)];                # stiffness damping
coefficient based on first and third modes
set a1_mod [expr $a1*(1.0+$n)/$n];                  # modified stiffness
damping coefficient used for n modified elements. See Zareian & Medina
2010.

# assign damping to frame beams and columns
# command: region $regionID -eleRange $elementIDfirst $elementIDlast -
rayleigh $alpha_mass $alpha_currentStiff $alpha_initialStiff
$alpha_committedStiff
# use "region" command when defining mass proportional damping so that
the stiffness proportional damping isn't canceled
region 4 -eleRange 111 222 -rayleigh 0.0 0.0 $a1_mod 0.0;# assign
stiffness proportional damping to frame beams & columns w/ n
modifications
region 5 -node 12 13 22 23 -rayleigh $a0 0.0 0.0 0.0;          # assign
mass proportional damping to structure (assign to nodes with mass)

# define ground motion parameters
set patternID 1;                          # load pattern ID
set GMdirection 1;                        # ground motion direction (1 =
x)
set GMfile "NR94cnp20.tcl";               # ground motion filename
set dt 0.005;                           # timestep of input GM file
set Scalefact 1.0;                      # ground motion scaling factor
set TotalNumberOfSteps 6000; # number of steps in ground motion
set GMtime [expr $dt*$TotalNumberOfSteps];    # total time of ground
motion + 10 sec of free vibration

# define the acceleration series for the ground motion
# syntax:  "Series -dt $timestep_of_record -filePath
$filename_with_acc_history -factor $scale_record_by_this_amount
set accelSeries "Series -dt $dt -filePath $GMfile -factor [expr
$Scalefact*$g]";

# create load pattern: apply acceleration to all fixed nodes with
UniformExcitation
# command: pattern UniformExcitation $patternID $GMdir -accel
$timeSeriesID
pattern UniformExcitation $patternID $GMdirection -accel $accelSeries;

# define dynamic analysis parameters
set dt_analysis 0.01;             # timestep of analysis
```

```
wipeAnalysis;                              # destroy all components of the
Analysis object, i.e. any objects created with system, numberer,
constraints, integrator, algorithm, and analysis commands
constraints Plain;                         # how it handles boundary
conditions
numberer RCM;                              # renumber dof's to minimize
band-width (optimization)
system UmfPack;                            # how to store and solve the
system of equations in the analysis
test NormDispIncr 1.0e-8 50; # type of convergence criteria with
tolerance, max iterations
algorithm NewtonLineSearch;       # use NewtonLineSearch solution
algorithm: updates tangent stiffness at every iteration and introduces
line search to the Newton-Raphson algorithm to solve the nonlinear
residual equation. Line search increases the effectiveness of the
Newton method
integrator Newmark 0.5 0.25; # uses Newmark's average acceleration
method to compute the time history
analysis Transient;                        # type of analysis: transient
or static
set NumSteps [expr round(($GMtime + 0.0)/$dt_analysis)]; # number of
steps in analysis

# perform the dynamic analysis and display whether analysis was
successful
set ok [analyze $NumSteps $dt_analysis];      # ok = 0 if analysis was
completed
if {$ok == 0} {
puts "Dynamic analysis complete";
} else {
puts "Dynamic analysis did not converge";
}

# output time at end of analysis
set currentTime [getTime];  # get current analysis time  (after dynamic
analysis)
puts "The current time is: $currentTime";
wipe all;
}
```

12.1 Appendix B

FRAME 2 NLTHA RESULTS

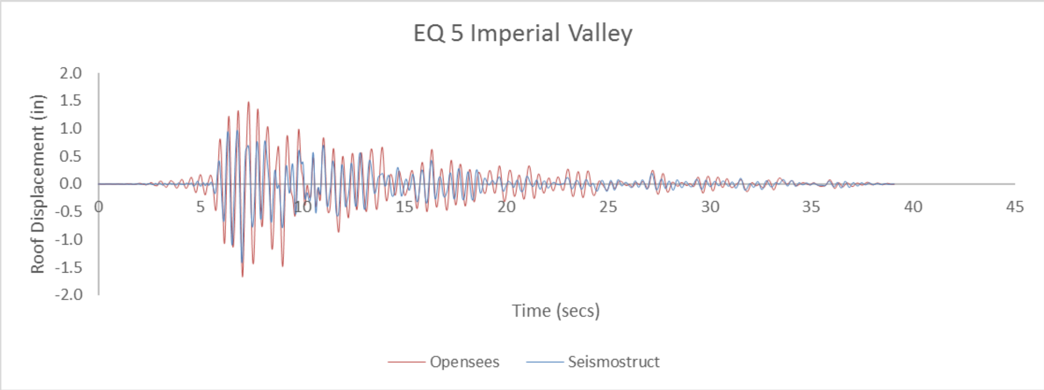

Figure : showing EQ 5 Imperial Valley time history analysis frame 2

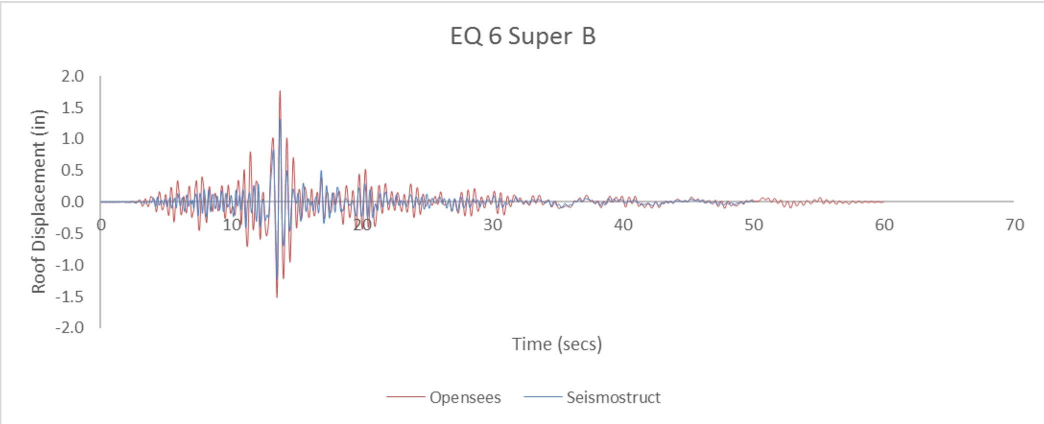

Figure: showing EQ 6 Super. Hills time history analysis frame 2

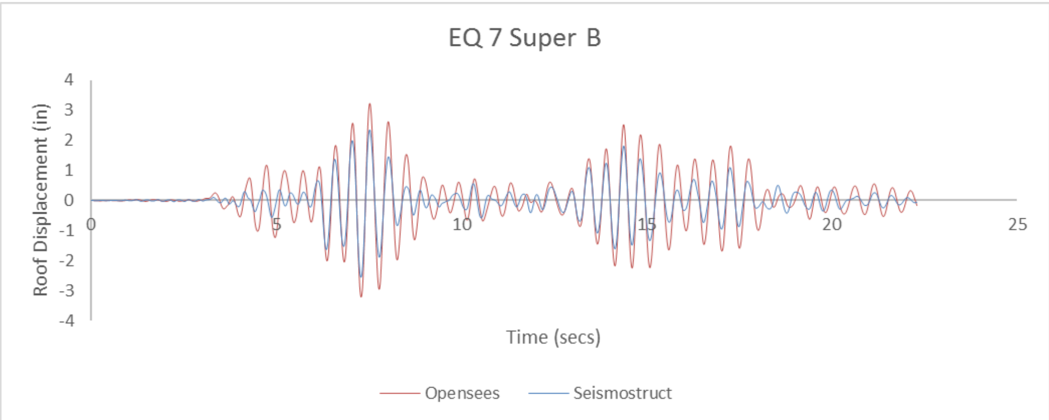

Figure: showing EQ 7 Super. Hills time history analysis frame 2

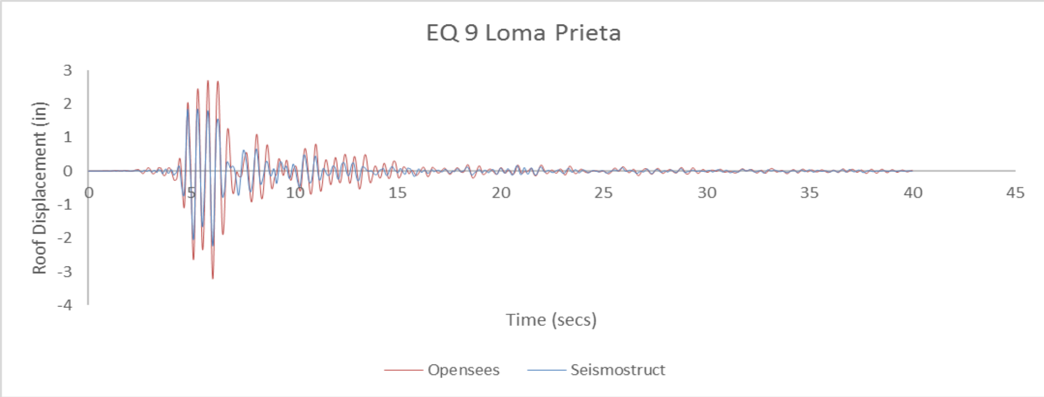

Figure : Showing EQ 9 Loma Prieta time history analysis frame 2

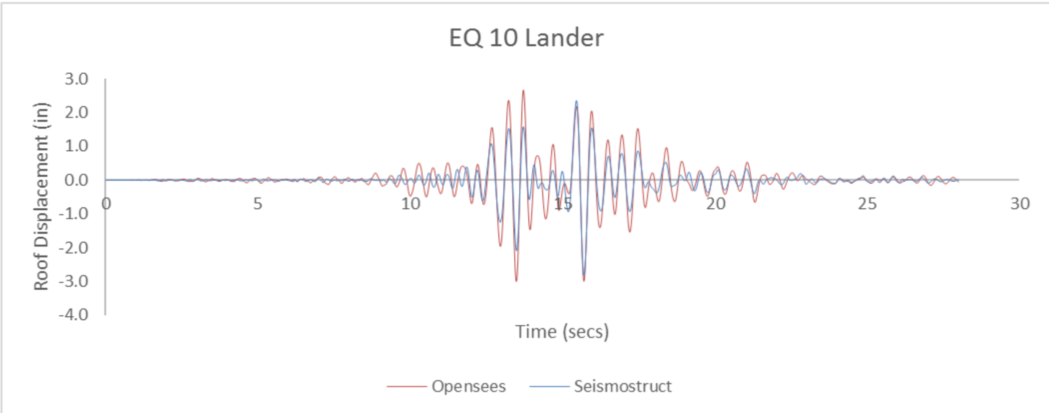

Figure : Showing EQ 10 Lander time history analysis frame 2

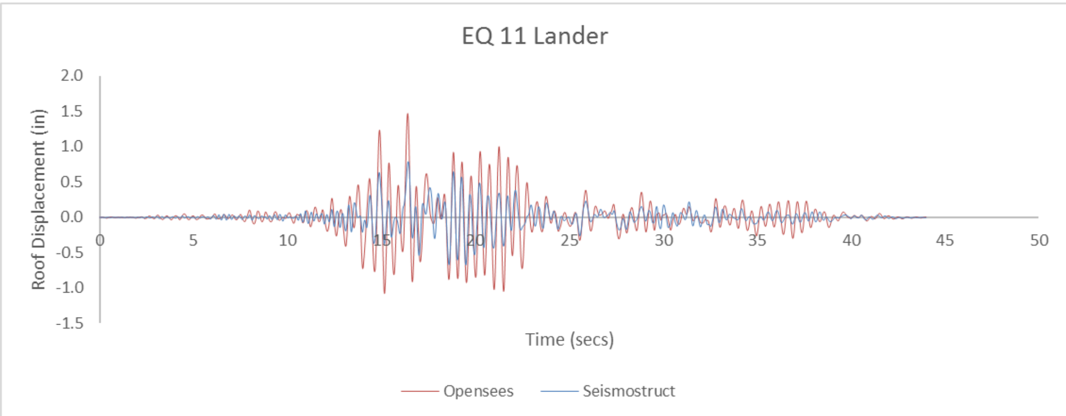

Figure : Showing EQ 11 Lander time history analysis frame 2

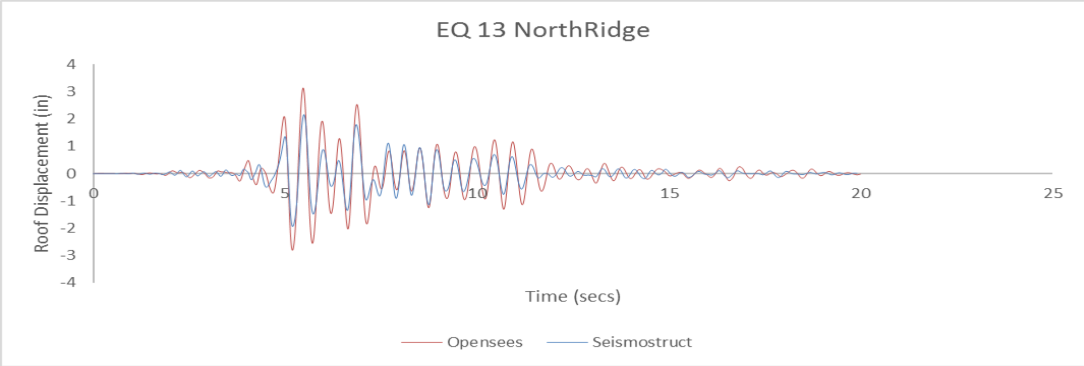

Figure : Showing EQ 13 Northridge time history analysis frame 2

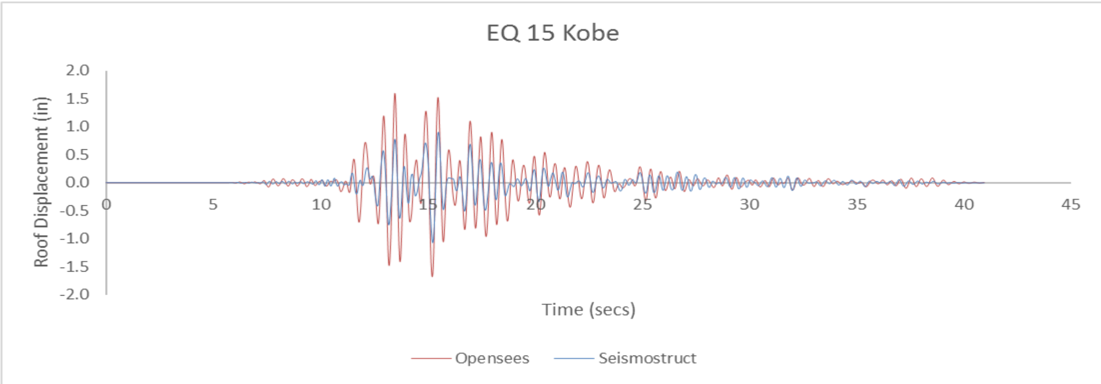

Figure : Showing EQ 15 kobe time history analysis frame 2

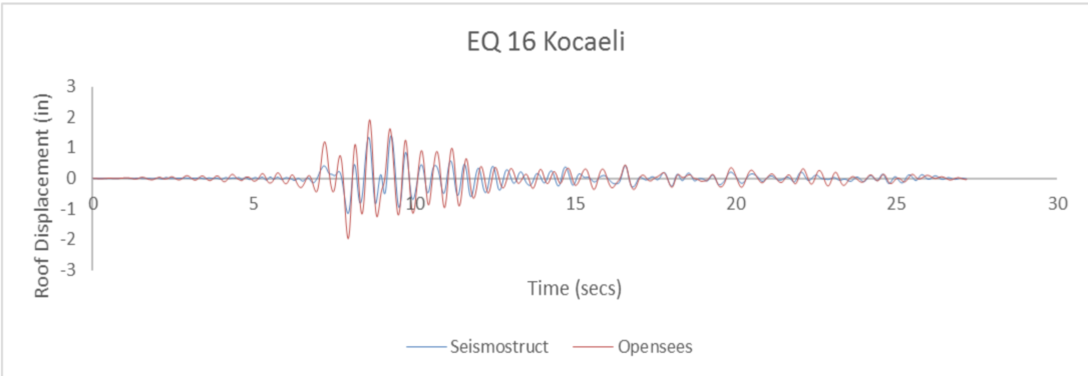

Figure : Showing EQ 16 Kocaeli time history analysis frame 2

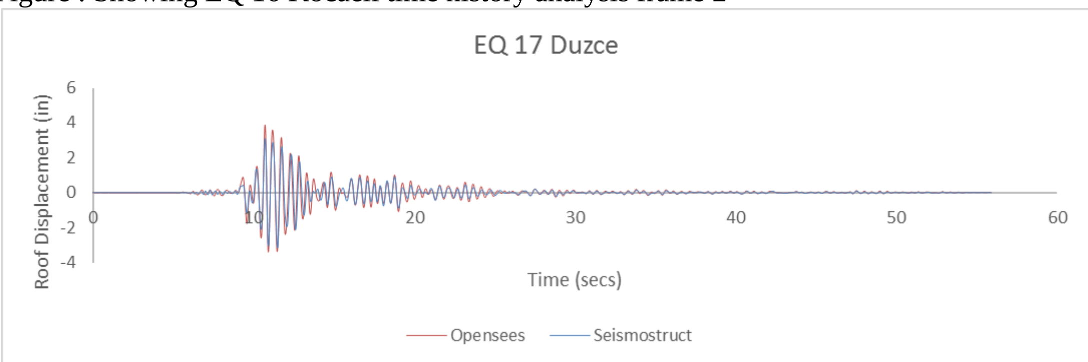

Figure : Showing EQ 17 Duzce time history analysis frame 2

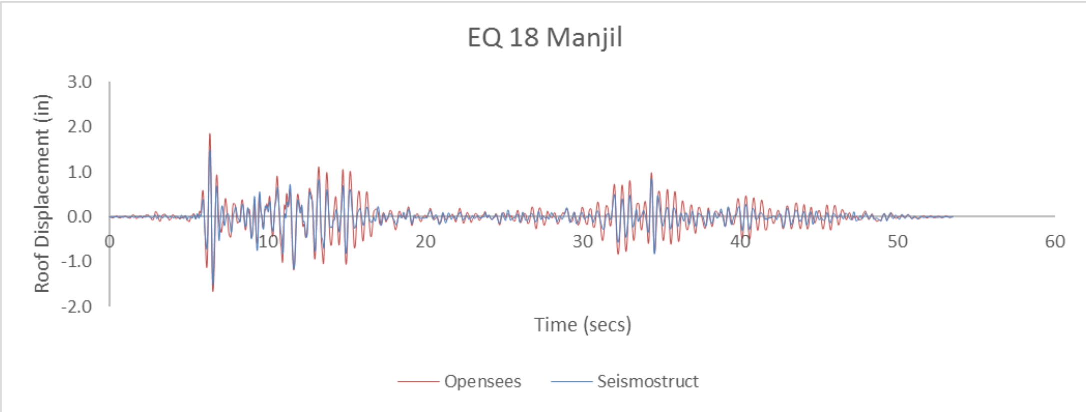

Figure : Showing EQ 18 Manjil time history analysis frame 2

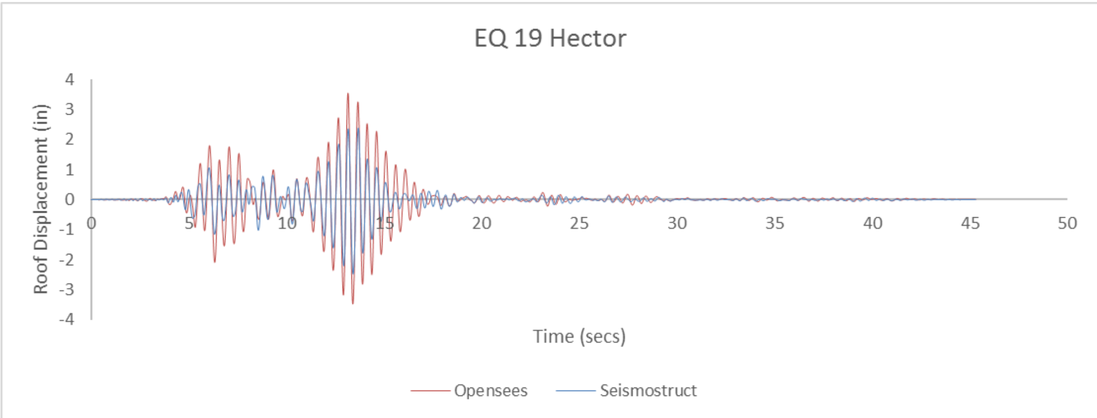

Figure : Showing EQ 19 Hector time history analysis frame 2

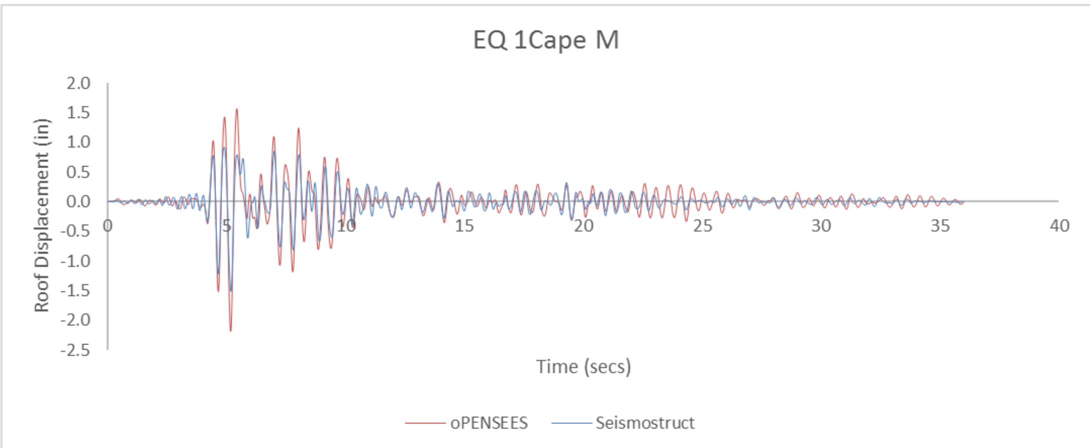

Figure : Showing EQ 1 Cape .M Lander time history analysis frame 2

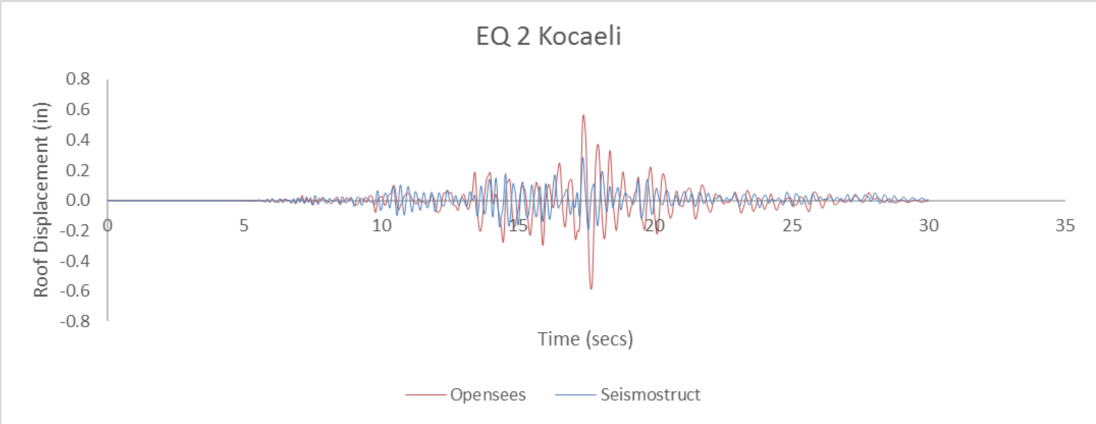

Figure: Showing EQ 2 Kocaeli time history analysis

Frame 3 NLTHA results

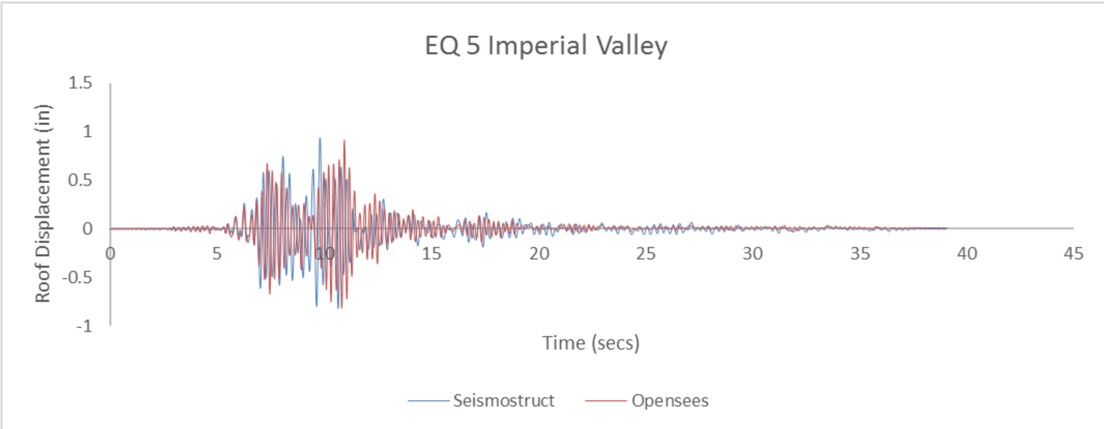

Figure : Showing EQ 5 Imperial Valley time history analysis frame 3

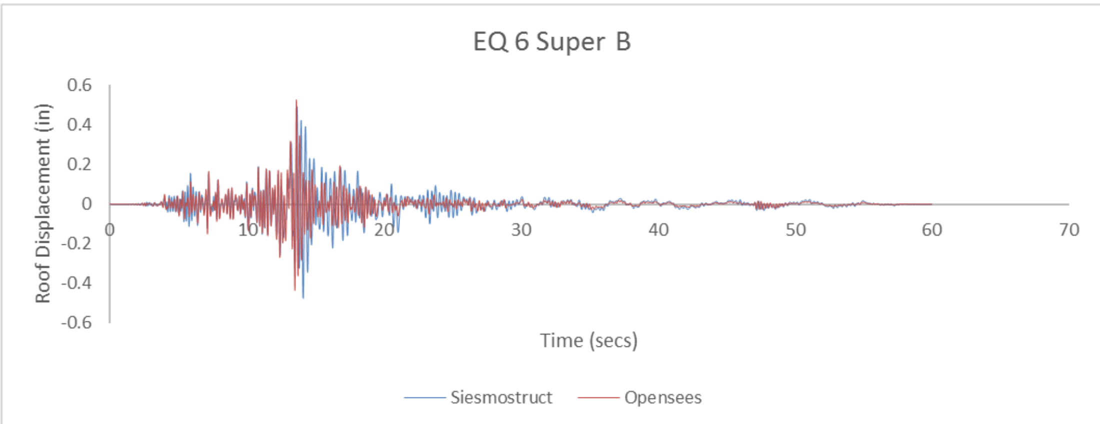

Figure : Showing EQ 6 Super Hills time history analysis frame 3

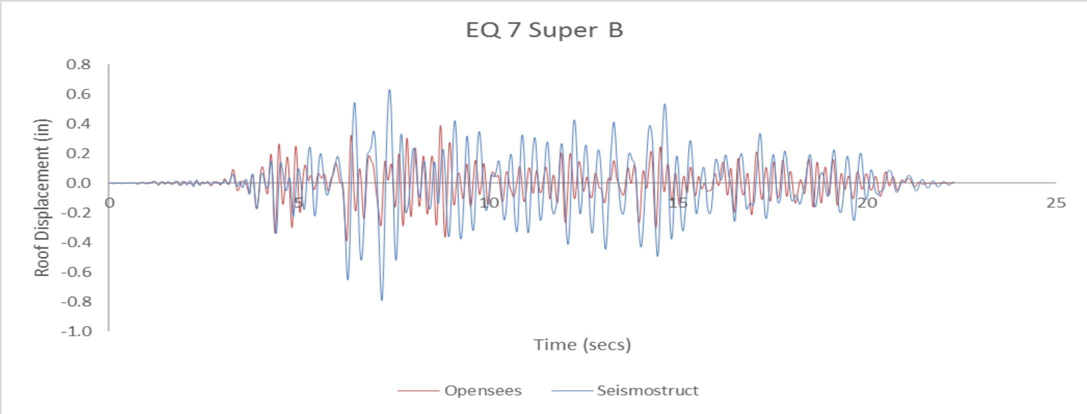

Figure : Showing EQ 7 Super Hills time history analysis frame 3

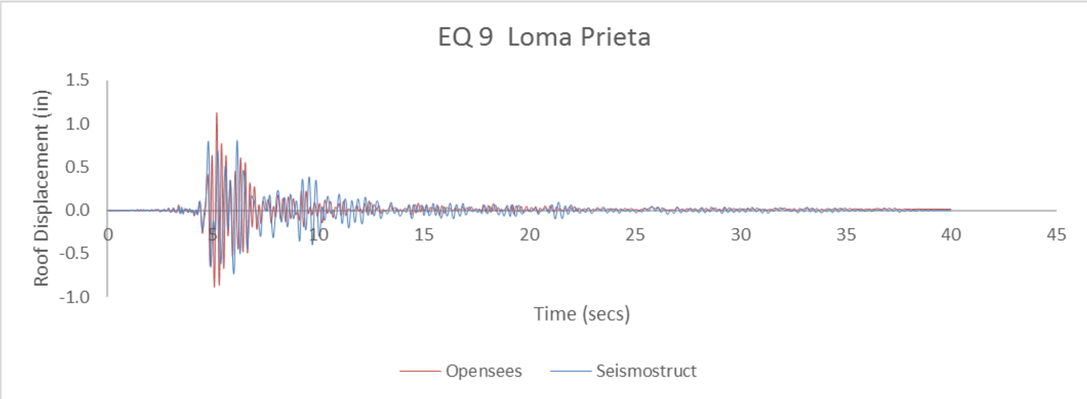

Figure : Showing EQ 9 Loma Prieta time history analysis frame 3

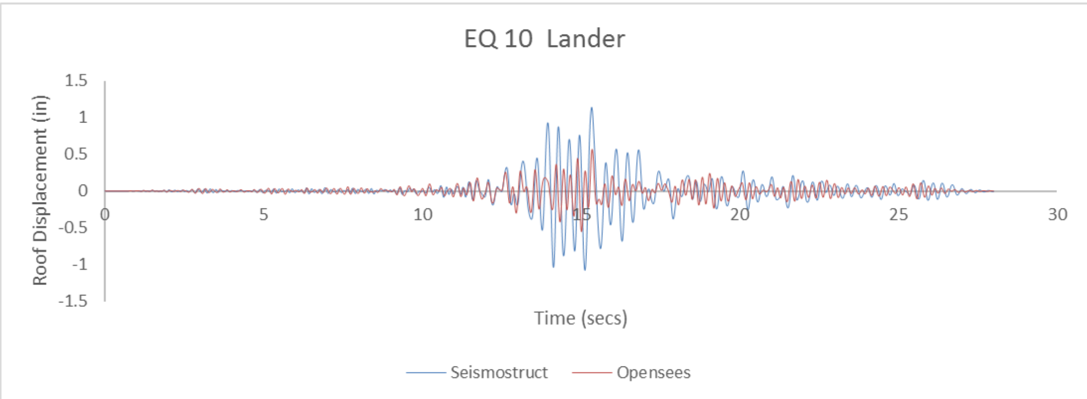

Figure : Showing EQ 10 Lander time history analysis frame 3

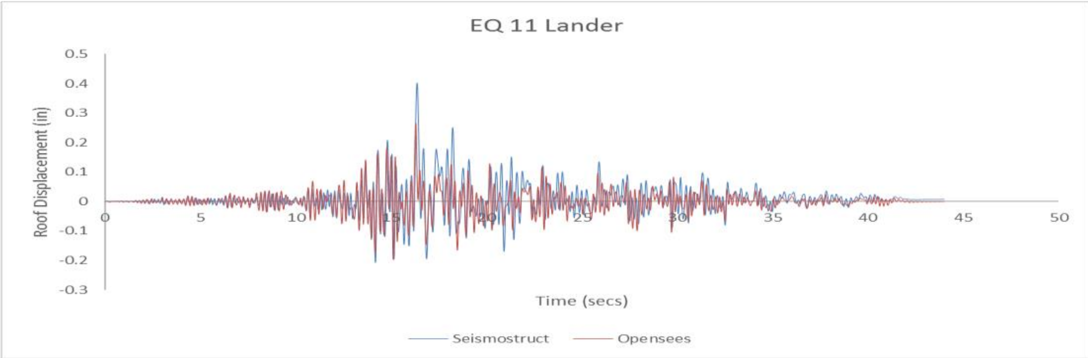

Figure : Showing EQ 11 Lander time history analysis frame 3

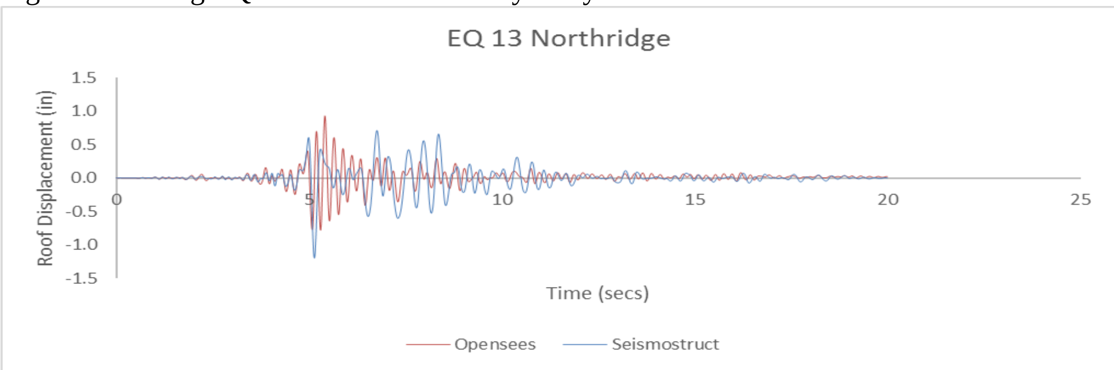

Figure : Showing EQ 13 North Ridge time history analysis frame 3

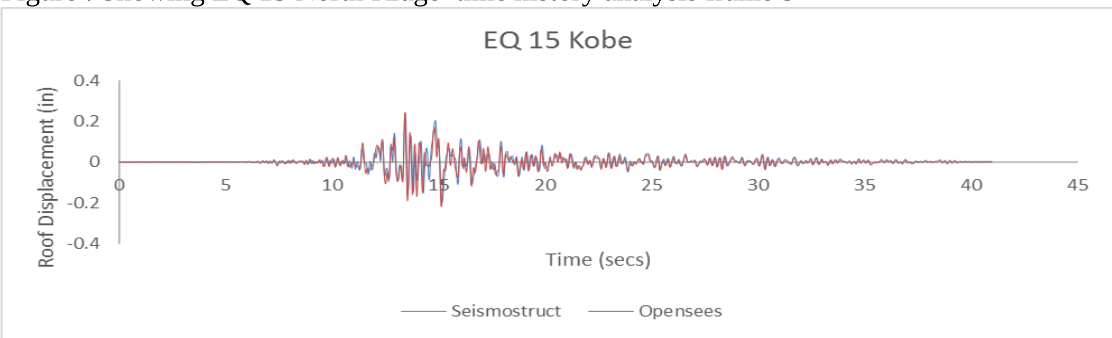

Figure : Showing EQ 15 Kobe time history analysis frame 3

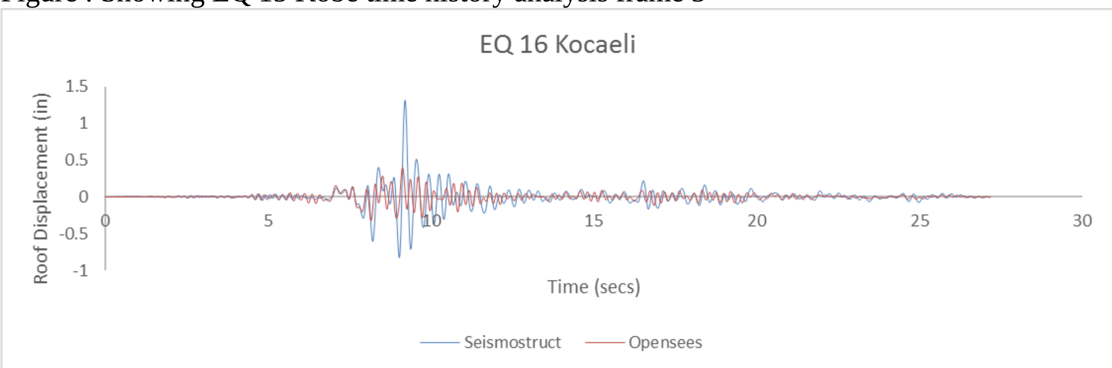

Figure : Showing EQ 16 Kocaeli time history analysis frame 3

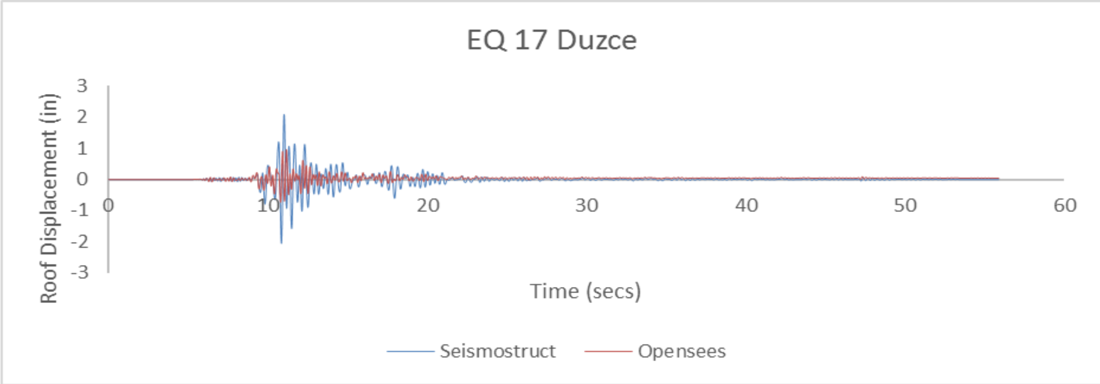

Figure : Showing EQ 17 Duzce time history analysis frame 3

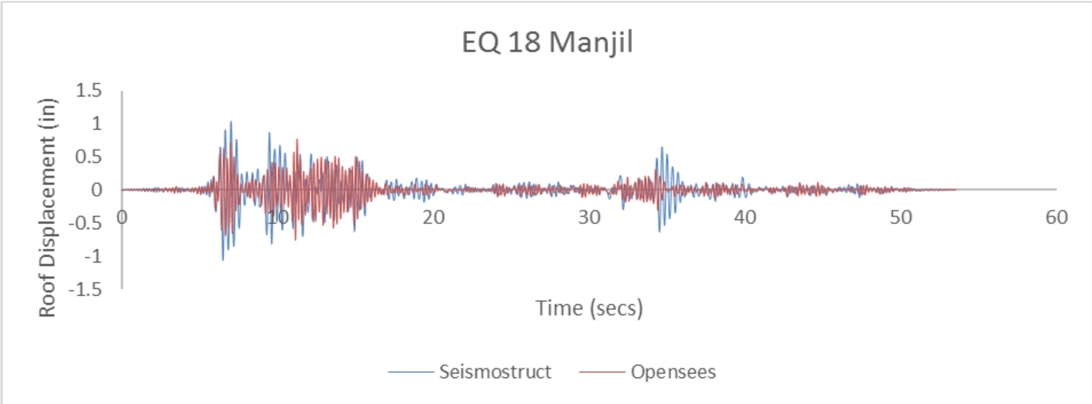

Figure : Showing EQ 18 Manjil time history analysis frame 3

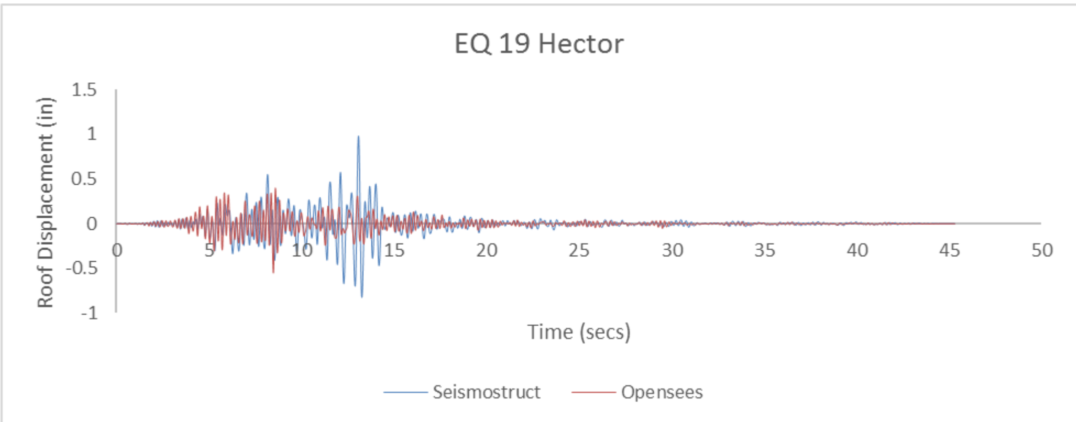

Figure : Showing EQ 19 Hector time history analysis frame 3

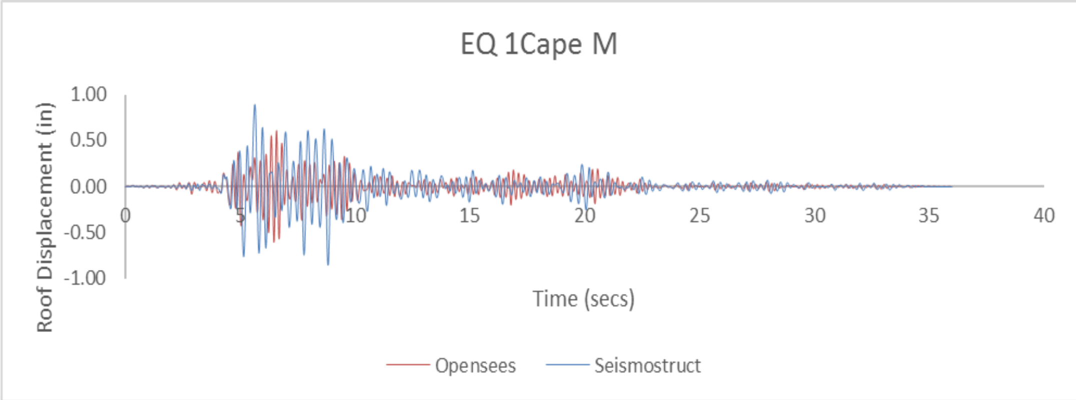

Figure : Showing EQ 1 Cape M time history analysis frame 3

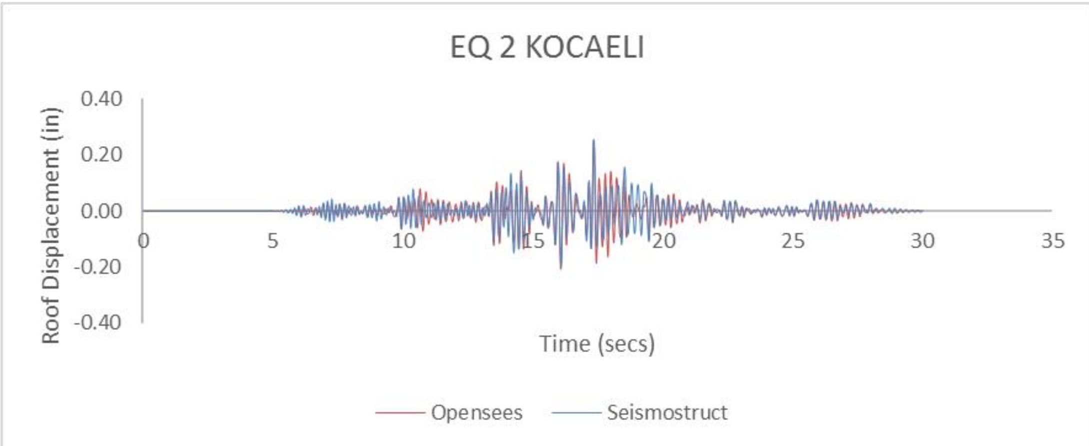

Figure : Showing EQ 2 Super Hills time history analysis frame 3

12.2 APPENDIX C

Table : Showing properties provided in Hasselton et al. (2007) Database

f'c	Characteristic compressive strength of concrete (MPa)
fyl	Yield stress of longitudinal reinforcement (MPa)
fyt	Yield stress of transverse reinforcement (MPa)
fsu long	Ultimate steel strength for longitudinal reinforcement(MPa)
fsu trans	Ultimate steel strength for transverse reinforcement(MPa)
B	Column Width (mm)
H	Column Depth (mm)
L	Length of equivalent cantilever (mm)
Bar Dia.	Diameter of transverse reinforcement (mm)
Spacing	Spacing of transverse reinforcement (mm)
Clear Cover	Distance between outer surface of column to outer edge of transverse reinforcement (mm)
Total # Bars	Number of longitudinal reinforcing bars
Diameter	Diameter of longitudinal reinforcement bars (mm)
Gross Area	Gross sectional area of column (mm2)
Vol. Trans	Volumetric transverse reinforcement ratio (reported)
Reinf. Ratio	Longitudinal reinforcement ratio (calculated)
Nv	Number of transverse shear bars in cross section
Configuration	C : Cantilever DC : Double Cantilever DE : Double Ended
Type of Confinement (Code)	(1) I: Interlocking ties (2) R: Rectangular ties (around perimeter) (3) RD: Rectangular and Diagonal ties (4) RI: Rectangular and Interlocking ties (5) RIJ: Rectangular and Interlocking ties, with J-hooks (6) RJ: Rectangular ties with J-hooks (7) RO: Rectangular and Octagonal ties (8) RU: Rectangular ties and U-bars (9) UJ: U-bars with J-hooks
P-D Codes	1 : Feff (=Mbase/L) Provided 2 : Shear Provided 3 : P Ram rotation decreases V 4 : P Ram rotation increases V -- : Not provided in report
Failure Type	1 : Flexure 2 : Shear

Table: Showing Frame 1 Maximum Inter-Storey Drift 1st Floor comparisons results

Names	Earthquake ID	SEISMOSSTRUCT	OPENSEES
		MIDR F1	MIDR F1
CapemendRio360	EQ1	0.023	0.0266
FriuliA-TMZ000	EQ2	0.011	0.0121
KOCAELI-ARC000	EQ3	0.005	0.0046
RSN169_IMPVALL	EQ4	0.217	0.0178
RSN174_IMPVALL	EQ5	0.019	0.0115
RSN721_SUPER	EQ6	0.024	0.0133
RSN725_SUPER.B_B	EQ7	0.016	0.0142
RSN752_LOMAP	EQ8	0.034	0.0199
RSN767_LOMAP	EQ9	0.010	0.0103
RSN848_LANDERS	EQ10	0.028	0.0147
RSN900_LANDERS	EQ11	0.033	0.0156
RSN953_NORTHR	EQ12	0.039	0.0295
RSN960_NORTHR	EQ13	0.018	0.0186
RSN1111_KOBE	EQ14	0.012	0.0126
RSN1116_KOBE	EQ15	0.020	0.0145
RSN1158_KOCAELI_	EQ16	0.045	0.2959
RSN1602_DUZCE	EQ17	0.027	0.0268
RSN1633_MANJIL	EQ18	0.013	0.0149
RSN1787_HECTOR	EQ19	0.025	0.0185
SFERNPEL090	EQ20	0.015	0.0149

Table: Frame 2 Maximum Inter-Storey Drift 1st floor comparisons results

Earthquake ID	SEISMOSSTRUCT	OPENSEES
	MIDR F2	MIDR F2
EQ1	0.0053	0.007387
EQ2	0.0041	0.005967
EQ3	0.0009	0.002127
EQ4	0.0042	0.00959
EQ5	0.0049	0.00540446
EQ6	0.0045	0.005906
EQ7	0.0088	0.01104
EQ8	0.0066	0.01444
EQ9	0.0078	0.01089
EQ10	0.0097	0.01012
EQ11	0.0026	0.005038
EQ12	0.0154	0.01708
EQ13	0.0073	0.01071
EQ14	0.0141	0.012467
EQ15	0.0037	0.005834
EQ16	0.0049	0.006702
EQ17	0.0107	0.01324
EQ18	0.0049	0.00624
EQ19	0.0086	0.01214
EQ20	0.0019	0.0037779

Table: Frame 3 Maximum Inter-Storey Drift at 1st Floor Comparison

Names	Earthquake ID	SEISMOSSTRUCT	OPENSEES
		MIDR F3	MIDR F3
CapemendRio360	EQ1	0.0032	0.00205278
FriuliA-TMZ000	EQ2	0.0024	0.0008615
KOCAELI-ARC000	EQ3	0.0009	0.00086154
RSN169_IMPVALL	EQ4	0.0022	0.0012464
RSN174_IMPVALL	EQ5	0.0033	0.00312
RSN721_SUPER	EQ6	0.0017	0.001794
RSN725_SUPER.B_B	EQ7	0.0028	0.00134
RSN752_LOMAP	EQ8	0.0064	-
RSN767_LOMAP	EQ9	0.0028	0.00397
RSN848_LANDERS	EQ10	0.0039	0.00195
RSN900_LANDERS	EQ11	0.0013	0.0009169
RSN953_NORTHR	EQ12	0.0049	0.0023191
RSN960_NORTHR	EQ13	0.0042	0.00316633
RSN1111_KOBE	EQ14	0.0044	0.0035226
RSN1116_KOBE	EQ15	0.0008	0.000825089
RSN1158_KOCAELI_	EQ16	0.0045	0.00138369
RSN1602_DUZCE	EQ17	0.0071	0.00334589
RSN1633_MANJIL	EQ18	0.0038	0.00258496
RSN1787_HECTOR	EQ19	0.0035	0.00185489
SFERNPEL090	EQ20	0.0019	0.00124

Table: Showing Tabulated PGA (g) and Sa (T1) g,,max roof displacement and drifts for frame 2

Earthquake ID	PGA (g)	Sa (T1)	SEISMOSSTRUCT		OPENSEES	
			Max Roof Displacement (in)	Max Roof Drift	Max Roof Displacement (in)	Max Roof Drift
EQ1	0.55	2.08	1.51	0.00	2.18	0.01
EQ2	0.35	0.74	1.24	0.00	1.79	0.01
EQ3	0.35	0.19	0.29	0.00	0.59	0.00
EQ4	0.37	0.53	1.19	0.00	2.84	0.01
EQ5	0.36	0.75	1.42	0.00	1.67	0.01
EQ6	0.47	0.58	1.32	0.00	1.77	0.01
EQ7	0.51	1.14	2.55	0.01	3.23	0.01
EQ8	0.56	1.83	1.94	0.01	4.00	0.01
EQ9	0.42	1.10	2.23	0.01	3.22	0.01
EQ10	0.24	0.97	2.82	0.01	3.00	0.01
EQ11	0.49	0.47	0.79	0.00	1.47	0.00
EQ12	0.47	1.08	4.24	0.01	4.74	0.01
EQ13	0.48	1.02	2.16	0.01	3.14	0.01
EQ14	0.23	1.60	3.96	0.01	3.59	0.01
EQ15	0.36	0.50	1.07	0.00	1.68	0.01
EQ16	0.74	1.21	1.39	0.00	1.97	0.01
EQ17	0.51	1.61	3.15	0.01	3.88	0.01
EQ18	0.33	1.08	1.50	0.00	1.85	0.01
EQ19	0.21	0.77	2.48	0.01	3.55	0.01
EQ20	0.22	0.46	0.59	0.00	1.08	0.00

Table: Showing Tabulated PGA (g) and Sa (T1) g, max roof displacement and drifts for frame 3

Earthquake ID	PGA (g)	Sa (T1)	SEISMOSSTRUCT		OPENSEES	
			Max Roof Displacement (in)	Max Roof Drift	Max Roof Displacement (in)	Max Roof Drift
EQ1	0.55	1.13	0.89	0.00	0.61	0.00
EQ2	0.35	0.62	0.70	0.00	0.44	0.00
EQ3	0.35	0.67	0.25	0.00	0.26	0.00
EQ4	0.37	0.69	0.66	0.00	0.37	0.00
EQ5	0.36	1.25	0.94	0.00	0.92	0.00
EQ6	0.47	0.93	0.49	0.00	0.53	0.00
EQ7	0.51	0.63	0.79	0.00	0.39	0.00
EQ8	0.56	1.33	1.89	0.01	0.82	0.00
EQ9	0.42	2.04	0.81	0.00	1.13	0.00
EQ10	0.24	0.60	1.14	0.00	0.57	0.00
EQ11	0.49	0.43	0.40	0.00	0.01	0.00
EQ12	0.47	1.16	1.40	0.00	0.67	0.00
EQ13	0.48	1.47	1.20	0.00	0.93	0.00
EQ14	0.23	1.47	1.22	0.00	1.00	0.00
EQ15	0.36	0.38	0.24	0.00	0.24	0.00
EQ16	0.74	0.64	1.31	0.00	0.40	0.00
EQ17	0.51	1.57	2.09	0.01	0.96	0.00
EQ18	0.33	1.70	1.07	0.00	0.77	0.00
EQ19	0.21	0.82	0.98	0.00	0.55	0.00
EQ20	0.22	0.65	0.55	0.00	0.36	0.00